Politecnico di Torino

Master's Degree in Biomedical Engineering

DEVELOPMENT OF MOLECULARLY IMPRINTED POLYMERS BY LIGHT-INDUCED 3D PRINTING

Supervisor:
Dott. Ignazio Roppolo

Co-supervisor:
Dott. Simone Marasso

Candidate:
Arianna Leone

Academic Year: 2022-2023

“Twenty years from now
you will be more disappointed
by the things you didn’t do
than by the ones you did do.
So throw off the bowlines,
sail away from the safe harbor.
Catch the trade winds in your sails.
Explore. Dream. Discover.“

Mark Twain

A me,
affinché io abbia il coraggio
di esplorare, sognare, scoprire.

Abstract

Molecularly Imprinted Polymers (MIPs) are artificial receptors fabricated through Molecularly Imprinted Technology, an interesting and emerging technique, which consists in creating cavities with the shape of a chosen template, within a polymeric matrix. So, MIPs can exhibit selectivity and specificity for a predetermined analyte, used in the imprinting procedure, and their aim is to mimic natural molecular recognition mechanism, typical of biological receptors.

Additionally, MIPs present several advantages, like superior physical robustness and strength, resilience to elevated temperatures and pressures, lower cost, ease of preparation, and versatility in the choice of template, compared to biological receptors.

Due to these characteristics, MIPs are gaining widespread attention over the last few decades in a variety of scientific and technological sectors, like drug delivery, artificial antibodies, chemo biosensing, separation science, purification, assay and sensors, and catalysis.

This thesis is focused on the development of 3D printed MIPs, using Digital Light Processing (DLP) technique, which allows the creation of complex and self-standing 3D structures. Generally, the constituents of MIPs are the molecule of interest, which will act as the template, embedded in a mixture of functional monomer, a small molecule that interacts with the template, crosslinker, a molecule that is employed to form the polymeric matrix, and finally an initiator, to induce the polymerization reaction.

In this work, the ingredients chosen are the antibiotic oxytetracycline (OTC) as the template; methacrylic acid (MAA) as the functional monomer; dipropylene glycol diacrylate (DPGDA) as the crosslinker and phenylbis (2,4,6-trimethylbenzoyl) phosphine oxide (BAPO) as the photoinitiator. Three formulations with different ratios between the ingredients (MAA, OTC and DPGDA) have been studied, optimizing for each of them the printing parameters, to obtain MIPs with complex geometries.

After assessing the ability of the investigated materials to operate as MIPs, by printing simple dots and by means of UV-Vis spectroscopy, more complex geometries were studied, i.e., filters constituted by the alternation of planes and pillars. Printing fidelity and the ability to capture template molecules were studied as well. At last, aiming at improving the surface area creating porosities within the matrix, formulations with salt were printed. As a result, 3D printed MIPs able to capture target molecules were successfully developed.

This thesis consists of five chapters: the first one describes the ingredients, their optimization for the fabrication of MIPs, and the different production techniques. The second one is focused on Additive Manufacturing and in particular on VAT polymerization and DLP. In the third chapter the experimental part is described, focusing on the materials and methods used during the thesis. Chapter four focuses on the optimization of printing parameters, along with analysis of results. Finally, conclusions are summarized, mentioning future perspectives.

Contents

Chapter 1: Molecularly Imprinted Polymers

1.1 Introduction

Nowadays, sensing the ambient environment has become crucially important; for example, in the past ten years, several investigations have found trace amounts of pharmaceuticals and personal care products in surface waters, drinking water, and wastewater effluents [1]. Others study have found antibiotics residues in animal derived foods, like oxytetracycline and fluoroquinolone, that are used to treat various infections in animals, aquaculture, and humans [2].

So, removal of these pollutants and antibiotic residues has become a top priority due to growing concerns about the effects of these toxins on the environment and human health [1].

The ultimate kind of sensing is molecular recognition, which is now the subject of many chemical studies. Although natural systems are capable of producing antibodies against a variety of foreign substances, using such receptors in chemical processes is complicated by issues like cost and susceptibility to external factors. So, the development of synthetic receptors that imitate the natural antibody-antigen interaction, with comparable specificity and sensitivity, is a focus of current sensor research [3].

These receptors, capable of detecting and monitoring targets in a non-invasive manner, are the so called “Molecularly Imprinted Polymers” (MIPs), fabricated through an interesting and emerging technique, called Molecularly Imprinted Technology (MIT).

Molecularly Imprinted Technology consists in creating cavities with the shape of the chosen template, within a polymeric matrix. This technique is based on the principle of recognition between enzyme and substrate, which is called the “lock and key” model, a metaphor used for the first time in 1894 by Emil Fischer in “Berichte der Deutschen Chemischen Gesellschaft”, showed in Figure 1.1.

In particular, the active binding site of an enzyme (lock) has a specific shape and therefore it’s complementary only to a certain type of substrate (key), which will then be bound to it, just as each key is specific to a lock. On the contrary, substrates that present different shapes and sizes will not be recognized by the enzymes and therefore will not bind [4]. Consequently, MIPs can exhibit selectivity and specificity for a predetermined analyte, used in the imprinting procedure, and their aim is to mimic natural molecular

recognition mechanism, typical of biological receptors, such as antibodies, nucleic acids, and proteins [5].

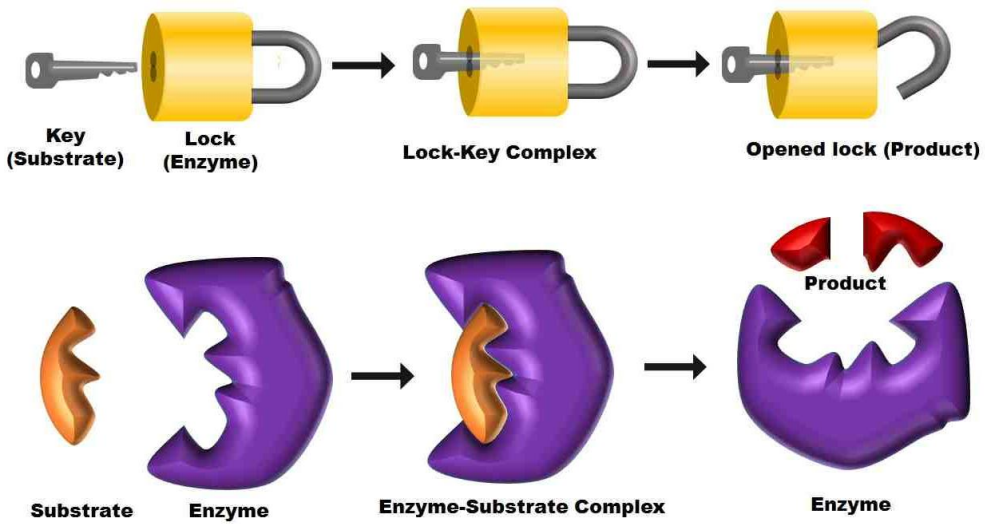

Figure 1.1 – Principle of recognition between enzyme and substrate, called "lock and key" model. [6]

Compared to biological systems, which typically require storage and application at temperatures in the range of the human body temperature, MIPs can usually be stored indefinitely, and they don't require particular environmental storage conditions [3]. Moreover, MIPs exhibit superior physical robustness, strength, and resilience to high temperatures and pressures. They are also inert towards acids, bases, metal ions and organic solvents. Moreover, they are less expensive and easier to prepare, require simple ingredients and have a very long storage life, retaining their recognition ability for several years at room temperature [5].

Another important advantage of MIPs is that they can be produced for almost any target molecule, such as pesticides, amino acids, steroids, pharmaceuticals, peptides and sugars, but also ions, cells and viruses [7].

Due to all these characteristics, MIPs have received widespread attention in a variety of scientific and technological sectors, like drug delivery, enantiomeric recognition and degradation, artificial antibodies, chemobiosensing, separation science, purification, assay and sensors, and catalysis [7].

1.2 Strategies for the synthesis of Molecularly Imprinted Polymers

The two most important mechanisms for the fabrication of MIPs are sol-gel process and free-radical polymerization (FRP); the latter in turn includes several productions' methods, like bulk polymerization, suspension

polymerization, emulsion polymerization, seed polymerization and precipitation polymerization [8]. Each of these methods is characterized by the presence of three fundamental elements:

- **Template**: the molecule of interest, used as mold in the imprinting procedure.
- **Functional monomer**: a small molecule that strongly interacts with the template.
- **Crosslinker**: a monomer with higher molecular weight, that form the matrix around the template-functional monomer complex.

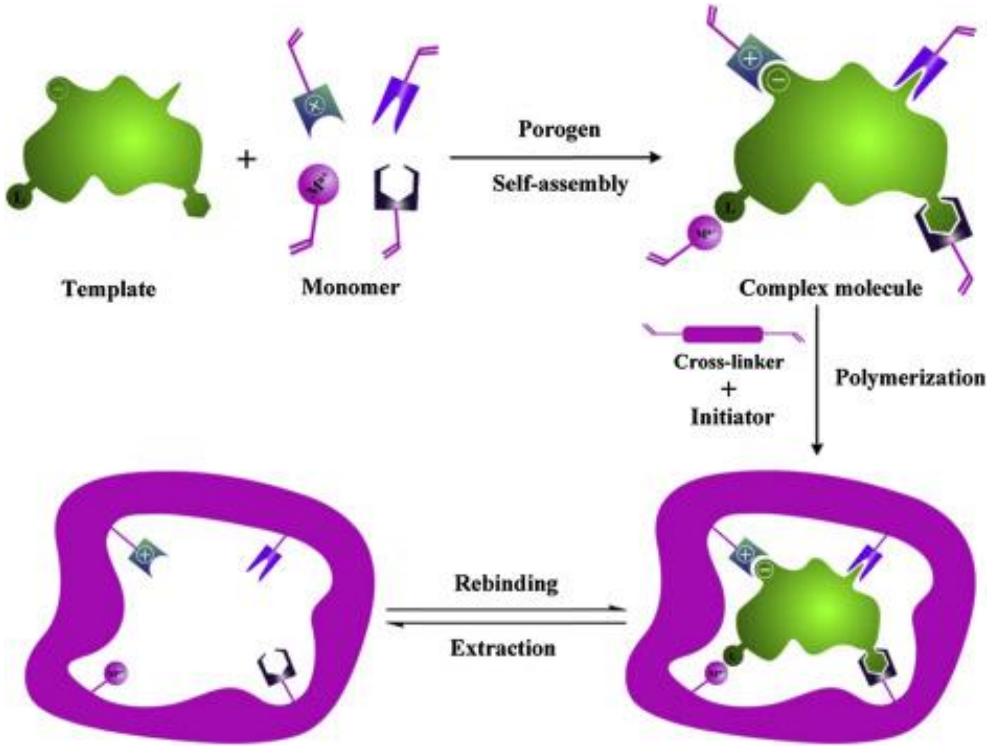

Figure 1.2 – Schematic representation of Molecularly Imprinted Polymer synthesis [9]

MIPs' production process proceeds step by step, as shown in Figure 1.2:

1) Formation of the pre-polymerization complex: the functional groups of the functional monomer strongly interact with those of the template molecule, to form the complex, and so basically the monomer is assembled around the template, after sufficient mixing and, if necessary, in presence of a solvent.
2) Polymerization process: the crosslinker and a polymerization initiator are added to the mixture; subsequently, by heating or ultraviolet radiation, the crosslinker polymerizes and forms a three-dimensional polymeric matrix around the complex template + functional monomer.

3) Removal of the template through washing techniques: in the matrix remain specific recognition sites complementary in shape, size and chemical functionality to the template molecule [7]. So, the resultant polymer recognizes and binds selectively the template molecules used during the imprinting procedure.

Based on the nature of interactions between the template molecule and the functional groups of the monomers in the pre-polymerization stage, the primary methods for creating MIP can be categorized into two groups: covalent and non-covalent (Figure 1.3). Additionally, there are semi-covalent imprinting, metal-mediated imprinting, and host-guest inclusion-based interactions, that are variations of these techniques [7]. In the following paragraphs the techniques most used are illustrated, namely the covalent, non-covalent and semi-covalent approach.

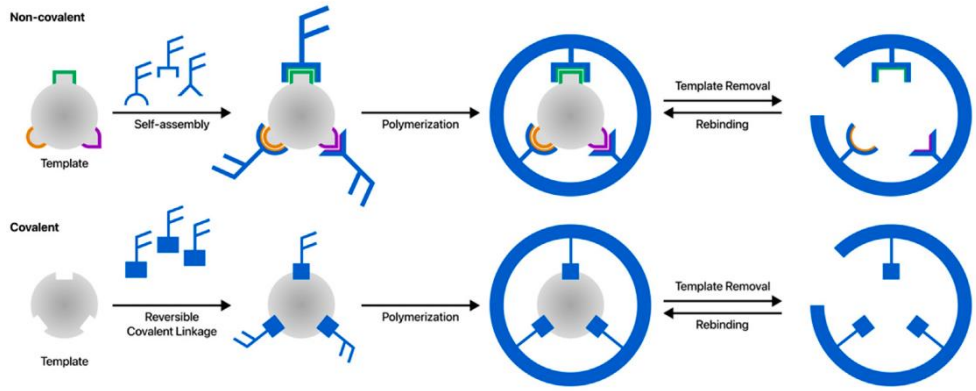

Figure 1.3 – MIP procedures: non-covalent and covalent imprinting [10]

1.2.1 Covalent imprinting approach

The covalent imprinting technique, also known as the pre-organized approach, was developed by G. Wulff and co-workers. It involves binding the template-monomer complex in solution prior to polymerization with reversible covalent bonds; as a result, molecular recognition is accomplished by the formation/breakage of these bonds [11].

A few examples of covalent interactions in molecular imprinting are:

- Schiff bonds: they are obtained by condensing an aldehyde or ketone with a primary amine, in an acidic environment, and by eliminating a molecule of water [12,13].
- Boronic ester bonds: they are obtained from boric acids in the presence of diols in aqueous solution [13,14,15].
- Ketal bonds: they are obtained from a ketone that reacts with an alcohol, in an acidic environment [16,17].

- Acetic bonds: they are obtained from the reaction between an aldehyde, or a ketone, and an alcohol, in an acidic environment [18].

Here, a significant amount of cross-linker is present during polymerization, in order to produce an insoluble stiff network. For template extraction, the covalent connections must be broken through chemical cleavage, resulting in well-defined binding cavities with the target molecule's complementary steric and functional topography.

The perfect stoichiometry of the template-monomer complexes enables the creation of polymers with binding groups exclusively positioned in the imprinted cavities, lowering the probability of non-specific interactions. This is one of the principal advantages of the covalent approach.

The resultant polymer networks exhibit homogeneous binding site distribution and superior selectivity than MIP produced using the non-covalent method, due to the high stability of the complexes during polymerization.

On the other hand, there are also some disadvantages: the choice of functional monomers and templates that can be used with this approach is limited to products such as alcohols, amines, aldehydes, ketones or carboxylic acids; there is the need to synthesize the template-monomer complex before polymerization and an increased effort is needed to remove the template after MIP synthesis, as well as for repeated use; finally, the reassociation kinetics is slow, due to the necessity to restore the covalent bond for target recognition [19]. MIPs prepared by this approach are usually used for catalysis [20].

1.2.2 Non-covalent imprinting approach

The non-covalent imprinting technique, also known as self-assembly approach, was developed by the Mosbach group [21]. It's based on non-covalent bonding between the template and the functional monomer, which include weak interactions such as van der Waals force, hydrogen bonds, $\pi - \pi$ interactions, dipole-dipole interactions, and ion-dipole interactions, which are easily obtained when all the components are mixed.

This method relies on common building blocks, so very little synthetic work is required. It's also rather flexible, since many functional monomers able to interact with almost any kind of target molecule are available [20]. The template molecule can be bound and removed from the polymer matrix with ease because weak non-covalent bonds are involved during the formation and breakdown stages. Moreover, the process is straightforward, so the need to chemically derivatize the template molecule prior to polymerization can be avoided [7]. Finally, this method gives the possibility of introducing a wide

variety of functionalities into the MIP [22]. These are some of the reasons why this approach is the most employed.

However, the monomer-template aggregate is labile, and doesn't maintain the stoichiometric ratio, and so, an excess amount of functional monomer is needed for completely bind template molecules [7]. This leads to a heterogeneous distribution of binding sites in the MIP with a variety of affinity constants [23]. Additionally, the remaining monomers that are not complexed, are randomly integrated into the polymer matrix, producing non-imprinted binding sites [20]. These are the main drawbacks of this technique.

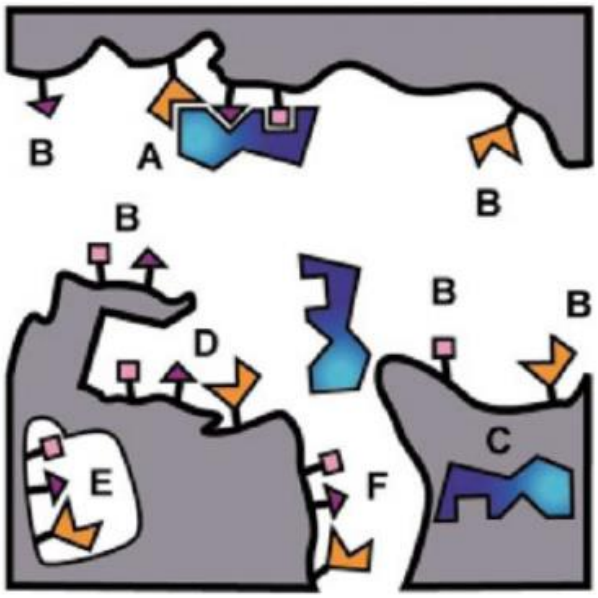

Figure 1.4 – Representation of binding sites' heterogeneity: high affinity site in macropore (A) and micropore (F); lower affinity sites in macropore (B); trapped template (C); embedded site (E), highest affinity site with shape selectivity from polymer (D). [20]

1.2.3 Semi-covalent imprinting approach

The semi-covalent imprinting technique was developed by Whitcombe and colleagues [24] to overcome one of the drawbacks of the covalent approach (the slow reassociation kinetics) and to combine the advantages of both approaches. This method employs covalent bonds only during the formation of the pre-polymerization complex between the template and the functional monomers, while the rebinding of the target to the MIP could be obtained by non-covalent interactions. Between the template and the functional monomer, a linker group or spacer is used, which is then removed during the bond rebinding of the template molecule.

Whitcombe and co-workers have demonstrated the feasibility of this approach on the example of a MIP specific for cholesterol, chosen due to its rigid structure, and because it is a representative of a group of molecules with significant biological and practical significance, the sterols [24].

A covalent template–functional monomer complex, cholesteryl (4-vinyl) phenyl carbonate ester, was imprinted. After polymerization with an excess of cross-linker, the resulting network was hydrolyzed by chemical cleavage, to release the template molecule (cholesterol) along with carbonic acid as the sacrificial molecule. This results in the formation of a noncovalent recognition site, bearing a phenolic hydroxyl group residue, to which cholesterol could rebind via a hydrogen bond [7,20]. So, this approach is characterized by both the high affinity of covalent binding and mild operation conditions of non-covalent rebinding [25].

1.3 Ingredients of Molecularly Imprinted Polymers and their optimization

As mentioned, the constituents of MIPs are functional monomer, template molecule, crosslinker, initiator and, if necessary, a solvent; since the performance of MIPs and their recognition properties depend on these elements, their role must be understood, and great consideration must be given to their selection. MIP synthesis is therefore a laborious process and numerous attempts are often needed to optimize the choice of these ingredients.

1.3.1. Crosslinker

As mentioned in paragraph 1.1, in the fabrication of MIP the crosslinker is employed to maintain the functional monomers around the template molecules during the polymerization process, leading to the production of a very stiff polymer matrix even after the template has been removed.

In particular, during the imprinting process, the crosslinker performs three main functions [5]:

a. Determine the morphology of the polymer network, which can be macroporous, microgel powder or gel type.

b. Stabilize the imprinted binding sites.

c. Give mechanical stability to the polymer network.

Some of the most used crosslinkers are listed in Figure 1.5.

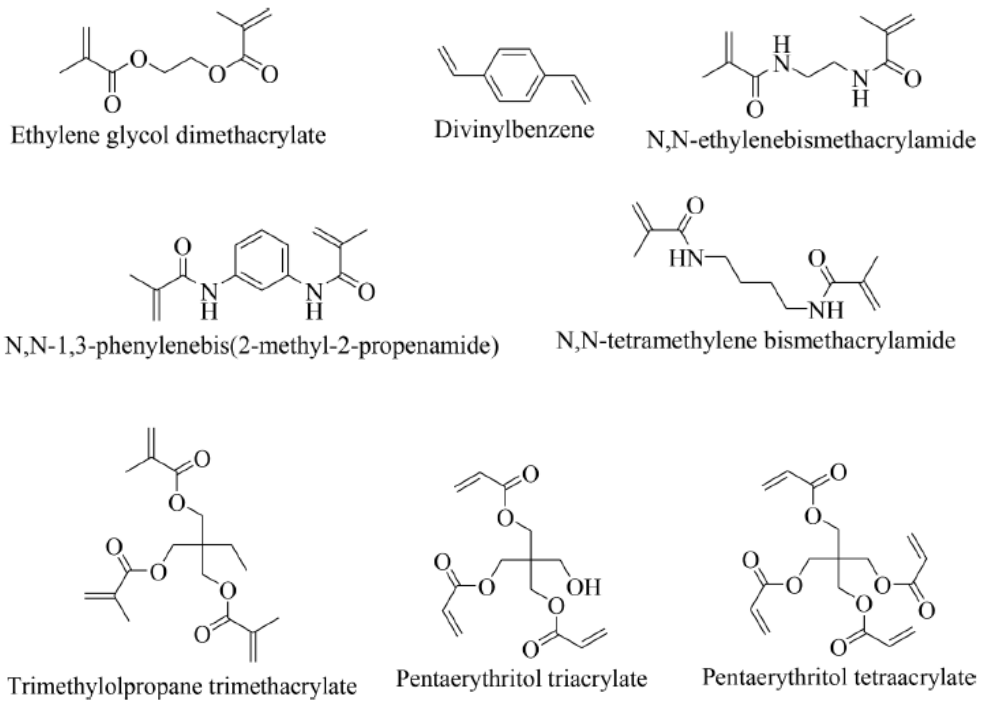

Figure 1.5 – Chemical structure of the most common crosslinkers used for MIP's fabrication [7]

1.3.2 Template

The template should have the following characteristics [7]:

- Be soluble in imprinting conditions.
- Generate binding sites with good cross-reactivity with targeted analysts.
- Not contain groups that inhibit polymerization [25].
- Exhibit excellent chemical stability during the polymerization reaction.
- Possibly be easily available in large quantities at a low cost.

One problem in molecular imprinting is that, even after the washing procedures, a small amount of template remains strongly bound to the polymer. This may not be a problem in preparative separations, but when the materials are used for sample preparation prior to analytical quantification, bleeding of this fraction will cause false results [26]. As a solution to this issue, some methods have been suggested, like parallel extraction on blank samples, post polymerization treatments [27], and dummy molecular imprinting. The latter, which creates MIPs using a structural analog of the target chemical as a template, is currently thought to be more efficient than previous approaches. Even though "dummy template leakage" happens during sample recovery, the method's accuracy is unaffected [28].

Some typical template molecules used in MIP fabrication process are amino acids, steroids, cells, viruses, pharmaceuticals, peptides, sugars and ions (Figure 1.6).

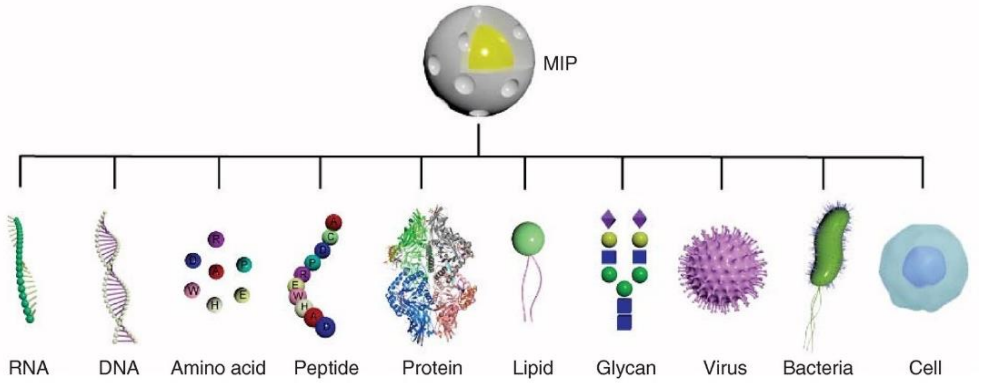

Figure 1.6 – Some typical templates used in MIPs' fabrication [29]

1.3.3 Functional monomer

The primary purpose of functional monomer is to bind its functional groups to those of the target molecule to form a suitable complementary pre-polymerization complex. Therefore, prior to polymerization, it is essential to choose the right functional monomer that interacts strongly with the template and produces selective donor-acceptor or antibody-antigen complexes [7].

The most used functional monomers, respectively in the covalent and non-covalent approach, are presented in Figure 1.7 and 1.8.

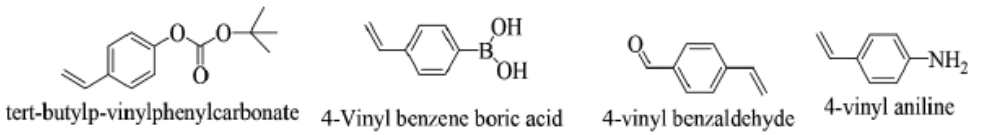

Figure 1.7 – Chemical structure of functional monomers commonly used in covalent imprinting [7]

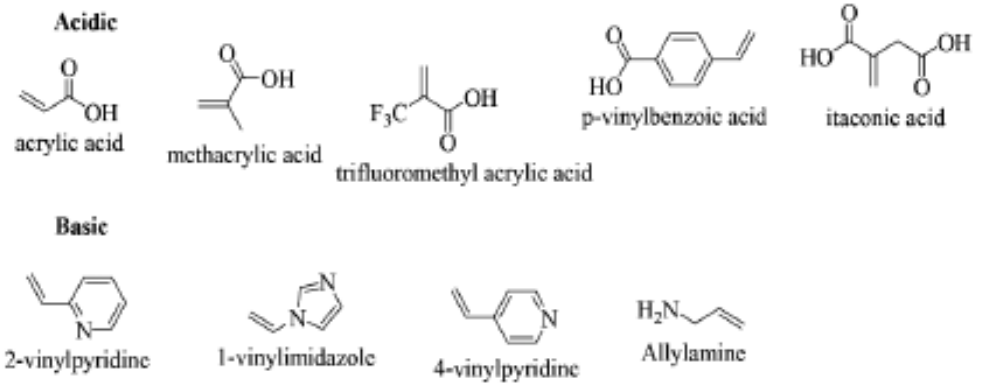

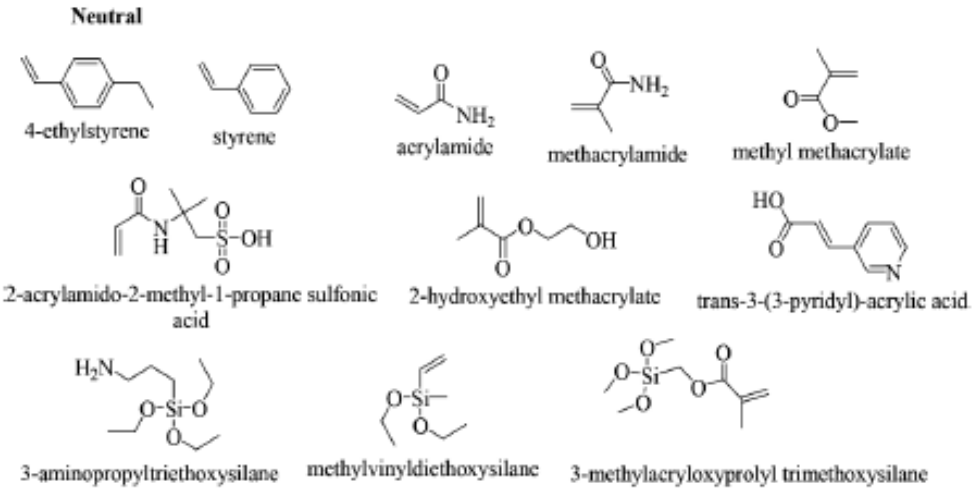

Figures 1.8 – Chemical structure of functional monomers commonly used in non-covalent imprinting [7]

1.3.4 Initiator

The most used technique for MIP synthesis is free radical polymerization (FRP); it is normally triggered by the photochemical, thermal, or electrochemical activation of a chemical initiator, depending on its nature. Typically, initiators are used in very small amounts compared to monomers, for example 1% in weight or 1% in moles compared with the total number of moles of polymerized double bonds. In Figure 1.9 some examples of initiators used in non-covalent approach are shown.

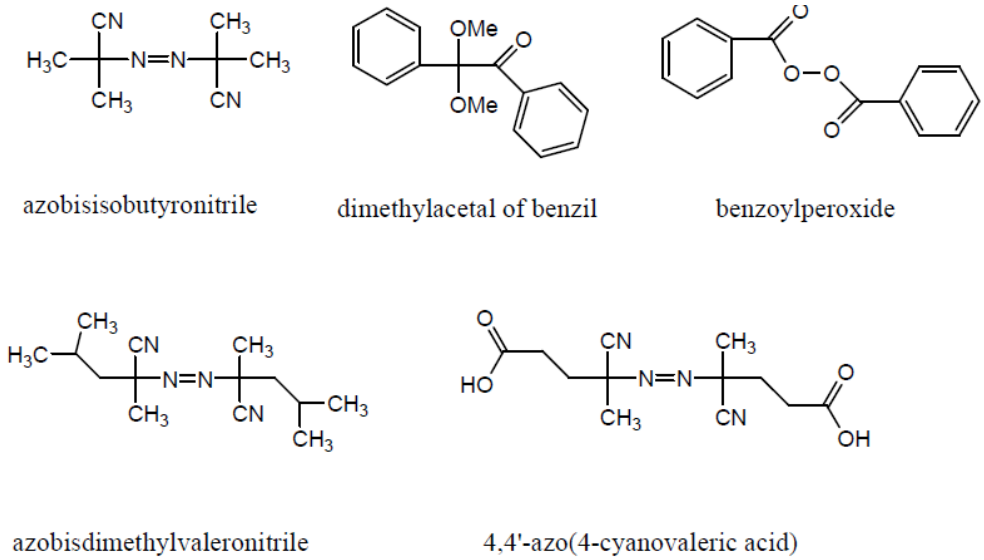

Figure 1.9 – Chemical structure of common initiators used in non-covalent imprinting [7]

In particular, there is a wide range of commercial photoinitiators that, according to their photochemical properties, are activated at different wavelengths, ranging from UV, through visible light to near infrared (NIR), as shown in Figure 1.10.

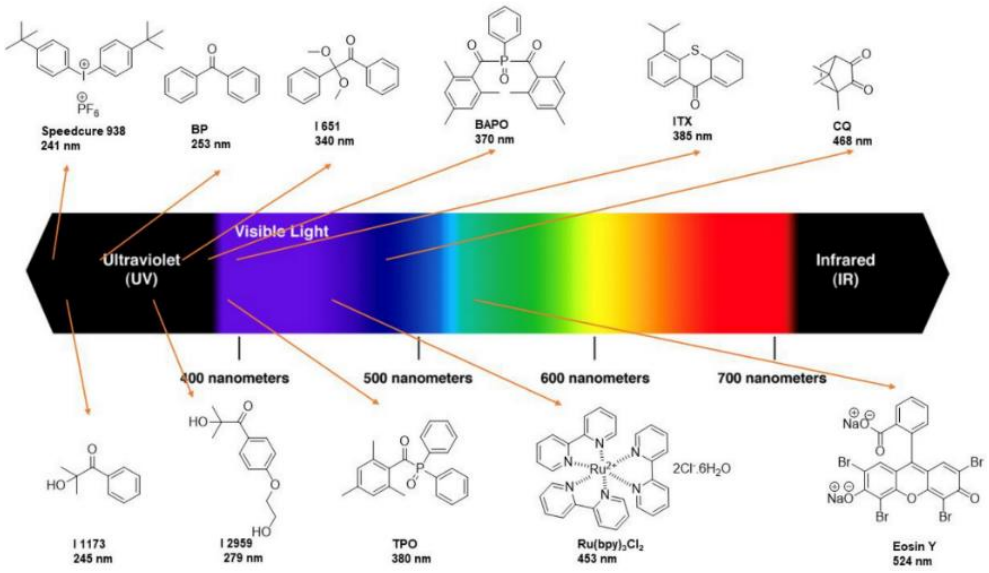

Figure 1.10 – Chemical structures and maximum absorption wavelength of some PIs used for 3D photopolymerization [30]

1.3.5 Solvent

The main role of the solvent is to act as dispersion media; thus template, monomer, initiator, and cross-linker should be soluble in it. On the other hand, other strategies can be used like employing partial solvents that can generate other phases. Consequently, solvent also determines the morphological characteristics of porosity and surface area of MIPs, and for this reason it's also called "porogen". Phase separation during polymerization between the porogen and the developing polymer is what causes porosity.

Low solubility phase porogens tend to separate early and generate materials with bigger holes and smaller surface areas; on the other hand, materials with smaller pore size distributions and more surface area are produced by porogens that phase separate later in the polymerization and have a higher solubility [31].

The effect that the solvent (and in particular its polarity) has on the complexation of functional monomers with the template before, during, and after polymerization is also crucial in the production of MIPs.

By applying Le Chatelier's principle, aprotic and less polar organic solvents, like chloroform, toluene, or benzene, will promote complex formation and facilitate polar non-covalent interactions, like hydrogen bonding and ionic salt bridge building; at the same time, they ensure optimum imprinting effectiveness. On the other hand, more polar solvents, particularly protic solvents, cause a high degree of disruption to hydrogen bonds and tend to dissociate the non-covalent contacts in the pre-polymer complex, due to the conflict for building interactions with both monomers and template [20,32].

So, generally, most MIPs are synthesized in organic solvents to preserve the hydrogen and electrostatic interactions between template and monomer. However, when organic solvents are used, MIPs show poor recognition ability for the target in aqueous environments because the presence of polar solvent can disturb the hydrogen bond formed between template and functional monomer [25], even though some of them can then be employed in aqueous solvents, though typically with a slightly altered selectivity [33,34].

And so, since many applications require MIPs capable of working in polar solvents, many studies are focused on finding useful approaches for the creation of MIPs that are compatible with water [25]. For example, one strategy was to adopt a two-step extraction method, but the procedures are complicated and time-consuming [35]; another one uses hydrophilic monomers, such as HEMA, b-CDs [36-39]. To further achieve recognition in aqueous media, hydrophilic modification of MIPs surface was proposed, which involved a two-step polymerization procedure [40,41].

Some interesting studies [41,42] show that the rebinding performance is optimized when carried out in the same solvent used for imprinting [41,42]. This effect may result from variations in the polymer structure's solvation in the microenvironment of the binding site. The shape and spacing characteristics that are built into the forming polymer may be influenced by the different solvation properties of different solvents. It's probable that the ideal rebinding settings demand the same or very similar solvation conditions as those employed for polymerization, to recreate and retain this shape and distance parameters [31].

1.4 Optimization of ingredients ratio

1.4.1 Crosslinker/Functional Monomer ratio (X/M)

To ensure the properties listed in paragraph 1.3.1, the amount of crosslinker is a crucial aspect. An insufficient amount of crosslinker, in fact, would result in unstable mechanical properties, due to the low degree of reticulation. On the other hand, an excess of crosslinker has pros and cons: it would allow to obtain macroporous materials, with high stability of recognition sites, but it would reduce the number of binding sites per mass unit of MIP [7,25]. The type of crosslinker employed, and its ratio with the functional monomer affect the MIP's selectivity and binding ability too.

The standards for choosing ingredients and their proportions differ depending on whether a covalent or non-covalent technique is used.

1.4.1.1 Covalent approach

In the study of Wulff et al., enantiomers of boronate ester template-bound functional monomers and three different crosslinkers with different ratios have been used: ethyleneglycol dimethacrylate (EGDMA), butanediol dimethacrylate (BDMA), and 1,4-divinylbenzene (DVB). They have demonstrated that, for covalent molecular imprinting, enantioselectivity and imprinting capability of MIPs are optimized by maximizing the amount of each cross-linking monomer in addition to the template functional monomer complex [43].

1.4.1.2 Non-Covalent approach

The optimization of X/M for non-covalent molecular imprinting has further complications due to the competing optimization of template/monomer ratio (T/M), which will be discussed in the next section.

Seminal studies by Sellergren [44] have investigated optimization of X/M in non-covalent imprinting systems while maintaining a fixed amount of template. In particular, they created MIPs using EGDMA as the crosslinker, methacrylic acid (MAA) as the functional monomer and L-phenylalanine-anilide as the template. They've also analyzed various EGDMA/MAA ratios.

As we can see in Figure 1.11, at first, as the mole % of MAA rises, the enantioselectivity for L-phe-an over D-phe-an increases. Above 20 mol% MAA, the slope starts to decline, and above 30 mol% MAA, enantioselectivity declines steeply. It has been assumed that imprinted polymers with more than 20–30 mol% MAA lose their selectivity for two reasons [44]:

a. An excessive amount of MAA (or any other functional monomer used) increases nonspecific binding, which lowers the overall average selectivity of the MIP.

b. Only a small quantity of crosslinker, such as EGDMA, is required to create a stiff enough polymer network to preserve the binding site's fidelity. The quantity of non-crosslinking functional monomer MAA that can be employed to create MIP binding sites is thus constrained [31].

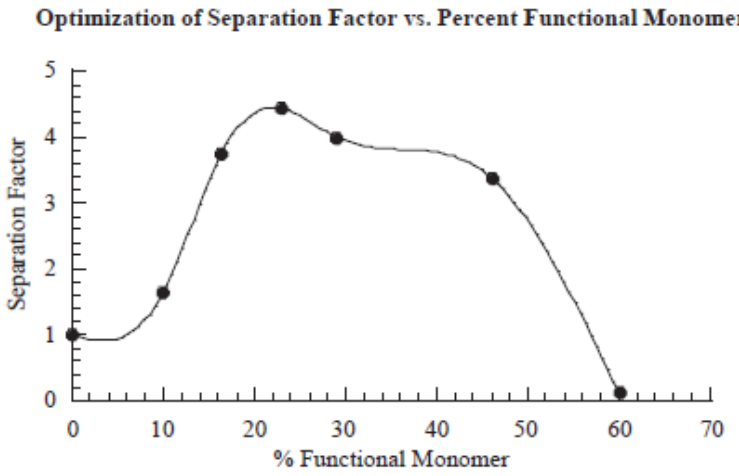

Figure 1.11 – Determination of percent functional monomer for optimum X/M ratio [31]

According to research by Wulff et al. [43] the degree of crosslinking has a significant impact on selectivity as well: when the degree of crosslinking is decreased from 100 to 50 mol%, the selectivity falls down gradually and abruptly decreases between 50 and 40 mol% crosslinking.

In conclusion, optimization of X/M in non-covalent MIPs must be empirically derived; nevertheless, most publications suggest that, depending on the functional monomer employed, an optimum crosslinker percentage can be established in the range of 50% to 80% [31].

1.4.2 Template/Functional Monomer ratio (T/M)

1.4.2.1 Covalent approach

The ratio between the template and the functional monomer depends directly on the availability of functional groups of the template, and/or on the structure of template molecule, that consequently determines how many functional monomers are required to create a covalent bond [7].

1.4.2.2 Non-Covalent approach

In non-covalent imprinting, once the X/M ratio has been determined, the template concentration can then be optimized with respect to the functional monomer [45]. The optimal template to functional monomer ratio must be determined empirically or computationally by comparing the binding properties of various polymers with increasing concentration of template molecules [46]. In particular, combinatorial synthesis accompanied with high throughput screening and molecular modeling can be used to speed up the optimization process and produce MIPs with the best recognition properties. The molecular modeling method screens a virtual library of monomers for a specific template using molecular modeling software, including the presence

of a solvent, if needed. Then, the appropriate MIPs are synthesized for experimental validation [47-49].

According to Le Chatelier's principle, the pre-polymer complex would increase if the constituent concentration or binding capability of the complex were to be increased in the pre-organized mixture. As a result, the imprinted polymer's binding cavities improve, increasing its selectivity for the target molecules [7].

The pre-polymer complex can be increased by increasing either the amount of functional monomer (M) or the amount of template (T), or both. Therefore, raising the monomer concentration causes the crosslinker concentration to drop in proportion, decreasing the X/M ratio. As was previously mentioned, there is a threshold amount of crosslinker that must be present in the MIP formulation before the X/M ratio becomes too low to maintain the fidelity of the binding site. According to MIP optimization experiments reported in the literature, this ratio (X/M) has a lower limit of roughly 1.0 and an optimal range of 4.0 [44].

On the other hand, raising the template concentration, while maintaining the (X/M) ratio at the ideal value of 4.0, can also result in a greater pre-polymer complex. This is an intriguing possibility since, in theory, the template can be increased to very high concentrations without affecting the composition of the final polymer. This is because the template is removed at the end of the imprinting process, and it is not covalently incorporated into the final polymer [31].

However, even if the amount of template is increased, when all the functional monomers have been complexed, any template in excess won't have any functional monomers to complex with, and eventually the number of binding sites will not increase. According to research by Andersson et al. [50], increasing the template amount did not improve MIP performance; rather, the peak performance was discovered at T/M ratios lower than 1.

Summarizing, the actual processes defining the final binding site structure are still unknown, being difficult to characterize it before and after polymerization. As a result, the T/M ratio still need to be empirically optimized, keeping in mind that lower T/M ratios induce fewer binding sites in polymers due to fewer template–monomer complexes, but over-high ones produce higher non-specific binding capacity, diminishing the binding selectivity [25].

As a general guideline, studies in the imprinting literature that empirically compared MIP performance to T/M ratio have frequently discovered that,

depending on the template used, T/M ratios in the range of 0.5-0.25 produce the best outcomes. [44,45].

Nevertheless, the optimization method becomes significantly more difficult when more than one functional monomer is utilized. Numerous studies report the successful employment of multiple functional monomers. In these cases, the components were optimized by varying the relative amounts of each functional monomer while maintaining a constant template concentration [51-53].

1.5 MIPs synthesis methods

As mentioned in previous sections, free-radical polymerization (FRP) is the most common method used for MIPs' fabrication. It's a method of polymerization by which a polymer forms by the successive addition of free-radical building blocks and proceeds in three steps: initiation, propagation, and termination.

FRP is the most used technique for many reasons: it is compatible with a wide range of monomers, the polymerization reaction is usually very rapid and may be initiated by several factors, polymers may be prepared successfully in a wide range of solvents at ambient temperature and pressure. Finally, the mechanism does not interfere severely with most imprint antigens [54].

However, FRP has a significant flaw: it is impossible to control the size, architecture, and number of the macromolecules that are formed. Moreover, the molecular weight of the polymer cannot be controlled or anticipated and so block copolymers and other polymers with complex architecture cannot be fabricated [20].

As time goes on, various techniques and innovative processes for MIPs preparation are subject to constant modifications. The schematic diagram of several MIP formats and synthesis methods is shown in Figure 1.12 and only the most used methods will be briefly explained.

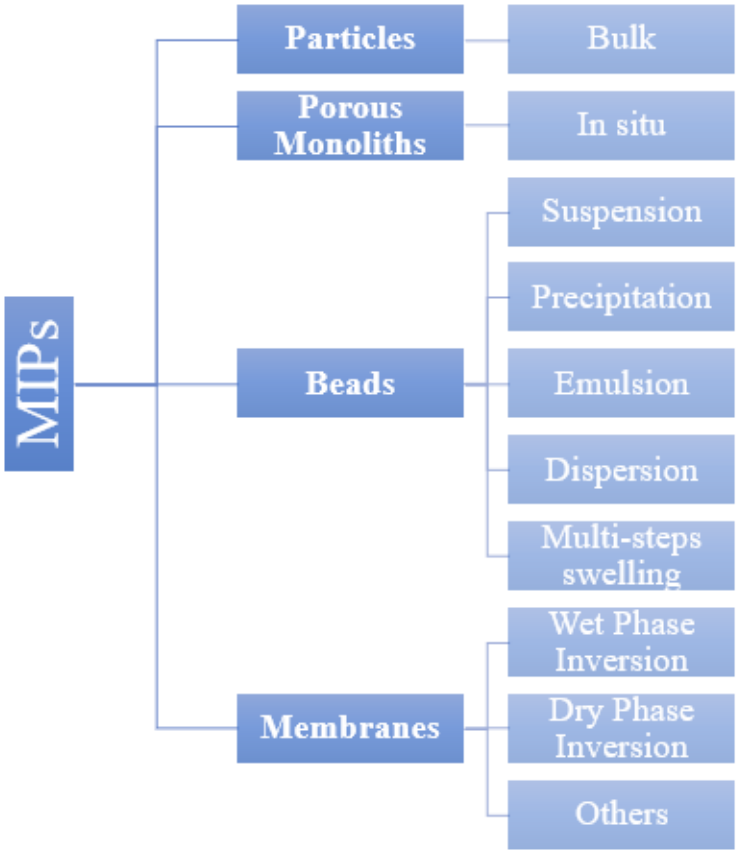

Figure 1.12 – Schematic representation of major formats and polymerization methods used for the preparation of MIPs. Adapted from [7]

1.5.1 MIP particles and bulk polymerization

MIPs particles are often prepared via bulk polymerization technique, which is the most extensively used free radical polymerization, due to its appealing qualities:

- Simplicity in preparation.
- No need for specialized or expensive instruments.
- Purity in the resulting MIPs.

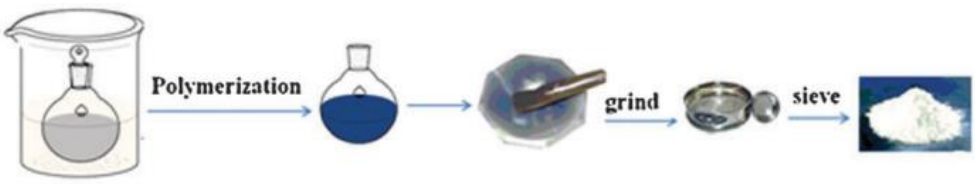

Figure 1.13 – Schematic diagrams of the molecular imprinting process for bulk polymerization [25]

The method consists in producing a monolithic polymer by bulk polymerization, which is then crushed, grounded, and sieved (Figure 1.13). This method is time consuming and has a low yield (only 30–40% of the total

polymer is recovered) [25]. Additionally, the grinding process produces particles that are irregular in size and shape as well as the destruction and conversion of some high-affinity binding sites into low affinity-sites, reducing the MIP loading capacity (Figure 1.4). Nonetheless, the binding site distribution is heterogeneous and it's difficult to remove the template from the core of the particles.

So, many appealing polymerization techniques have been employed to overcome these drawbacks of bulk polymerization: suspension polymerization, emulsion polymerization, seed polymerization, and precipitation polymerization. These methods lead to the formation of different types of MIPs, like beads, membranes, monoliths, and nanoparticles.

1.5.2 MIP monoliths

MIP monolith, also known as continuous polymer bed or continuous polymer rod, denotes a porous one-piece polymer. It is created by combining a template, functional monomer, crosslinker, solvent, and initiator inside a column, a glass rod, or a capillary tube, leading to a growing single structural piece of polymer with specific binding sites after template removal [55,56]. Monolithic MIPs have been demonstrated to have superior chiral recognition properties to those of conventionally made bulk polymers [56].

1.5.3 MIP beads and precipitation polymerization process

To overcome the drawbacks of the previous methods, like irregular shapes, new processes were developed to obtain regular and spherical beads, whose size range from a few hundred micrometers to nanometers [7]. The MIP beads have been created utilizing a variety of polymerization techniques, and the most used is precipitation polymerization process. Apart from a higher amount of porogen, this method enables the creation of imprinted beads using the same reaction mixture as the bulk method. Once the beads reach a sufficient dimension, they become insoluble in the reaction mixture and precipitate, and then they are recovered with washing and centrifuging procedures (Figure 1.14).

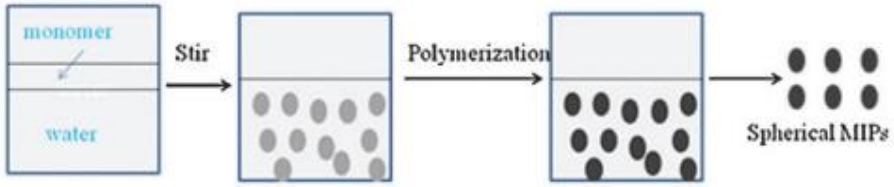

Figure 1.14 – Schematic diagrams of the molecular imprinting process for precipitation polymerization [25]

This process produces beads relatively monodisperse in size and shape; it takes less time than bulk polymerization [5]. Moreover, the binding sites are situated at or near the material's surface, which minimizes the diffusion distances of molecules and results in high performance of the MIPs [7].

1.5.4 Surface imprinted MIP

Another method, known as surface imprinting, has been developed especially for "large" imprint antigens, like proteins and cells. First, functional monomers in solution are allowed to form complexes with the imprint antigen, which are then bound to an activated surface, such as silica wafers or glass surfaces. Thus, a designed imprinted surface is obtained using this process. [54].

As mentioned before, in bulk polymerization, the strong cross-linking nature of MIPs makes it challenging to extract the original templates from the interior region of bulk materials. This could lead to partial template removal, limited binding capacity and delayed mass transfer, as it's shown in Figure 1.15.

Figure 1.15 – Partial template removal and rebinding in MIP fabricated with bulk polymerization (black triangles: templates in MIPs; red triangles: rebound templates in recognition sites) [25]

In surface imprinting, instead, the imprinted templates are located at the surface or close to the material's surface, and so their removal is easier, as shown in Figure 1.16 [57].

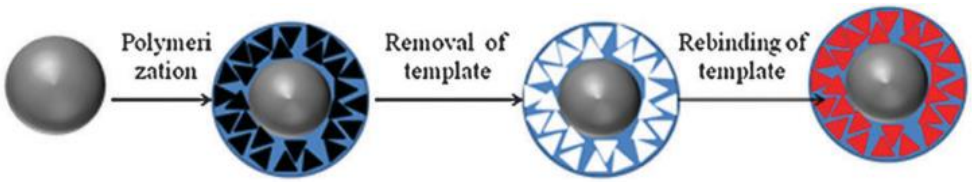

Figure 1.16 – Template removal and rebinding in MIP fabricated with surface imprinting (black triangles: templates in MIPs; red triangles: rebound templates in recognition sites) [25]

Moreover, surface imprinted polymers have a larger binding capacity than conventional MIPs, as well as quicker mass transfer and binding kinetics. [25]

1.5.5 Conclusion

To sum up, there are plenty of techniques to create MIPs, and only a few of them have been discussed in the preceding sections, each with their pros and cons.

However, none of these methods was used in this thesis work, which instead introduces a 3D printing technique, specifically Digital Light Processing (DLP), for the realization of MIPs. This is an innovative approach that, to the best of our knowledge, has not been explored, except by Rezanavaz et al. in 2022 [58], and it will be described in detail in the next chapters.

1.6 Template removal procedure

In the production of Molecularly Imprinted Polymers (MIPs), template removal is an essential step. This is a challenging procedure due to the polymer network's built-in properties and the imprinted cavities' affinity for the template. Efficiency will decrease if the MIPs still include template molecules because fewer cavities will be available for rebinding; additionally, mistakes will happen if template leakage takes place during analytical applications [59].

Unfortunately, even after numerous washing cycles, it is often difficult to completely remove the template; this is primarily because the solvent cannot reach highly cross-linked regions, or the template is not soluble enough in the solvent to disrupt the interactions with the imprinted cavity. Even in the case of MIPs created by a self-assembly or non-covalent method, the template's adherence to the imprinted cavity's components might be so intense that extraction under extreme circumstances is necessary, like extreme pH or temperature applied for a long time [60].

The consequences of too much extreme washing condition can be distortion or rupture of the cavities, producing MIPs with low selectivity and recovery [15]. Additionally, modifications in the MIP network's degree of swelling during extraction and subsequent desiccation can cause the cavities to collapse, sterically obstructing the entrance of the target molecule, or distorting the binding sites or the intensity of the interactions [61] (Figure 1.17).

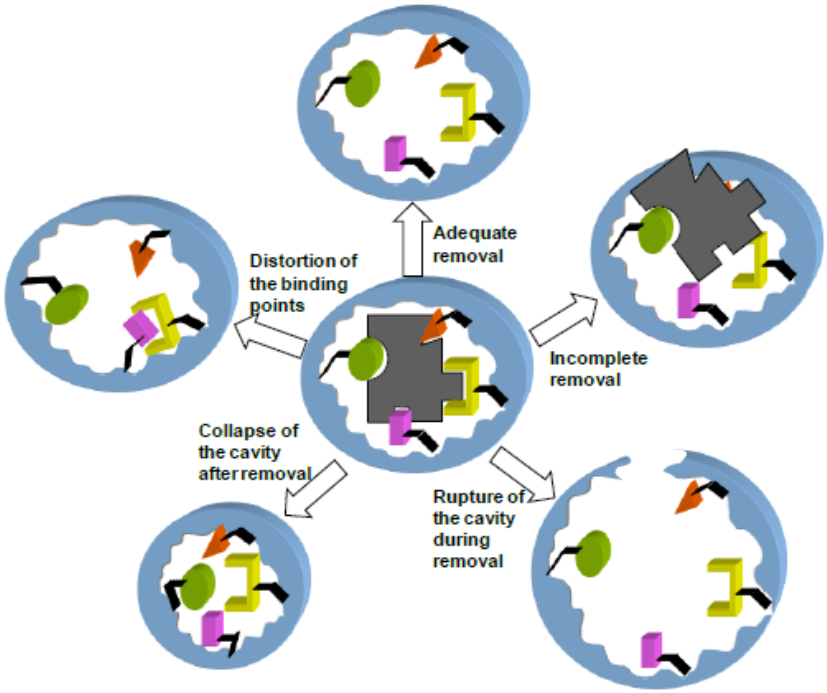

Figure 1.17 – Scheme of the changes induced in MIPs during the removal of the template [59]

The three basic methods for removing templates are: solvent extraction using ordinary solvents, solvent extraction with physical assistance, and fluid extraction using subcritical or supercritical fluids (Figure 1.18):

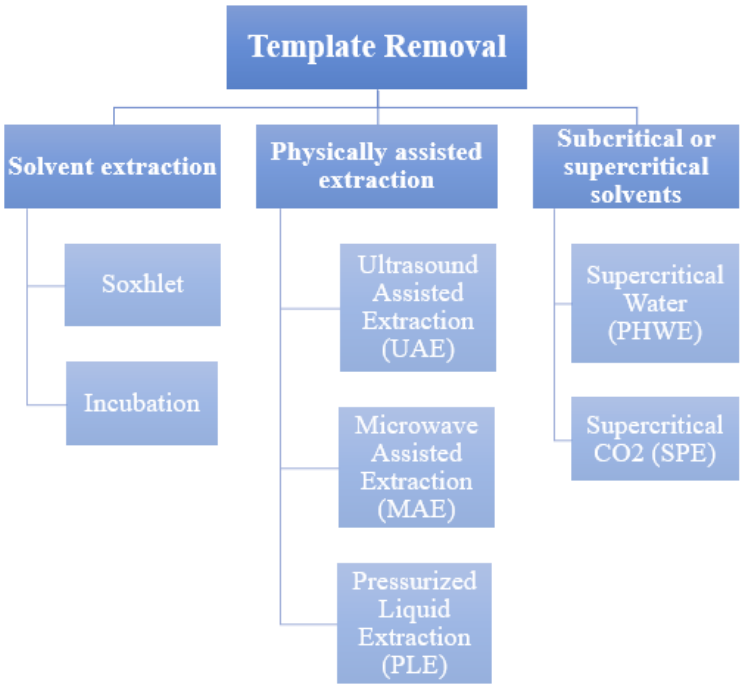

Figure 1.18 – The three main approaches available for template removal: extraction with common solvents, physically-assisted solvent extraction, and extraction with subcritical or supercritical fluids. Adapted from [59]

Since the nature and stability of both the template and the MIP should be taken into consideration, it is difficult to select the right extraction method, taking also into account that each of these methods has benefits and drawbacks. Nevertheless, the following general guidelines should be considered [51]:

- Ease of use.
- Speed of operation.
- Use of eco-friendly solvents.
- Use of a small volume of solvent.
- Cheap cost.
- Potential for industrial scale application.

1.6.1 Common solvent extraction

1.6.1.1 Conventional Soxhlet Extraction

Since its invention nearly 135 years ago, extraction with organic solvents using a Soxhlet apparatus has been a standard procedure, and it is frequently used as the benchmark to assess the effectiveness of other techniques. This method entails packing a porous cartridge inside the extractor chamber with finely crushed MIP particles. In a flask attached to the lower end of the extractor chamber, the extracting solvent—typically an organic solvent with acid or base additives—is poured; then it is heated and goes up. When the condensed vapor contacts the MIP particles inside the cartridge, it removes the template; the solvent containing the dissolved template descends through a siphon to the flask when a particular level of liquid is reached. It is possible to think of the procedure as a continuous extraction because the solvent is continuously cycled through the MIP particles.

Following is a list of the primary benefits of Soxhlet extraction [62]:

- The extraction is conducted with a hot solvent, which may encourage the solubilization of the template.
- The MIP particles are periodically rinsed with new quantities of the extracting solvent.
- After the extraction, there is no requirement for filtration to collect the MIP particles.
- The apparatus is very inexpensive, and the operator can be trained easily.
- It can be applied to practically any polymer matrix.

However, several drawbacks might also be mentioned [62]:

- Long extraction times (6-24 h) are required.
- Risk of temperature-induced degradation of labile templates.
- Large amounts of organic solvent (50-300 mL) used, which may suggest environmental concerns.
- MIP particles that are mostly static throughout the process slow down solvent flow and prolong the extraction process.
- Automation is challenging.

1.6.1.2 Incubation with solvents

The simplest technique for extracting the template is to submerge MIPs in solvents that can cause the network to enlarge while also favoring the template's breakdown. The approach is often used in mild environments, and the networks' chemical stability remains unchanged contrary to what may happen during Soxhlet extraction [59]. Although in general the removal still takes several hours, it can be sped up by using a large volume of medium (required to establish a high gradient concentration between the MIP and the solvent at the bulk), heating and agitating the solvent medium, or oscillating the entire system.

1.6.2 Physically assisted extraction

This approach aims to maximize the solvents' ability to extract while reducing solvent volume, operational expenses, and operational time.

1.6.2.1 Microwave-Assisted Extraction (MAE)

Microwave-assisted extraction (MAE) is a process that uses microwave energy to heat solvents in contact with a sample to partition analytes from the sample matrix into the solvent [63].

In comparison to conventional procedures, MAE typically uses 10 times fewer amounts of solvent (25–50 mL) and takes considerably less time (3–1 h). When compared to traditional extraction, these properties result in a beneficial decrease in the prices of the solvents, energy, and time.

High Microwave power may cause the template removal to happen quickly in the context of MIPs; however, in the case of labile MIPs, too high temperatures must be avoided [59].

1.6.2.2 Ultrasound-Assisted Extraction (UAE)

Ultrasound is a cyclic sound pressure with a frequency higher than 20 kHz, whose energy causes the so-called cavitation effect, which results in the mechanical erosion or rupture of solid particles as well as the production of tiny bubbles in liquid media. Solubility and diffusivity are favored by local increases in temperature, and penetration and transport are favored by increases in pressure [59].

A typical ultrasound-assisted extraction (UAE) process involves placing the polymer sample in contact with a predetermined volume of solvent, followed by the application of ultrasounds for 3–60 minutes. In most cases, the solvent is changed after many cycles.

1.6.2.3 Pressurized Liquid Extraction (PLE)

The PLE uses heated organic and aqueous solvents in the liquid phase at pressures high enough to prevent boiling. Due to a reduction in viscosity and surface tension, high temperatures (50–200 °C) and pressures (10–14 MPa) greatly facilitate the penetration of the solvent into the target matrix, necessitating less solvent (15 mL for a 10 g sample) and shorter extraction times (10–25 min) [59].

The sample is typically prepared for PLE by drying it previously and grinding it into particles smaller than 2 mm, then depositing it in a stainless-steel chamber, which is subsequently filled with the solvent. After 5 to 10 minutes of static extraction at a specified temperature and pressure, the solvent is then fed to a collector. After nitrogen gas is used to purge the chamber of all solvent, a fresh solvent can be added to begin a new extraction cycle.

The versatility of the solvents that can be used for the extraction makes this technique appropriate for the removal of almost any compound; additionally, the simultaneous or sequential extraction of a relevant number of samples can be easily automated. It is, however, considerably more expensive than MAE or the extraction using supercritical fluids (SFE) [59].

1.6.3 Supercritical or subcritical fluids extraction

1.6.3.1 Supercritical Fluid Extraction (SFE)

Supercritical fluids have characteristics that fall in between those of liquids (high solvation ability) and gases (high diffusivity), which is very helpful for solubilizing a wide range of compounds and for diffusion through solid networks; for these reasons they are very appealing for extraction.

A SFE extractor's primary parts are a high purity supercritical fluid source, a pump to provide the fluid at constant pressure and flow, a thermostated extraction chamber, a valve to allow for a controlled depressurization of the chamber, and a trap to catch the extracted materials.

To maximize the extraction from each material, a number of interconnected factors should be adjusted: the flow of the supercritical fluid, the pressure, the temperature, the extraction modes (static, dynamic or recirculation), the presence of a co-solvent, the extraction time, and the system to collect the extracted substances [59].

1.6.3.2 Subcritical Water Extraction (SWE)

High pressure (10-60 bar) and high temperature (100-374 °C) can help water, the cheapest solvent, to remove templates more effectively; superheated-water extraction (SWE), another name for subcritical water extraction, is based on the substantial loss of polarity that liquid water experiences when heated to a high temperature. The ability to solubilize a variety of polar, ionic, and non-polar molecules is a benefit of this method, as is the increase in diffusivity and mass transfer rate. In addition, the high pressure allows water to permeate otherwise inaccessible locations. The technique's principal drawback, instead, is that it is unsuitable for polymer matrices and labile templates [59].

Chapter 2: Additive Manufacturing

2.1 Advantages of 3D printing in MIP's production

The undefined architecture of MIPs is one of the main obstacles to their widespread practical use (47-49,43); this is a particular issue when dealing with metal ions, which have an angstrom-sized ionic radius and require an active cavity with precise dimensions [58].

The use of Additive Manufacturing (AM) techniques in the creation of MIPs offers the best method for creating a precisely defined and self-standing three-dimensional object that retains all properties required for target recognition [64,65]. Moreover, 3D printing can provide a highly ordered and complex 3D structure that is extremely adaptable to a filter structure and capable of managing huge volumes and turbulent flows, as opposed to filter packing with traditionally made MIPs.

Additionally, due to the lack of mold or other tools, these approaches enable the production of items with high resolution in a relatively quick and affordable manner; finally, further benefit of 3D printing is the ability to modify the mechanical, physical, and chemical properties of the finished product by carefully selecting the precursors and printing techniques.

For all these reasons, in this thesis work it has been chosen to realize MIPs using 3D printing techniques, in particular Digital Light Processing (DLP).

2.2 3D polymeric printing

AM, also called 3D printing or rapid prototyping, is a group of technologies that use layer-by-layer deposition of materials to create three-dimensional geometries [66].

Those techniques differ from computerized numerical-controlled machining (CNC), because the latter is a subtractive production technique, that starts with a full block of material and gradually removes it until the desired object is produced. Conversely, AM allows for a substantially smaller amount of material waste, as depicted in Figure 2.1.

Figure 2.1 – summary scheme of Computerized Numerical-Controlled machining (A); summary scheme of Additive Manufacturing (B).[67]

Generally, a 3D printing process is characterized by a series of steps (Figure 2.2):

1) **Creation of a 3D model** of the object, using computer-aided design (CAD) software; it's also possible to scan the object, for example with Magnetic Resonance Imaging, laser scanning or Computer Tomography [66].

2) **Creation of STL file**, that is the standard file type for AM machines; in particular, once a CAD model is created, it should be saved in STL (STereo Lithography interface format or acronym of "Standard Triangulation Language") format, through the CAD software. STL file translates the surface of the CAD model to a mesh of triangles, whose number and size control the precision of the printing [66].

3) **Slicing of the 3D model**, performed by the slicing software.

4) **Generation of G-code,** performed by the slicing software, that converts the STL file to G-code, i.e., in the series of commands that are sent to the printer with the printing instructions, such as how each individual layer must be printed, printing time, layer thickness, print orientation, temperature, etc.

5) Then, the actual process of **printing** begins.

6) **Post processing** of the final object, such as curing, sintering, and cleaning.

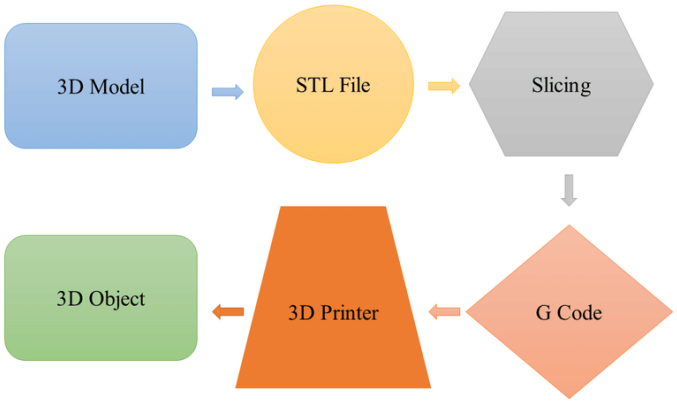

Figure 2.2 – Workflow of 3D Printing Process [68]

Compared to traditional production techniques, AM offers several advantages, such as:

- Digital design: it ensures that the created part precisely represents the designer's intention, thereby reducing the production inaccuracies.
- Increased complexity of object's geometry.
- Time-to-market: AM speeds up the product development process and therefore improves the time it takes to market the product [69].
- Personalization: every component can be designed with specific peculiarities. For instance, healthcare items can be fabricated specifically for each patient's needs, which are predicted to have a substantial positive impact on population welfare [70].
- Energy and raw material utilization are reduced, which makes a significant contribution to environmental sustainability [70].
- On-demand manufacturing, which offers the chance to reorganize the manufacturing supply chain to speed up the delivery of less expensive items to consumers while using fewer resources [70].

However, due to the following shortcomings, additive manufacturing (AM) technology still cannot totally replace traditional manufacturing, particularly in the field of mass production [70]:

- Size limitations: to create object layers, AM methods frequently use liquid polymers, or a powder made of plaster or resin; these materials prevent AM from producing large-scale items, whose construction process takes a very long period.
- Imperfections: a rough and ribbed surface finish is a common feature of parts made utilizing AM techniques; this effect is caused by plastic beads or huge powder particles that are layered on top of one another, giving the final product an unfinished appearance.

- Cost: AM equipment is seen as an expensive investment; without counting in the price of accessories, resins, or other operational materials, the cost of entry-level 3D printers ranges from a few hundred euros to hundreds of thousands of euros for higher-end models.
- Finally, especially in biomedical field, not all the 3D printable materials fulfill the established standards required for specific applications.

2.3 3D printing methods

3D printing techniques can be classified in three main groups [71]:

- Extrusion-based techniques: these methods are based on the transition of phase of thermoplastic filaments from a solid to a liquid state; the filaments move through a hot nozzle, which makes them melt and directs their deposition where it is required; then, the material quickly cools and solidifies. Fused Filament Fabrication (FFF) is the technique that is most frequently utilized, together with Direct Ink Writing (DIW).
- Powder-based techniques: these procedures require the deposition of a thin layer of powders that are then pressed and compacted; the powders are then melted at the desired locations using a binder or laser radiation. Selective Laser Sintering (SLS) is the most known method that fits within this category.
- Photopolymerization-based methods: in these methods, a photocurable resin (composed by photopolymers and photoinitiator), when subjected to suitable light irradiation, undergoes photopolymerization reaction, whit rapid solidification. These procedures don't require high temperatures, they are quick and simple [72]. This category includes Digital Light Processing (DLP) and other stereolithographic processes. This process will be explained in detail since it was used in this Thesis work.

2.3.1 Photopolymerization mechanisms

Photopolymerization is a chemical process that, using light as an energy source, can transform reactive molecules in the liquid state to a solid macromolecular part. [73] Photopolymerization can be activated at different wavelengths; however, this process is most frequently triggered by radiation in the UV-visible spectrum (250 - 450 nm). A photocurable mixture must contain a photoinitiator, a molecule that absorbs radiation and transforms it into chemical energy in the form of reactive intermediates, like free radicals or cations. Those then react with monomers, generating polymeric material. Consequently, an overlap between the used light source's emission and photoinitiator's absorption spectra is essential [74].

We refer to the photopolymerization process as either a radical, cationic, or anionic photopolymerization mechanism depending on whether the reactive species is a radical or an ion.

- Radical mechanism: initiation, propagation, and termination are the three basic phases that can be identified; light activates the photoinitiator during the initiation process, producing a reactive species called a radical, which interacts with monomers to form monomeric radicals; then these interact with more monomers to cause a chain reaction during the propagation phase. In the termination phase, the reaction stops, usually by combination: two growing chains meet, and the radicals inactivate. [73].
- Ionic mechanism: in this instance, the reactive species is an ion, which is often a cation; because cationic photopolymerization proceeds more slowly than radical photopolymerization and occasionally necessitates additional heat treatment to improve monomer conversion, it is less frequent than radical photopolymerization, especially in 3D printing [73].

2.3.2 VAT photopolymerization

VAT photopolymerization is another name for the photopolymerization-based printing technique, precisely because the starting liquid resin is placed inside a vat.

The light employed to enable 3D printing can come from two ways: from above in the case of the free surface approach, or from below through a transparent vat in the case of the constrained surface approach. Consequently, one the term top-down 3D printer is used for former, while bottom-up refers to the latter. Irradiation can be carried out either by projecting the complete pixelated picture onto the layer in Digital Light Processing (DLP-SLA) or by scanning each point of the desired cross-section with a laser in Laser-SLA (Figure 2.3) [75]. The object is printed using a platform as substrate, layer by layer.

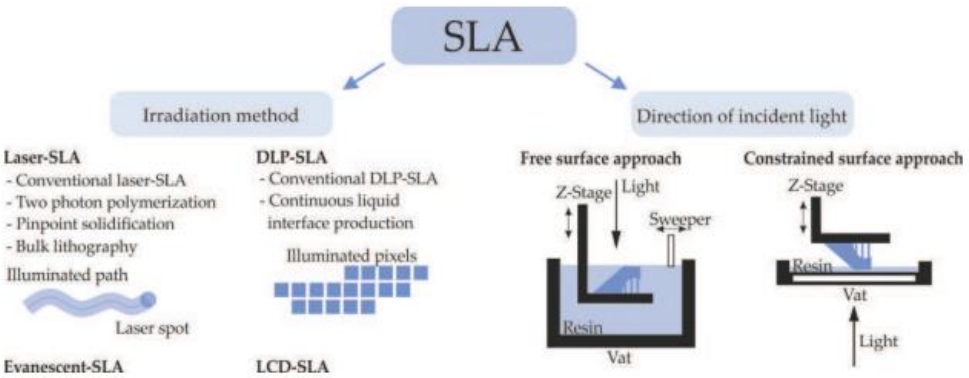

Figure 2.3 – Classification of SLA according to irradiation method (left) and direction of incident light (right) [75]

When compared to other 3D printing processes, photopolymerization has some advantages:

- Best resolution and smallest characteristic size (down to 25 μm) [71].
- Due to the capacity to change the chemistry of the starting resin, these procedures also provide the greatest flexibility in terms of the object's ultimate qualities [76].
- The resin does not need to have any specific surface tension, viscosity, or volatility characteristics, which must be carefully regulated for other techniques, such as FFF [71].
- No backing material is needed because the uncured material itself serves as a support [71].

Even though photopolymerization is now often utilized in several 3D printing procedures, it has drawbacks [76], including:

- The single polymerizable layer has a relatively low thickness since UV photons only penetrate at shallow depths. This increases the printing time, which might be problematic, especially for large objects.
- Products or reagents may deteriorate after being exposed to UV radiation for an extended period of time.
- The use of UV radiation during bio-printing, which involves putting cells into polymer resin, could result in cellular photodamage.
- Since the object is printed inside a solution in the bath, only one material at the time may be utilized [71].

2.3.2.1 Laser-SLA

Laser-SLA or often simply referred to as SLA (stereolithography), is a technique that uses a punctual laser as the light source; the building platform on which the printed part grows is situated in a tank of resin and coated with a liquid resin film (Figure 2.4). The initial layer is cured by illumination of the required cross section from above the resin bath (top-down configuration) or from below (bottom-up configuration); this x-y motion of the laser is implemented by two galvanometers in combination with a dedicated optical system. The developing portion of the platform (the z-stage) is lowered further into the tank after each layer, and a motorized sweeper coats new resin on top. This prepares the way for the next layer.

Once the final object is finished, a post-processing step is required. This step can be broken down into 4 parts [77]:

1. Removal of the object from the building platform.
2. Cleaning of the object, that entails the removal of non-polymerized resin from its surface using air jets or by submerging it in organic solvents like isopropanol or ethanol.
3. Post-curing process that uses external UV light; this step enhances the long-term structural stability of the printed structure, increasing the final cross-linking density, and the degree of polymerization [30].
4. Removal of any printing supports.

SLA can reach resolutions of 5–10 μm, depending on resin composition, scanning speed and diameter of the laser spot [75].

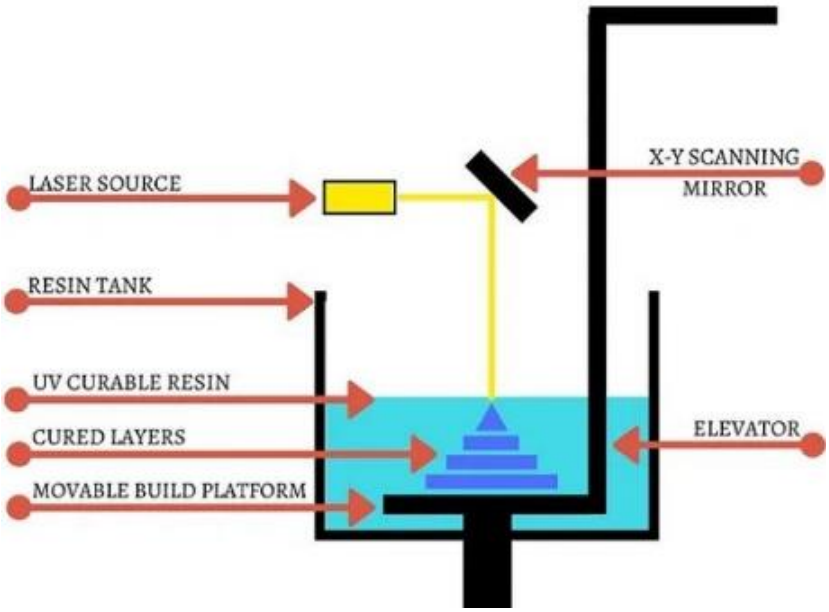

Figure 2.4 – Schematic diagram of Laser-SLA 3D printer configuration [78]

2.3.2.2 DLP-SLA

DLP-SLA or often simply referred to as DLP (Digital Light Processing), is a technique that allows the simultaneous illumination of an entire layer of resin, leading to solidification of an area instead of one spot at a time. To do this, a digital micro-mirror device (DMD) is placed in the laser's optical path [79]; it is composed by thousands of movable micro-mirrors arranged in an array, and each one may be switched between being "on" and "off" depending on whether it reflects light from the source or not. So, the DMD enables the projection of the full image of the layer at once and the object is then printed using repeated exposures, layer by layer [80]. In DLP printing there is a top-down configuration, if the light source comes from above, or bottom-up, if it comes from below. In Figure 2.5 is represented a schematic diagram of DLP-SLA printer configuration.

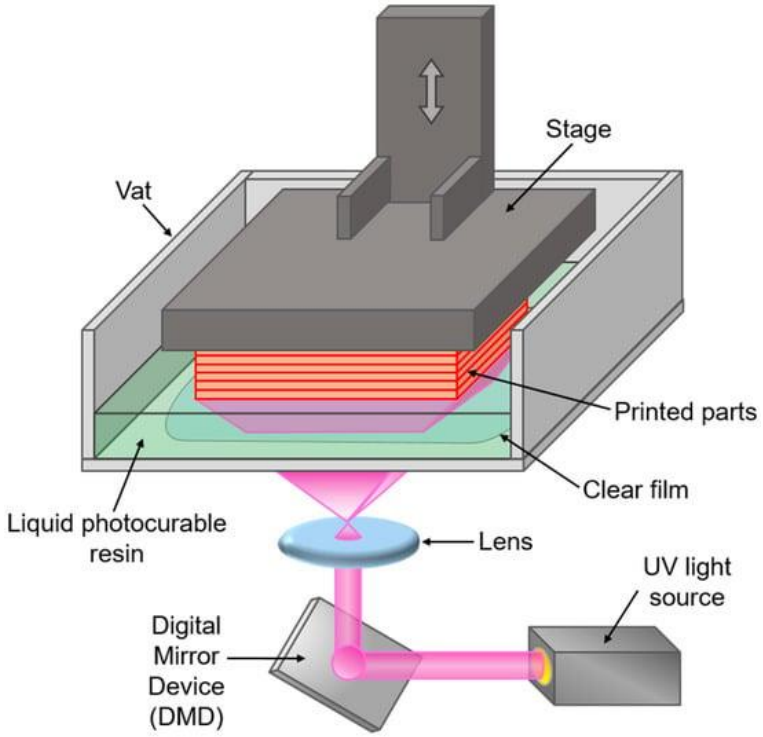

Figure 2.5 – Schematic diagram of DLP-SLA 3D printer configuration [81]

A DLP printer uses a light source with a typical wavelength of 365 or 405 nm [72] and can achieve a resolution of 25 µm [75].

Once the final object is finished, a post-processing step is required, which is the same as described in the previous section for SLA.

Comparing DLP to SLA, there are various benefits: first, illuminating a complete layer at once drastically cuts down on printing time; moreover, since the sample does not have to be completely submerged in the vat, less resin is used, which also results in a cost savings. DLP printers may also use light sources with a variety of wavelengths and are faster and more effective [79]. Smooth surfaces may be generated with accuracy down to 0.1-1 µm [75] thanks to the precision of platform movement along the z-axis.

However, the principal drawback of DLP is connected to the attraction forces that must be resisted in order for the newly solidified layer to attach to the earlier layers between the molded object and the vat floor. The application of hydrophobic coatings to the tank's bottom is one technique used to lessen the strength of these forces. Curved surfaces may become rough using this technique because the exposure mechanism is pixel-based. Therefore, using the proper optical technologies, the pixel size must be decreased if high resolution is necessary. The DMD's set number of mirrors causes image compression, which lowers the geometry's maximum size. [75]

In conclusion, DLP, the equipment used in this Thesis, has faster printing and lower costs despite SLA's superior resolutions. [79]

2.3.2.3 Two-photon polymerization (TPP)

TPP was initially proposed by Strickler et al. [82] as an AM technique. Since then, it has been thoroughly explored, and despite its expensive cost, TPP was even commercialized by Nanoscribe GmbH in 2007. Resolutions around 100 nm and surface roughness smaller than 10 nm are achievable [75].

In TPP, as opposed to conventional SLA, the excitation of the photoinitiator in the resin and subsequent activation of the curing reaction only takes place in the area of the laser's focal point, known as a volume pixel or voxel. Two photons can be simultaneously absorbed by molecules when a powerful femtosecond pulsed laser is used. In TPP, a titanium-sapphire laser with near-infrared (NIR) light at twice the wavelength (i.e., half the energy) replaces UV light. The energies of the two separate photons are nevertheless combined to produce the energy required for excitation [75].

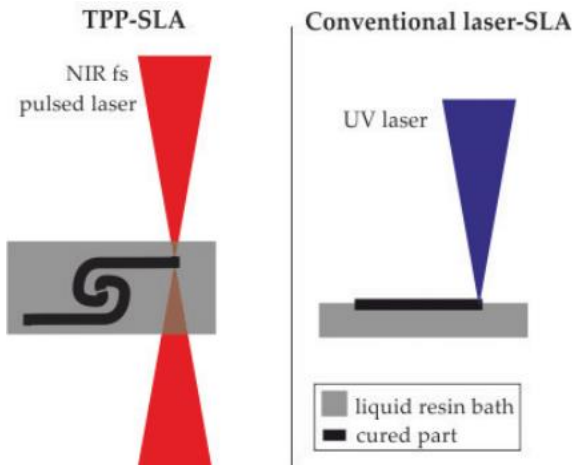

Figure 2.6 – Scheme of TPP vs. conventional laser-SLA 75]

The spatially limited 3D voxel in TPP, as shown in Figure 2.6, enables the curing of forms inside the resin bath rather than only on its surface. As a result, layer-wise production is no longer necessary, and highly complicated geometries with freely moving elements can be manufactured without the need for extra support structures [75].

However, the limitation to extremely small geometries in the mm range and the slow writing speed of the laser lines are two issues that still face TPP [67]. Also the cost of TPP printers is in the order of hundreds of thousands of euros.

2.3.3 Synthesis of DLP 3D printable formulation

A common photocurable formulation, that can be used for 3D printing, is composed of the following obligatory components:

- **Precursors**: they can be monomers, oligomers, or prepolymers that solidify after exposure to light. Their selection is primarily guided by

functionality (mono-, di-, or poly-), viscosity, reaction kinetics, hydrophobicity/hydrophilicity, shrinkage, costs, shelf life, volatility, toxicity, and the final mechanical and functional properties of the product [76]. It is important to understand that the reactive groups primarily determine the kinetics of a photocurable formulation, whereas the backbone mostly affects the physicochemical and mechanical properties (strength, brittleness, and hydrophilicity) of the polymer [30]. Some of the most common resins are composed by acrylates, that are preferred over other materials because of their quick reactivity in relation to their chain growth-polymerization mechanism and oxygen inhibition, which promotes strong adhesion between printing layers [76]. However, after curing, they frequently shrink, resulting in poor resolution, internal stress, or even damage to printed objects. Methacrylate monomers, instead, mitigate the shrinking issue with a slower rate of cure [30]. Some of the most common precursors used in 3D printing are polyethylene glycol diacrylate (PEGDA), triethylene glycol dimethacrylate (TEGDMA), bisphenol A-glycidyl methacrylate (Bis-GMA).

- **Photoinitiator**: to start the polymerization process, a photoinitiator (PI) converts the absorbed light into the reactive species. Depending on the starting reactive species they produce, PIs can either be radical or cationic. To have an effective initiation, the chosen PI's absorption wavelength must coincide with the emission of the 3D printer used [30]. The majority of radical PIs absorb light in the UV and visible range, making them suitable for all VP techniques, especially DLP.

Then, other elements can be inserted, to enhance the printability of the resin or provide specific properties [30]:

- **Dye**: is included in some of the formulations because it absorbs incident light, improving 3D printing control, resolution, and preventing uncontrolled polymerization. Typical dyes (such as those in the azobenzene and benzotriazole groups) are UV and visible light absorbers; they can be covalently bonded to the monomer/polymer chains or dispersed in the liquid formulation [30]. It is important to choose the right dye by considering both its absorption spectrum and the emission wavelength of the used 3D printer.

- **Fillers**: they are elements that can be added to the resin to get specific features like electrical or thermal conductivity, luminescence, rigidity, electromagnetic shielding, or antibacterial qualities. Additionally, fillers could reduce shrinking, resulting in improved accuracy. The most frequently employed fillers are carbon materials (e.g., graphene and nanotubes), ceramic and metal powders, glassy and fibrous materials

(e.g., as cellulose), minerals (e.g., as titanium), and bio-fillers (e.g., as coffee grounds and wood flour) [30].

- **Radical scavenger**: it is a chemical that is added to a polymer mixture to eliminate or deactivate contaminants and undesirable reaction products [30].

Chapter 3: Materials and Methods

3.1 Formulation's ingredient

All the materials used in this thesis work were purchased from Sigma-Aldrich (Merck Company, Milan, Italy).

3.1.1 Functional monomer

In this work methacrylic acid (MAA), an organic compound, has been chosen as functional monomer, since the carboxyl group functions as a hydrogen donor and a hydrogen acceptor at the same time [83]. Moreover, it interacts strongly with the chosen template, described in the next section.

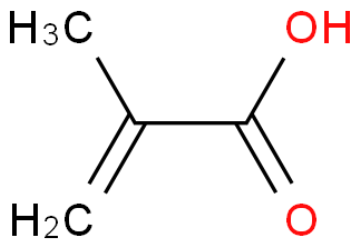

Figure 3.1 – Chemical structure of methacrylic acid [84]

3.1.2 Template

The chosen template is oxytetracycline (OTC), that belongs to tetracyclines, a group of broad-spectrum antibiotics; it is produced by strains of *Streptomyces rimosus* and was introduced in 1950 (Figure 3.2). Tetracycline antibiotics (TCs) are frequently used in veterinary medicine as a feed additive or in drinking water to increase growth, to prevent illness (for example pneumonia, endometritis and septicemia in cows), to extend the freshness of milk; in other words, they are used to ensure the best possible animal health for food production [85].

Once the drug is administered it is necessary to wait for a time called "Withdrawal Time" (WDT), i.e., a time of suspension, so that the concentrations of the drug and of any metabolites in animal tissues decrease below the tolerance value, or below the concentration of the medicine considered safe for human consumption [86].

However, it is possible that this WDT is not observed, and consequently antibiotic residues could remain in milk and edible animal tissues meant for human consumption; these residues may represent a major hazard to human health, causing allergies, harmful effects, bacterial resistance, gastrointestinal disorders, hypersensitivity, bone and dental problems in children [87].

As a result, the maximum residue limit (MRL) for tetracycline antibiotics in milk has been set at 0.1 mg kg^{-1} by the Chinese Ministry of Agriculture, the European Union (EU), and the US Food and Drug Administration (FDA) [87].

So, to ensure food safety within these bounds, sensitive and targeted technologies for detecting antibiotic residues in food must be developed and this is where molecular imprinting technology and MIPs developed in this thesis work come into play.

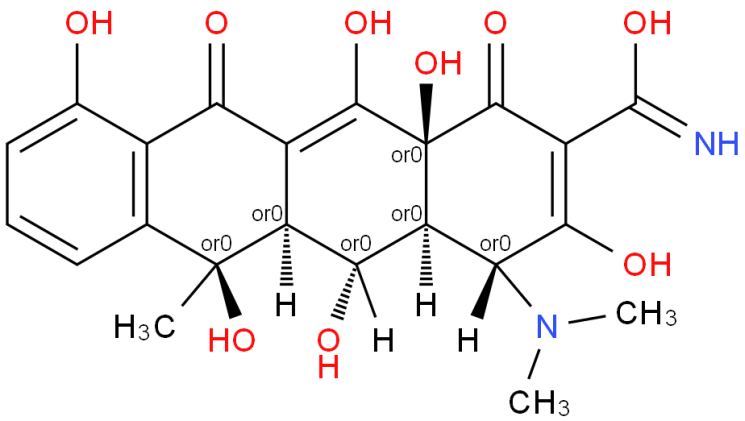

Figure 3.2 – Chemical structure of oxytetracycline [84]

3.1.3 Crosslinker

The crosslinker used is Dipropylene Glycol Diacrylate (DPGDA), a difunctional reactive diluent that polymerizes when exposed to sources of free radicals. DPGDA is particularly useful in coatings and inks where improved flexibility and adhesion are desired in combination with good moisture resistance [88].

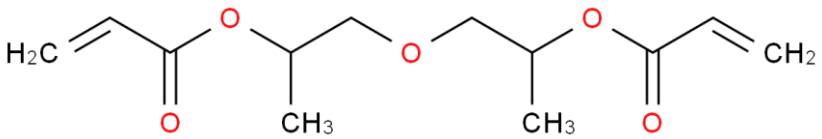

Figure 3.3 – Chemical structure of Dipropylene Glycol Diacrylate [84]

3.1.4 Solvent

The chosen solvent is Dimethyl Sulfoxide (DMSO), a polar aprotic solvent, because it will promote monomer-template complex formation and facilitate polar non-covalent interactions.

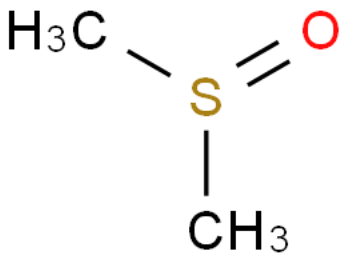

Figure 3.4 – Chemical structure of Dimethyl Sulfoxide [84]

3.1.5 Photoinitiator

As photoinitiator phenylbis (2,4,6-trimethylbenzoyl) phosphine oxide (BAPO) has been chosen, since it adequately absorbs the emission wavelength of the 3D printer used (385 nm).

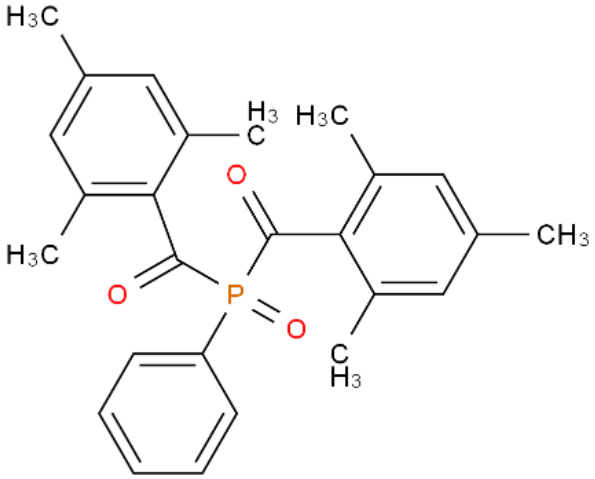

Figure 3.5 – Chemical structure of phenylbis (2,4,6-trimethylbenzoyl) phosphine oxide [84]

3.1.6 Dye

The selected dye is (N-ethyl-N-(2-hydroxyethyl)-4-(4-nitrophenylazo) aniline), also known as Disperse Red 1 (DR1).

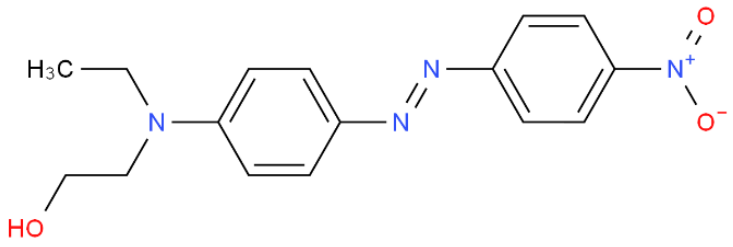

Figure 3.6 – Chemical structure of (N-ethyl-N-(2-hydroxyethyl)-4-(4-nitrophenylazo) aniline) [84]

3.2 DLP 3D printer

The Asiga MAX UVX27 printer, made by the company Asiga, was utilized for the printing stage (Figure 3.7). The LED light source used in this DLP printer emits light with a wavelength of 385 nm; on the x-y plane, pixels have a resolution of 27 µm, while along the z plane, it is between 1 and 500 µm. The construction platform has a surface area of 51.8 x 29.2 mm^2, and the tallest object that may be printed is 75 mm high.

Figure 3.7 – Asiga MAX UVX27 printer [89]

Because of the bottom-up printer setup, the platform moves vertically from bottom to top, and the sample is printed backwards; an internal set up of Asiga MAX UVX27 printer is represented in Figure 3.8. Layer thickness, light intensity, and time to irradiate are the three main factors that can be changed compared to the default values set by the Asiga Composer software.

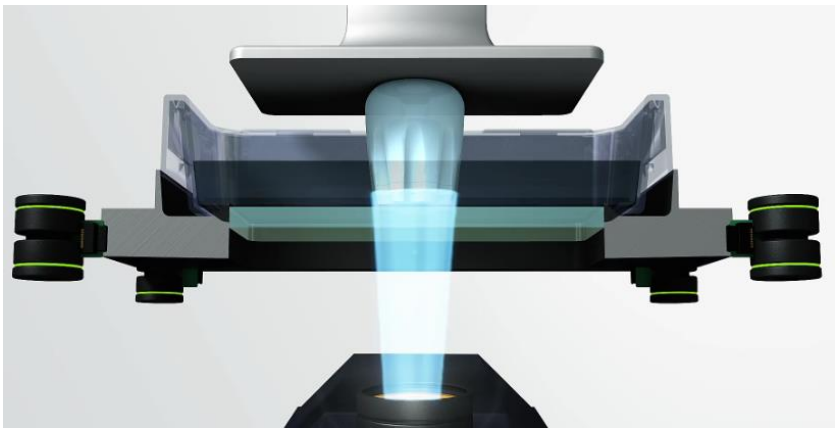

Figure 3.8 – Internal set up of Asiga MAX UVX27 printer [89]

The printing process can be split into the following phases:

1) **Optimization of printing parameters**: in this preliminary phase, it's important to select the right parameters to ensure the success of the printing procedure.
2) **Approach phase**: the platform is first brought closer to the vat, where the resin is already present, up to a distance equal to the layer thickness indicated at the print parameter selection stage.
3) **Irradiation phase**: after the first phase is finished, the LED lights up to irradiate the resin for the chosen irradiation time.
4) **Detachment phase**: the platform is pulled out from the vat to allow the formation of a continuous layer of liquid resin, and the process then repeats with a new approach phase.

In addition to the parameters mentioned above, it may be necessary to adjust other parameters, such as the speed of the platform's movement during the approach or detachment phase or the length of waiting intervals between phases of the single layer printing process; this last parameter may need to be raised to prevent bubble formation, which may cause internal flaws in the printed samples. Moreover, it's possible to change the temperature of the printing environment up to 50°C.

The early layers, namely *burn in* layers, are typically printed with longer irradiation time or intensities than of the following layers, to aid the adhesion of the material to the platform.

After printing, a blade is used to peel the printed object from the printing platform; to get rid of any remaining resin, it is sonicated for 10-30 seconds in an ethanol-filled beaker. The object is then post-cured in a broad-band UV chamber from Asiga (light intensity 10 mW/cm^2) for 1-3 minutes. This post-curing process has been made for all the items printed for this thesis work.

3.3 Formulation's preparation

Three photocurable formulations were prepared with different weight ratios between template (OTC) and functional monomer (MAA), while the weight of crosslinker (DPGDA) doesn't change:

1) OTC:MAA:DPGDA = 1:4:20
2) OTC:MAA:DPGDA = 1:5:20
3) OTC:MAA:DPGDA = 1:6:20

In each formulation was then added 0.8 phr (per hundred resins) of BAPO and 15 phr of DMSO.

In the first step, a batch of BAPO, DMSO, and DPGDA—collectively referred to as "base"—must be prepared; in particular, BAPO and DMSO are mixed first and sonicated until the BAPO is dissolved; then DPGDA is added, and the mixture is sonicated again.

In the second step, following the non-covalent approach, the pre-polymerization complex is prepared by magnetic stirring OTC and MAA, until OTC is dissolved, with speeds of about 200 rpm.

Finally, the two preparations are mixed together and sonicate again, to make a homogeneous final resin, ready for printing.

It's important to prepare the resin in a black falcon to avoid polymerization due to visible light.

In this thesis work these 3 formulations were used to print both MIPs and NIPs (Non-Imprinted Polymers) dots; these latter are used as sample control, and they are made like MIPs but without the template. One of the aims is to understand which of the 3 formulations provides the best results; moreover, the formulation with the ratio OTC:MAA = 1:4 was used to print different MIPs geometries, like two different filters and to test different molarity of the rebinding solution (50, 100 and 150 μm).

3.3.1 Creation of porosity with salt-leaching technique

Porosity is an important feature required in a wide variety of materials for numerous applications, such as lightweight constructions, biomedical scaffolds, and catalytic supports [90]. The advantages of pores' creation are light weight, high surface area, and variable density.

The most widespread technique is *salt leaching*, that makes it simple to create porous materials using a wide range of chemistries. This method is based on the use of salt particles as templates, which are then filled with the target material and then dissolved from the solid scaffold material to provide porosity [91]. The following benefits contribute to the selection of sodium chloride (NaCl) in this thesis: it is a plentiful, inexpensive and harmless substance that quickly dissolves in water without the requirement for chemical solvents. In addition to environmental concerns, NaCl can be applied to a wide variety of scaffold materials, it is biocompatible, and has great thermal and chemical stability [90,91].

However, this templating method has so far been limited to the fabrication of structures with random porosity and relatively simple macroscopic shapes. Fortunately, new developments in additive manufacturing (AM) have increased design freedom in the production of porous materials, allowing for

the creation of complex grid-like structures with tightly regulated porosity and pore sizes at the macroscale [90].

So, it's possible to combine the ease of salt leaching with the complex shaping possibilities given by additive manufacturing (AM) [90] and this is exactly what was done in this thesis, with the purpose of increasing the surface area of samples and understand if, in this way, the performances of MIPs improve.

Three formulations have been prepared, with ratio OTC:MAA=1:5 and different salt percentages:

4) OTC:MAA:DPGDA = 1:5:20 and 60 phr of salt
5) OTC:MAA:DPGDA = 1:5:20 and 40 phr of salt
6) OTC:MAA:DPGDA = 1:5:20 and 20 phr of salt

It was used common edible salt, manually grinded with the use of a mortar and then added to other ingredients, i.e., 0.8 phr of BAPO and 15 phr of DMSO. The steps for the preparation of these resins are the same as that explained in the previous section.

All three formulations were used to test the printability of simple dots; the third one was used to print a more complex geometry too, that will be described in Chapter four.

3.4 Choice of the extraction method

The information about the extraction methods provided in section 1.6 makes it quite evident that choosing an efficient removal method is a difficult process, largely due to the MIP's tailored nature.

The method chosen for the experiments conducted during the thesis is the Ultrasound-Assisted Extraction, along with the use of a rocking platform; in particular, an ultrasound bath has been used. The composition of the washing solution and other details will be discussed in Chapter four.

3.5 Batch rebinding method

Once MIPs have been fabricated, one of the finest techniques for evaluating their binding sites and so to analyze their ability to capture the target molecule, is *batch rebinding*. This technique consists of incubating MIPs within a solution that contains the template used for the imprinting process.

The quantity of template still present in solution after adsorption to the polymer is measured and referred to as Cf (the concentration of free substrate) after a predetermined amount of MIP has been added to a solution of substrate (S). Next, Cf is subtracted from the total amount of substrate added (Ct) to

determine the amount of substrate bound (Sb) to the MIP. Given that the polymer is a solid, the amount of bound substrate per gram of polymer is calculated by dividing the amount of bound substrate by the weight of the polymer [31].

Another parameter used to check the performance of MIPs is the *partition coefficient* K_p, which is the ratio between the substrate bound to the MIP and the substrate still present in solution [31]:

$$K_p = \frac{S_b}{C_f}$$

In this thesis, to evaluate the selectivity and the binding ability of 3D printed MIPs, batch rebinding and partition coefficient have been used. In particular, the composition of the rebinding solution and the complete procedure will be explained in more detail in the next chapter, in section 4.1.6.

3.6 Characterization methods

In this section will be analyzed the characterization methods used during the experiments.

3.6.1 UV/visible spectroscopy

The creation, measurement, and interpretation of spectra that result from the interaction of electromagnetic radiation with matter are all aspects of spectroscopy. There are numerous distinct spectroscopic techniques available to solve a variety of analytical issues; the techniques vary depending on the species to be studied (for example, molecular or atomic spectroscopy), the radiation-matter interaction to be observed (for example, absorption, emission, or diffraction), and the area of the electromagnetic spectrum being studied. The most frequently used techniques are based on the absorption or emission of radiation in the ultraviolet (UV), visible (Vis), infrared (IR), and radio (Nuclear Magnetic Resonance, NMR) frequency ranges [92].

Indeed, in this thesis the UV/visible spectroscopy has been used; it is based on the principle that when light radiation passes through a substance, this selectively absorbs certain light wavelengths. So, a light source generates radiation that spans a large variety of UV-visible wavelengths (200 nm – 780 nm); then, a detector measures the amount of light absorbed by the sample to be tested, in relation to its wavelength, by picking up the light that passes through it (Figure 3.11).

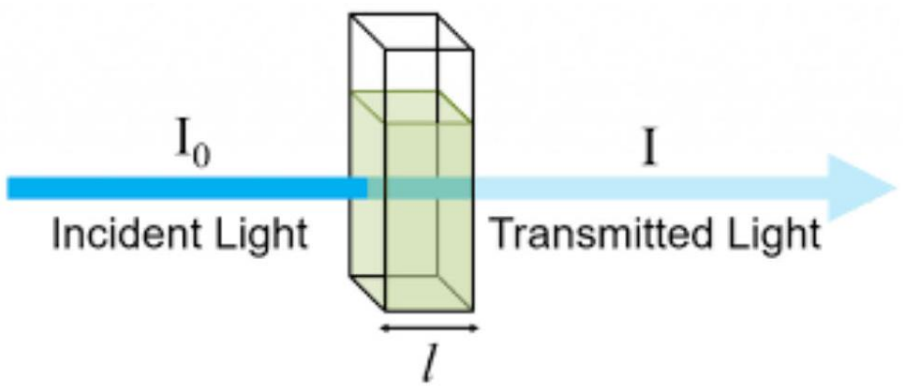

Figure 3.11 – Schematic representation of Lambert-Beer Law [93]

The mathematical-physical foundation for light-absorption measurements on gases and solutions in the UV, visible, and infrared regions is the Bouguer-Lambert-Beer law [94]:

$$A = \log(I_0 \cdot I) = \varepsilon \cdot l \cdot c$$

which then gives:

$$\varepsilon = \frac{A}{c \cdot l}$$

where:

- A is the absorbance.
- I_0 is the intensity of the monochromatic incident light (so before passing through the sample).
- I is the intensity of the monochromatic transmitted light (so after passing through the sample).
- ε is the molar extinction coefficient of the substance that causes the absorption of radiation.
- c is the concentration of the light-absorbing substance.
- l is the optical path length of the sample.

By plotting the absorbance versus the wavelength (or the wavenumber) the absorbance spectrum will be obtained.

The Lambert-Beer law is only strictly valid when some fundamental conditions are fulfilled [95]:

- Strictly monochromatic measuring light.
- Homogeneous distribution of the molecules in the sample.
- Passage of the complete measuring beam through the sample.

- Absence of light scattering and of photochemical reactions in samples.
- No secondary emission of the absorbed light by fluorescence.
- An ideal detection and processing of the intensity values I_0 and I.

Focusing on the last point, we consider the insufficiency of the detection and signal processing unit for absorbance measurements: the two signals, I_0 and I, that differ by a factor of 10 in amplitude, must be processed during detection and signal conversion in order to measure an absorbance of 1; in particular, they need to be amplified and digitalized with enough accuracy to calculate I_0/I. The resolution of an analog signal depends on how it is digitalized, so, for example, a signal of 1 V that is digitized at a resolution of 10 bits is divided into $2^{10} = 1024$ discrete steps that are each approximately 1 mV. Instead, if the absorbance is higher than 1, it will be needed analog-to-digital converter with considerably higher resolution; they are technically feasible, but their price increases and their speed decreases [95].

Moreover, we go closer to a division by zero the higher the absorbance and the smaller I is in comparison to I_0, and large changes in the outcome will result from small absolute variations in the measurement of I. So, this is another reason to keep absorbance low [95].

The UV/Visible spectroscopy has been used in this thesis for analyzing the OTC rebinding solutions during the experiments, to check the performances of the 3D-printed MIPs. In particular, the BioTek™ Synergy™ HTX Multi-Mode Microplate Reader (Figure 3.12) was used, performing absorption tests between 250 nm and 450 nm with 1 nm intervals.

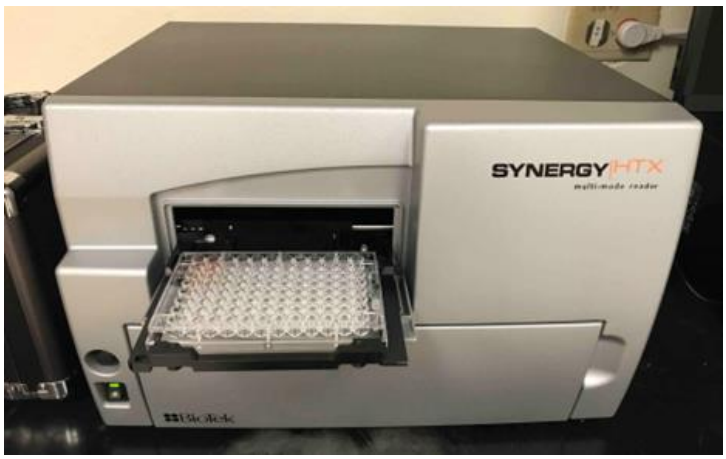

Figure 3.12 – BioTekTM SynergyTM HTX Multi-Mode Microplate Reader

3.6.1.1 Calibration curve

A fundamental step that must be taken for the analysis of the experiments is the creation of a calibration curve, which is used to understand the instrumental response to an analyte and to predict the concentration in an unknown sample.

So, if the molar extinction coefficient (ε) for the substance in question is not already known, a calibration curve between absorbance and concentration must be made. First step consists in preparing a series of formulations with known concentrations of the substance dissolved in a solvent (water, alcohol or organic solvents), then make the "base line" (the instrument is calibrated to zero absorption) with the cuvette full of the solvent alone and finally read the absorbance of the various concentrations known by putting the respective cuvette in the instrument one after the other.

Many spectroscopic photometers can measure one absorption read at a particular wavelength and are configurable to one wavelength at a time. Additionally, there are series diode spectroscopes that can quickly read all sample absorptions across a spectrum of wavelengths (often UV/visible). The outcome of this second sort of instrument is the 'absorption spectrum', which represents the absorbance vs. the wavelength; a molecule can then absorb at various spectral points, producing absorption curves with peaks and areas of no absorption. This second type of instrument is used in this thesis.

Once the absorption spectrum has been obtained, it is the turn of the calibration curve: a single wavelength is chosen (typically where there is the absorbance peak) and the absorbance at that chosen wavelength vs. the concentrations of the solutions is represented; then a linear regression is performed and the best-fit line is determined: the output should be an equation in the form $y = m\,x + b$; it's also possible to calculate R^2-value and if it is near 1 it means that a good fit has been obtained.

At this point, once the calibration curve is ready, it can be used to determine the unknown concentration of the sample under analysis: it will be sufficient to prepare a dilution in the same solvent, determine the value of absorbance and, thanks to the curve created with the known standards, calculate the corresponding concentration value [96].

3.6.2 3D scanner

For evaluating the printing fidelity of some of the sample, a 3D scanner was utilized to compare the printed geometry to the one created using CAD software. The 3Shape E4 scanner, manufactured by 3Shape A/S in Copenhagen, Denmark, has been used (Figure 3.13); it has four 5 MP cameras

with a measurement accuracy of 4 µm, and Convince software from 3Shape was used to analyze scan data. The sample is put on the scanner platform after being lightly dusted with magnesium stearate, to limit the reflection of light [97]. The scanner then generates a digital model of the tested object.

Figure 3.13 – 3Shape E4 scanner [98]

This digital model is than compared with the initial CAD model. The final output is a colorimetric map in which discrepancy between the two files are reported.

3.6.3 Scanning Electron Microscope (SEM)

One of the most adaptable tools for examining and analyzing the microstructure morphology and chemical composition of materials is the Scanning Electron Microscope (SEM). At the ideal viewing distance of 25 cm, the unaided eye can distinguish objects extending to around 1/60° of a visual angle, with a resolution of ~0.1 mm; instead, the maximum resolution achievable with SEM is ~2000 $\mathring{A}$, due to the optical lens's ability to magnify the field of view [99].

Figure 3.14 shows a column structure of a conventional SEM, with its major components.

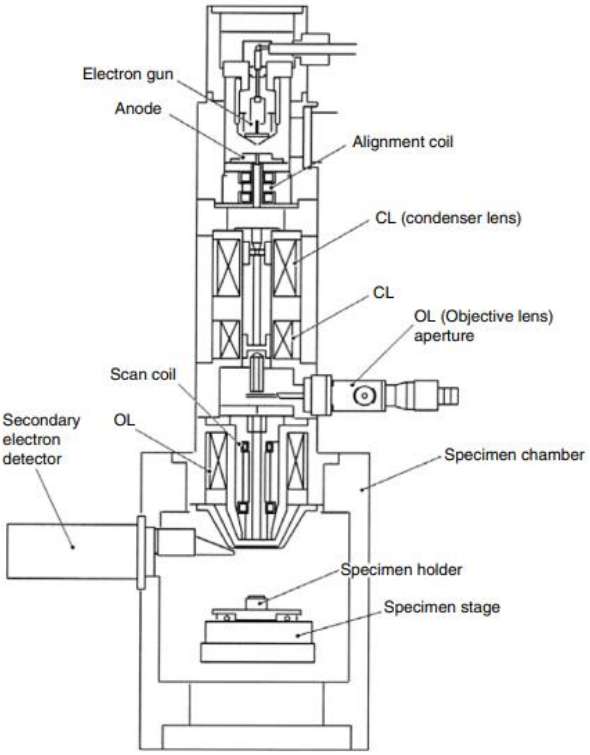

Figure 3.14 – Schematic diagram of a scanning electron microscope [99]

The electrons are created and accelerated to an energy level of 0.1 to 30 keV by the electron gun, which is located at the top of the column. To take a high-resolution picture, the electron beam produced by the hairpin tungsten gun must be smaller than its diameter. So, to concentrate and define the electron beam and create a narrow-focused electron spot on the specimen, electromagnetic lenses and apertures are utilized. To prevent air from scattering electrons throughout their path, a high vacuum environment is required too. Real-time observation and picture capturing of the specimen surface are made possible by the specimen stage, electron beam scanning coils, signal detection, and processing equipment [99].

SEM uses a focused beam of high-energy electrons, which interacts with the sample to analyze; in particular, when the primary beam hits the sample surface, ionizing the specimen's atoms, secondary electrons - also known as loosely bound electrons- may be released (Figure 3.15). These electrons are collected by a detector and are used to form a 2-dimensional image, that reveals information about the sample external morphology (texture), chemical composition, crystalline structure and orientation of its materials [100].

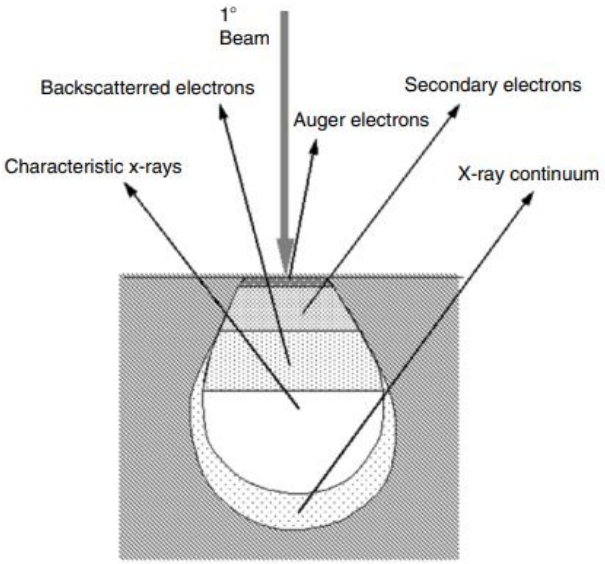

Figure 3.15 – Illustration of several signals generated by the electron beam–specimen interaction in the Scanning Electron Microscope [99]

In this thesis, the Field Emission Scanning Electron Microscopy (FESEM, Zeiss Supra 40) was used to analyze the surface morphology and the internal structure of printed samples, at magnifications of 10x to 300x (Figure 3.16). Compared to the SEM, the Field Emission SEM produces clearer, less electrostatically distorted images with spatial resolution down to 1 1/2 nanometers – three to six times better [101].

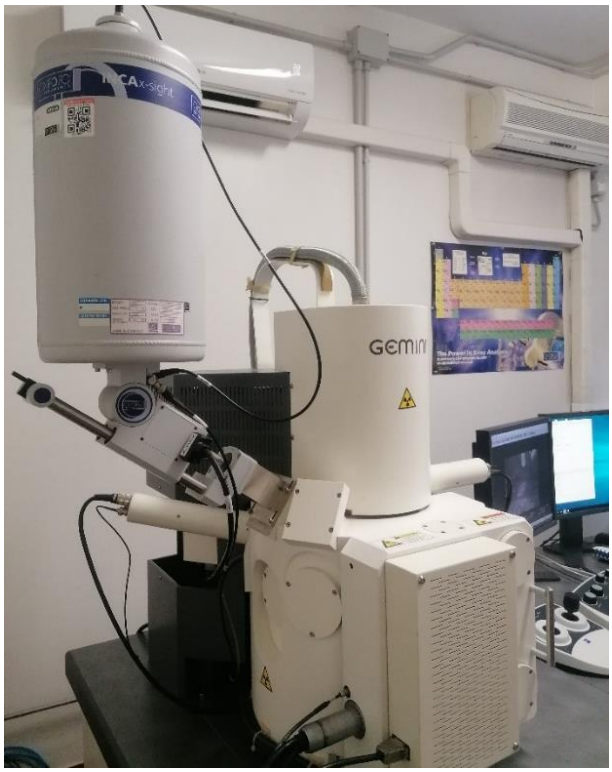

Figure 3.16 – Field Emission Scanning Electron Microscopy (FESEM Zeiss Supra 40)

The samples considered, which are not conductive, were metalized with platinum (30 mA/50 s) before they could be observed via FESEM, and they were cut into pieces to analyze the cross-section (Figures 3.17).

Figures 3.17 – Samples coated with platinum

Chapter 4: Samples printing and results analysis

As already mentioned in the previous chapters, the aim of this investigation was to fabricate Molecularly Imprinted Polymers through Additive Manufacturing, in particular DLP 3D printing, which is a pretty innovative approach. To the best of our knowledge, the use of DLP for MIPs' fabrication is not yet developed within the scientific community, so it needs research efforts and in-depth analysis. Consequently, this thesis reports the first steps and hopefully can lay the foundations for future activities.

4.1 Experiments' steps

During this work, all samples have been printed following a series of steps, listed below, and that will be described in detail in the next sections:

a. Preparation of the formulation.
b. Design of CAD geometry.
c. Optimization of the printing parameters and printing process.
d. Post curing of samples.
e. Removal of the template molecule.
f. Rebinding process.
g. Data analysis.

4.1.1 Formulation's preparation

The complete procedure for preparing the different formulations is described in section 3.3 and two summary tables are provided below (Table 4.1 and Table 4.12):

	OTC:MAA:DPGDA
Formulation 1	1:4:20
Formulation 2	1:5:20
Formulation 3	1:6:20

Table 4.1 – Formulations with different OTC:MAA:DPGDA ratios

	OTC:MAA:DPGDA	Salt content
Formulation 4	1:5:20	60 phr
Formulation 5	1:5:20	40 phr
Formulation 6	1:5:20	20 phr

Table 4.2 – Formulations with different content of salt

4.1.2 CAD geometry

Rhinoceros® is the program employed to realize all the CAD needed for the experiments. First, it's important to highlight that all the geometries that have been used have the common diameter of 10 mm. This choice was made for practical reasons, to allow the dots and filters to fit exactly inside the 48-multiwell plate, used during the following experiment's steps.

Dots

The geometry employed for the first printing attempts was a simple dot with a diameter of 10 mm and a height of 550 µm (Figures 4.1):

Figures 4.1 – Dot geometry, with 10 mm diameter and 550 µm height

Then, two other CAD were realized, with a more complex geometry, i.e., six-floor filters, to improve the performance of the MIPs. The aim was to obtain a self-standing geometry with a larger surface area, through which the rebinding solution could flow more easily.

Filter 1

The first filter (that we will call *Filter 1* in the next sections) has six levels 300 µm thick, that are equal but rotated on the xy plane and separated by pillars 500 µm high (Figures 4.2).

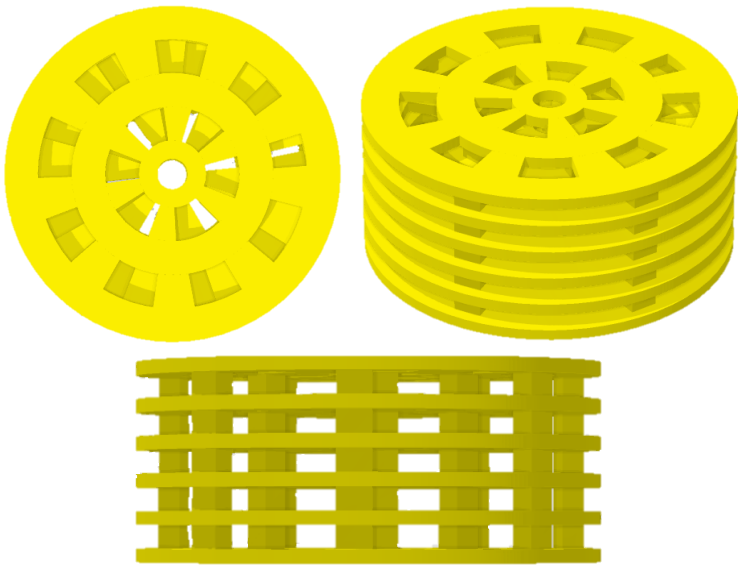

Figures 4.2 – Filter 1 geometry, with six levels 300 µm thick, separated by pillars 500 µm high

Filter 2

The second filter (that we will call *Filter 2* in the next sections) has six levels 250 µm thick, equal and rotated, separated by pillar 500 µm high, and each level is characterized by smaller features in the x-y plane (Figures 4.3):

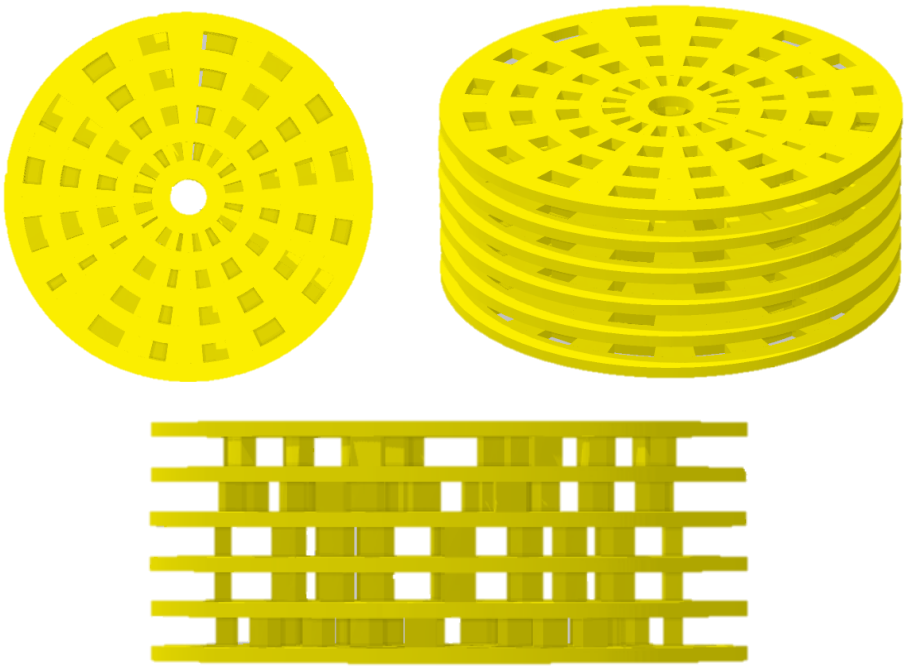

Figures 4.3 – Filter 2 geometry, with six levels 250 µm thick, separated by pillars 500 µm high

Filter 3

Finally, during the experiments there was the need to realize another CAD, that we'll call *Filter 3*, used to print MIPs with the addition of salt. It's a filter without pillars, 1.2 mm high, with the same features of *Filter 1* on x-y plane (Figures 4.4).

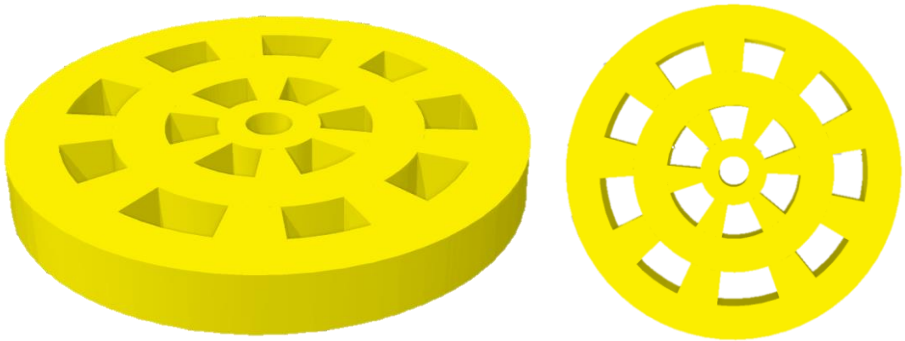

Figures 4.4 – Filter 3 geometry, with 1.2 mm height and without pillars

4.1.3 Optimization of printing parameters

The first step of a 3D printing process, after preparing the resin, is to find the right printing parameters; this is a time-consuming process and lots of attempts are necessary, because every resin and every geometry is different

from each other. The most important parameters that must be optimized are exposure time, light intensity and slice thickness.

The optimization of MIP and NIP dots' parameters came first, for each of the three formulations with different OTC/MAA ratio; then, the resin with OTC:MAA=1:4 has been chosen to print MIP filters (*Filter 1* and *Filter 2*) and so the parameters for both geometries have been re-optimized. Finally, resin with OTC:MAA=1:5 has been used to print MIP dots and filters with different percentages of salt.

Two summary tables (Table 4.3 and Table 4.4) of the different formulations and geometries are provided below:

	Composition	Printed geometry
Formulation 1	OTC:MAA:DPGDA=1:4:20	
Formulation 2	OTC:MAA:DPGDA=1:5:20	
Formulation 3	OTC:MAA:DPGDA=1:6:20	

Table 4.3 – Formulations without salt, and the respective printed geometries

	Composition	Printed geometry
Formulation 4	OTC:MAA:DPGDA=1:5:20 + 60 % of salt	
Formulation 5	OTC:MAA:DPGDA=1:5:20 + 40 % of salt	
Formulation 6	OTC:MAA:DPGDA=1:5:20 + 20 % of salt	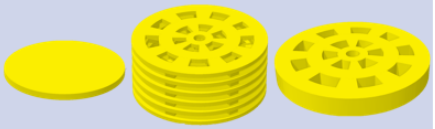

Table 4.4 – Formulations with salt, and the respective printed geometries

Concerning dots, they are composed of two distinct elements: the so called "base", 500 µm high, and the active layer of NIP/MIP, 50 µm high, as it can be seen in the schematic picture below (Figure 4.5):

Figure 4.5 – Schematic representation of the two components of printed dots: base (grey) and MIP/NIP layer (yellow)

The aim of this distinction is to have an extremely thin active layer, as if it were the functionalization of a surface.

Consequently, MIP and NIP dots were printed with two different resins:

- the first 500 µm with the so called "base resin" described in section 3.3, composed by DPGDA, DMSO and BAPO.
- the remaining 50 µm with NIP and MIP resin, i.e., the "base" plus MAA (for NIPs) and MAA+OTC (for MIPs).

For this reason, through Asiga Composer program, it was necessary to create ranges with different parameters for the first 500 µm and for the last 50 µm. Moreover, the use of two different formulations requires the printer to stop when the base is printed, manually change the resin within the vat and then continue the printing process.

Concerning filters, instead, there is no distinction between "base" and active layer; they are entirely printed with NIP/MIP resin. By the way, also for filter geometry ranges have been created with different parameters for distinguishing the 6 planes from the pillars.

Moreover, as explained in section 3.2, for all the geometries, the *burn in* layers have been printed with increased irradiation time or intensities to allow the adhesion of the material to the platform.

Finally, the optimal parameters for each formulation and geometry are listed in the sections below, with some pictures of the printed items.

4.1.3.1 DPGDA dot with *Formulation 1*

To print dots with Formulation 1, three ranges have been created: *burn-in* and range 1 are made with "base" resin, while range 2 is made with NIP and MIP resin, with ratio OTC:MAA:DPGDA=1:4:20. The printing parameters are summarized in Table 4.5 and Table 4.6; images obtained with an optical microscope are inserted below (Figure 4.6 and Figure 4.7).

NIP

	Burn-in	Range 1	Range 2
	0 - 100 µm	*100 - 500 µm*	*500 - 550 µm*
Light intensity (mW/cm²)	20	20	40
Exposure time (s)	4.5	3.5	5
Slice thickness (µm)	50	50	25

Table 4.5 – Optimized printing parameters for NIP dots with Formulation 1

Figure 4.6 – Top view of dot printed with NIP resin, with Formulation 1

MIP

	Burn-in	Range 1	Range 2
	0 - 100 µm	*100 - 500 µm*	*500 - 550 µm*
Light intensity (mW/cm²)	20	20	48
Exposure time (s)	4.5	3.5	33.5
Slice thickness (µm)	50	50	25

Table 4.6 – Optimized printing parameters for MIP dots with Formulation 1

Figure 4.7 – Top view of dot printed with MIP resin, with Formulation 1

The coloration of all MIPs that have been printed is due to the presence of the antibiotic OTC, which is a powder that has a yellow color.

4.1.3.2 DPGDA dot with *Formulation 2*

For Formulation 2, with ratio OTC:MAA:DPGDA=1:5:20, parameters are equal to those of Formulation 1, both for NIP and MIP (Table 4.5 and Table 4.6), and there is also no variation in appearance.

4.1.3.3 DPGDA dot with *Formulation 3*

For formulation 3, with ratio OTC:MAA:DPGDA=1:6:20, the printed dots have the same aspect of the previous one and we cannot clearly notice any differences between them. Nevertheless, the printing parameters are different, and they are summarized in Table 4.7 and 4.8.

NIP

	Burn-in	Range 1	Range 2
	0 - 100 µm	*100 - 500 µm*	*500 - 550 µm*
Light intensity (mW/cm²)	20	20	30
Exposure time (s)	4.5	3.5	4.5
Slice thickness (µm)	50	50	25

Table 4.7 – Optimized printing parameters for NIP dots with Formulation 3

MIP

	Burn-in	Range 1	Range 2
	0 - 100 µm	*100 - 500 µm*	*500 - 550 µm*
Light intensity (mW/cm²)	20	20	48
Exposure time (s)	4.5	3.5	33.5
Slice thickness (µm)	50	50	25

Table 4.8 – Optimized printing parameters for MIP dots with Formulation 3

4.1.3.4 DPGDA *Filter 1* with *Formulation 1*

NIP

The starting point was printing *Filter 1* with NIP resin, composed of DPGDA, BAPO, DMSO and MAA; numerous attempts to optimize the parameters have been made, but resolution along z axis was not good and no filter could be printed. So, to increase the resolution, it was proposed to incorporate a red dye (DR1) into the formulation, specifically 0.01 phr. After several tries, however, the outcome was unchanged: the resolution along the z axis has not improved and there has been an accumulation of unpolymerized resin

between the three layers. Despite several ethanol washing with the help of ultrasound, it was not possible to remove the excess resin without damaging the filter (Figures 4.8).

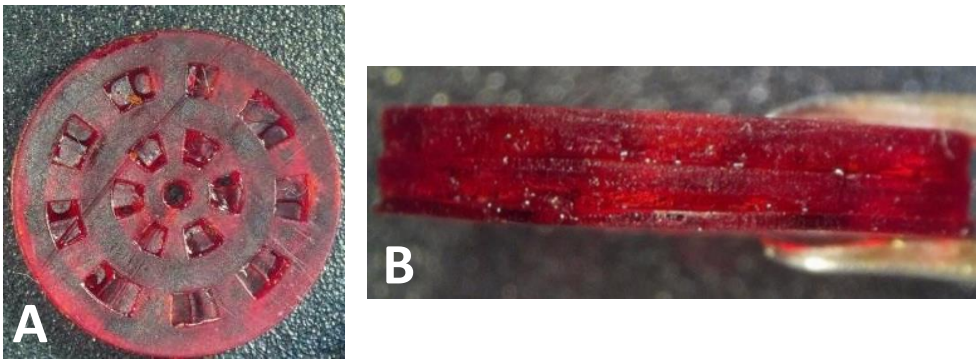

Figures 4.8 – Filter 1 printed with NIP resin, with Formulation 1; top view (A) and side view (B)

Then, another attempt was made to change the printing conditions: the initial CAD was modified, obtaining *Filter 4* (Figure 4.9), increasing the height of the pillars to 1 mm, to facilitate the removal of the resin between the various layers:

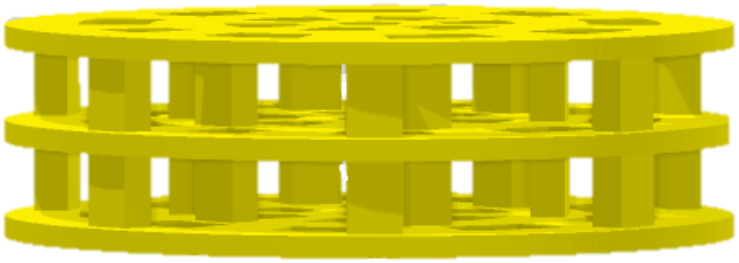

Figure 4.9 – Filter 4, with three levels 300 µm high and 1 mm high pillars

A slight improvement was seen, but it was possible to print a filter with only 3 levels, instead of 6 (Figures 4.10). The optimized parameters listed below have provided the best result, shown in Table 4.9.

	Burn-in	Range 1	Range 2	Range 3	Range 4	Range 5
	0 - 100 µm	*100 - 300 µm*	*300 - 1.3 mm*	*1.3 - 1.6 mm*	*1.6 - 2.6 mm*	*2.6 - 2.9 mm*
Light intensity (mW/cm²)	40	40	45	40	45	40
Exposure time (s)	5	5	7	5	7	5
Slice thickness (µm)	0.05	0.05	0.05	0.15	0.05	0.15

Table 4.9 – Optimized printing parameters for NIP Filter 4 with Formulation 1

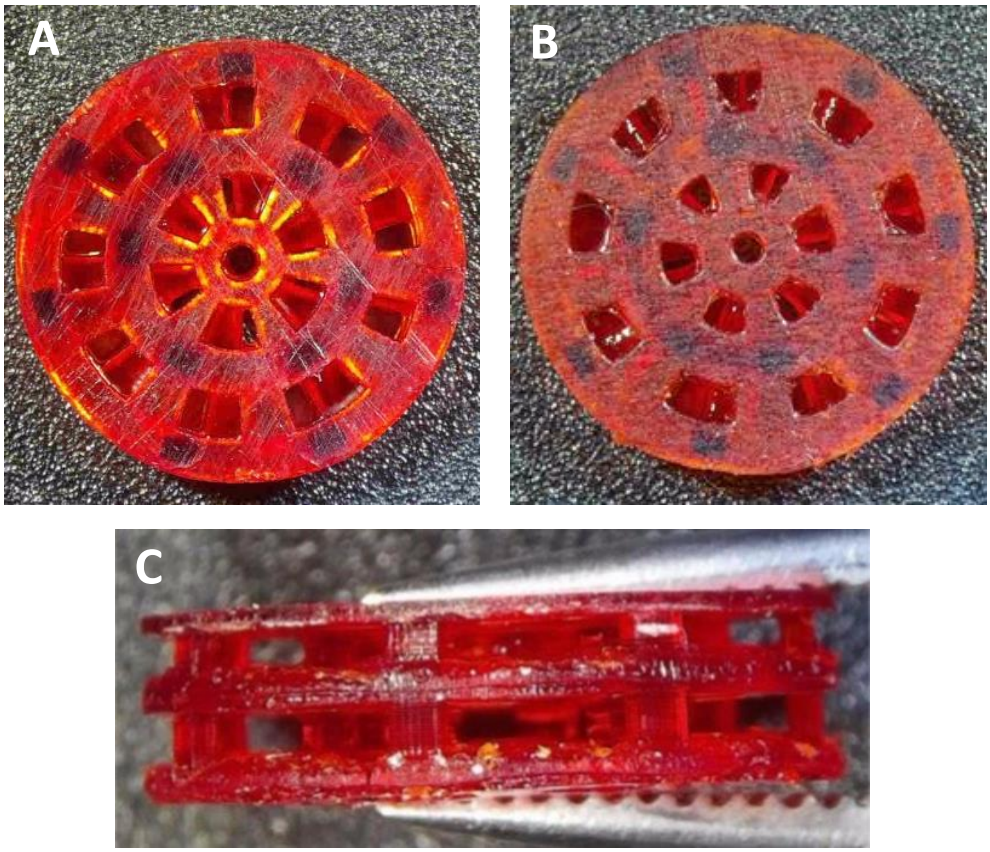

Figures 4.10 – Filter 4 printed with NIP Formulation 1; top view (A), bottom view (B), side view (C)

The resolution on the x-y plane is high, in fact it's possible to distinguish all the holes on the surface (Figure 4.10 – A); however, the resolution along the z axis is not good, indeed the most obvious defect of this filter is the incorrect thickness of the layers, which should be of 300 µm, but is instead much higher (~ 1 mm), along with a non-optimal surface finish (Figure 4.10 – C).

MIP

For printing MIP *Filter 1*, 11 ranges have been created, to distinguish the parameters for the 6 planes and for pillars; the optimized parameters are summarized in Table 4.10.

	Burn-in	1	2 (pillar)	3	4 (pillar)	5
	0-100 µm	*100-300 µm*	*300-800 µm*	*800-1.1 mm*	*1.1-1.6 mm*	*1.6-1.9 mm*
Light intensity (mW/cm²)	40	40	41	40	41	40
Exposure time (s)	30	30	32	30	32	30
Slice thickness (µm)	50	50	50	50	50	50

	6 (pillar)	7	8 (pillar)	9	10 (pillar)	11
	1.9-2.4 mm	*2.4-2.7 mm*	*2.7-3.2 mm*	*3.2-3.5 mm*	*3.5-4 mm*	*4-4.3 mm*
Light intensity (mW/cm^2)	41	40	41	40	41	40
Exposure time (s)	32	30	32	30	32	30
Slice thickness (µm)	50	50	50	50	50	50

Table 4.10 – Optimized printing parameters for MIP Filter 1 with Formulation 1

From Figures 4.11 it is quite clear that the print resolution is quite good, both on the x-y and the z planes. The size of the filter was also measured using caliber, obtaining a total height of 4.3 mm, as expected from CAD.

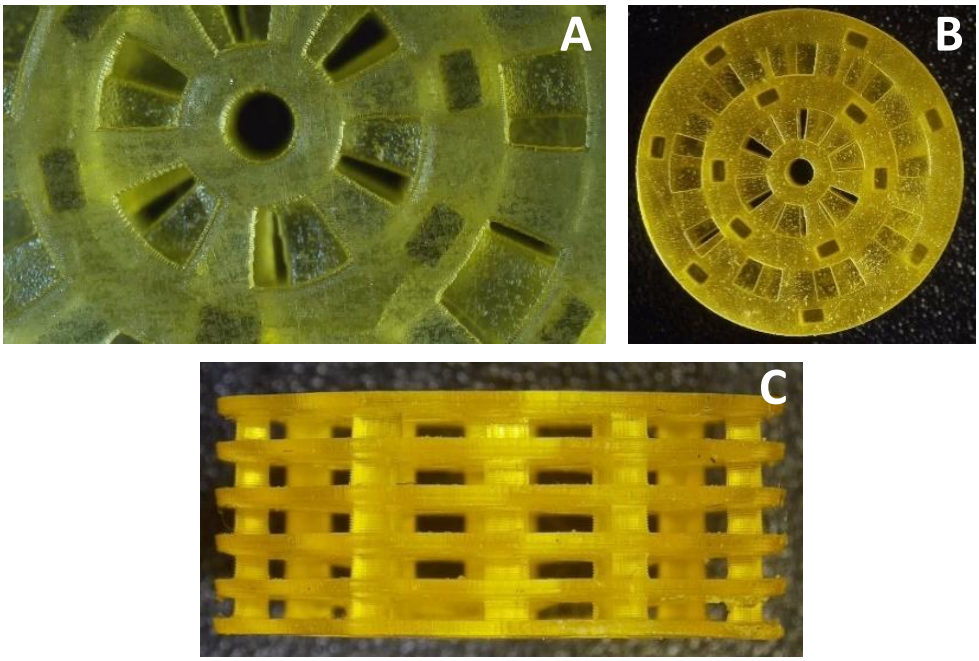

Figures 4.11 – Filter 1 printed with MIP Formulation 1; top view (A, B) and side view (C)

In addition, the 3D scanner was used, to compare the printed geometry to the one created using CAD software. As we can see from Figures 4.12, good print fidelity is reached, with discrepancies within the range ± 50 µm compared to the CAD. Larger deviations (red color) are related to the impossibility of the scanner to measure internal cavities of the component.

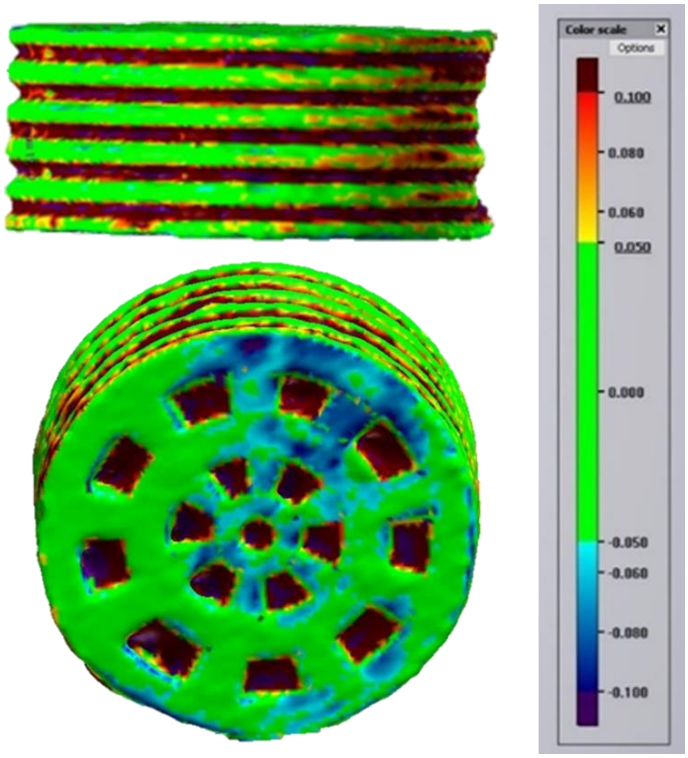

Figures 4.12 – 3D scanning of filter 1 printed with MIP Formulation 1

4.1.3.5 DPGDA *Filter 2* with *Formulation 1*

For printing MIP *Filter 2*, 11 ranges have been created, to distinguish the parameters for the 6 planes and for pillars; the parameters in Table 4.11 have provided the best result.

	Burn-in	1	2 (pillar)	3	4 (pillar)	5
	0-100 µm	*100-250 µm*	*250-750 µm*	*750-1 mm*	*1-1.5 mm*	*1.5-1.75 mm*
Light intensity (mW/cm²)	40	40	41	40	41	40
Exposure time (s)	30	30	32	30	32	30
Slice thickness (µm)	50	50	50	50	50	50

	6 (pillar)	7	8 (pillar)	9	10 (pillar)	11
	1.75-2.25 mm	*2.25-2.5 mm*	*2.25-3 mm*	*3-3.25 mm*	*3.25-3.75 mm*	*3.75-4 mm*
Light intensity (mW/cm²)	41	40	41	40	41	40
Exposure time (s)	32	29	32	29	32	29
Slice thickness (µm)	50	50	50	50	50	50

Table 4.11 – Optimized printing parameters for MIP Filter 2 with Formulation 1

Unfortunately, as we can see from Figures 4.13, the filter is not perfect: between the first two layers there is an accumulation of unpolymerized resin that cannot be completely removed by washing the filter in ethanol or water;

moreover, the layers are very fragile, and they could shatter and break if left in the washing solution in the ultrasonic bath for too long.

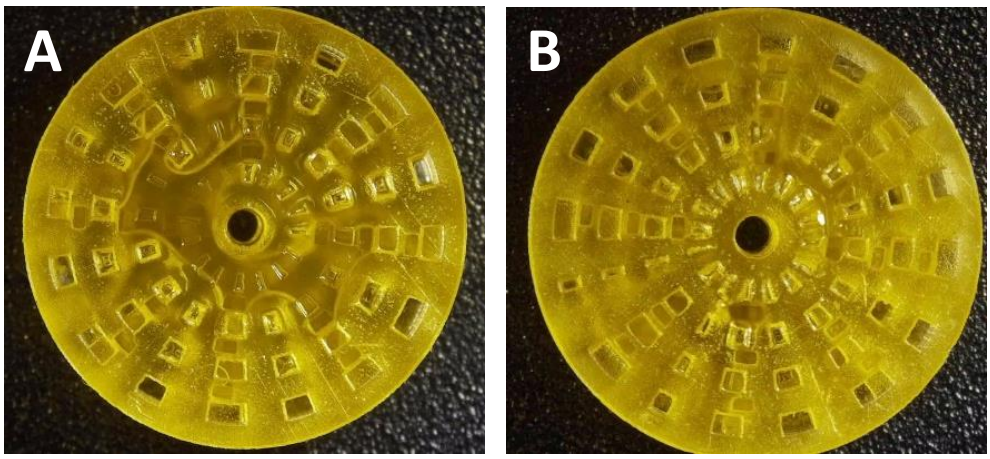

Figures 4.13 – Bottom view (A) and top view (B) of filter 2 printed with MIP Formulation 1

It was originally thought that a blade might be used to remove the final layer where there is an excess of resin (Figures 4.14); however, doing so increases the risk of seriously damaging the filters, making this an impractical solution for the long term.

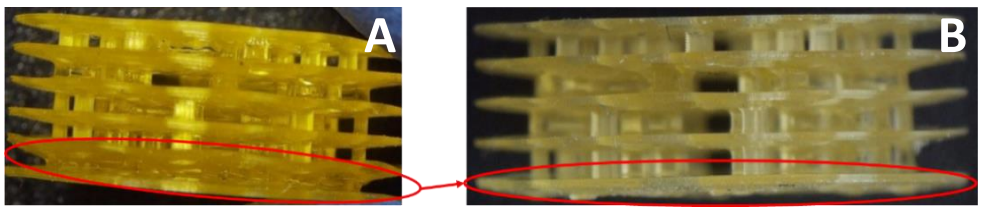

Figures 4.14 – Side view of filter 2 printed with MIP Formulation 1; it is highlighted the accumulation of resin between the first two layers (A) and the subsequent removal of the first layer (B)

So, further attempts to optimize the parameters are needed and, if necessary, CAD can be modified too.

4.1.3.6 Dots with salt

For printing dots with salt, three ranges have been created: *burn-in* and range 1 are made with "base" resin, while range 2 is made with NIP and MIP resin with the adding of salt. Numerous attempts have been made and a problem sometimes observed during printing procedure was the "approach failed after X seconds". This is an error of the printer, that is unable to reach the target after X seconds (Figure 4.15), and this could be caused by build platform misalignment, material debris, vibration sources, not sufficient resin in the vat, partial or entire detachment of the model [102]:

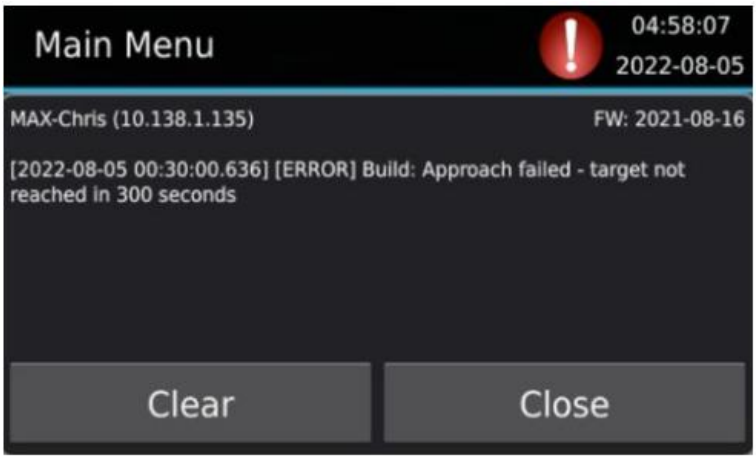

Figure 4.15 – printer error: approach failed; target not reached in X seconds [102]

In this case, the error could be caused by the presence of salt particles larger than the thickness of the layer to be printed, considering that they were grinded manually and there was no control over their size. Additionally, the NIP/MIP layer, that should be 50 µm thick, is instead roughly 150-200 µm thick. Finally, as can be seen in Figures 4.16, sometimes the salt particles are not dispersed uniformly within the resin.

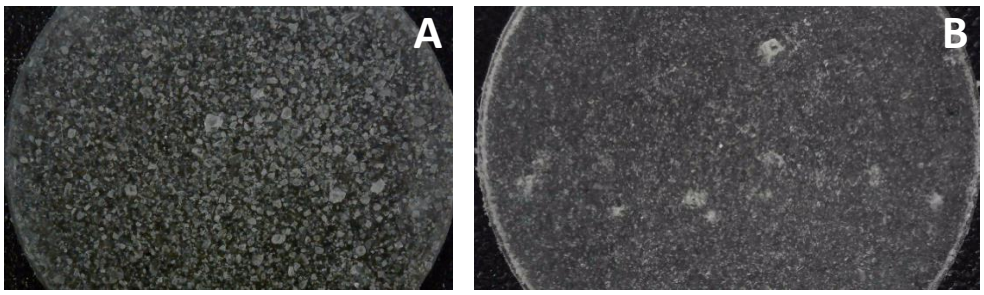

Figures 4.16 – Top view of dot printed with NIP Formulation 5 (A) and Formulation 4 (B)

4.1.3.6.1 DPGDA dot with *Formulation 4*

For NIP/MIP dots with Formulation 4 (OTC:MAA:DPGDA=1:5:20 and 60 % of salt) the optimized parameters are summarized in Tables 4.12 and 4.13.

NIP

	Burn-in	Range 1	Range 2
	0 - 100 µm	*100 - 500 µm*	*500 - 550 µm*
Light intensity (mW/cm²)	20	20	49
Exposure time (s)	4.5	3.5	15
Slice thickness (µm)	0.05	0.05	0.05

Table 4.12 – Optimized printing parameters for NIP dots with Formulation 4

MIP

	Burn-in	Range 1	Range 2
	0 - 100 µm	*100 - 500 µm*	*500 - 550 µm*
Light intensity (mW/cm²)	20	20	50
Exposure time (s)	4.5	3.5	47
Slice thickness (µm)	0.05	0.05	0.025

Table 4.13 – Optimized printing parameters for MIP dots with Formulation 4

4.1.3.6.2 DPGDA dot with *Formulation 5*

For printed NIP/MIP dots with Formulation 5 (OTC:MAA=1:5 and 40 % of salt) the optimized parameters are summarized in Tables 4.14 and 4.15.

NIP

	Burn-in	Range 1	Range 2
	0 - 100 µm	*100 - 500 µm*	*500 - 550 µm*
Light intensity (mW/cm²)	20	20	49
Exposure time (s)	4.5	3.5	10
Slice thickness (µm)	0.05	0.05	0.025

Table 4.14 – Optimized printing parameters for NIP dots with Formulation 5

To verify the presence of porosity within the sample matrix, images using FESEM were taken. As can be seen from Figure 4.22, the removal of salt from the sample after printing created some pores, but they are not interconnected as expected. Furthermore, having grinded the salt manually, the size of the pores is not homogeneous.

Moreover, from Figure 4.21 it's clear that the sample has a distinct composition: 500 µm were printed using the base resin, so without salt, and 50 µm were printed using the salt-containing formulation.

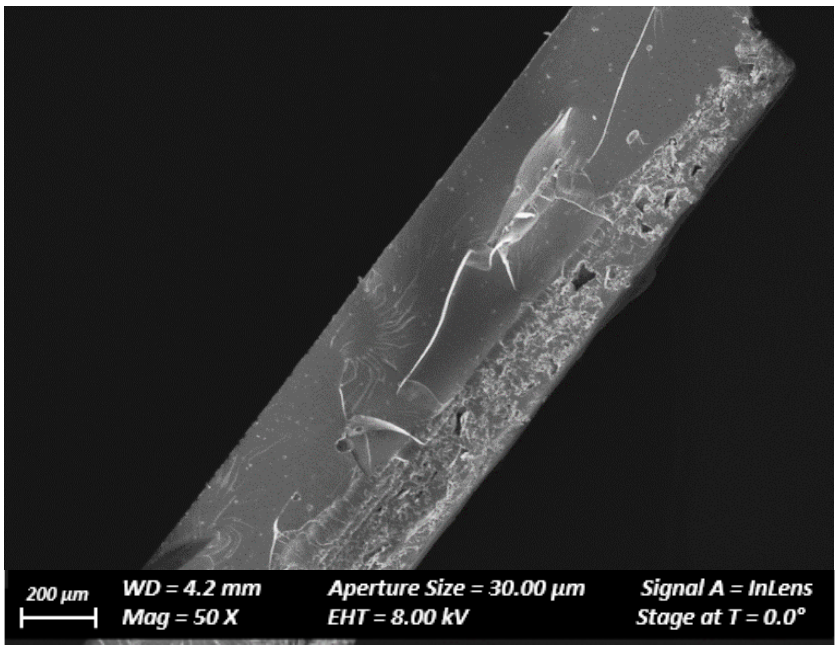

Figure 4.21 – FESEM image of NIP dot, with Formulation 5

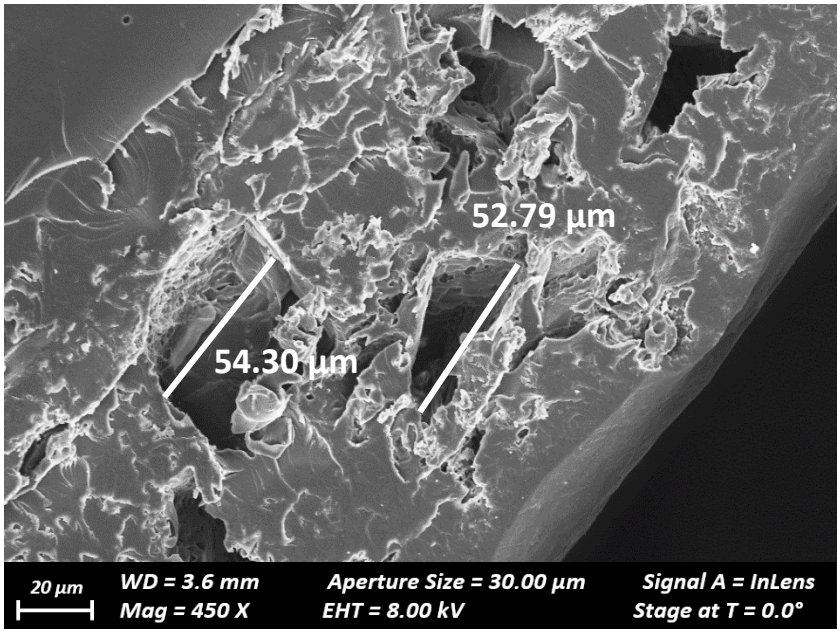

Figure 4.22 – FESEM image of NIP dot, with formulation 5

MIP

	Burn-in	Range 1	Range 2
	0 - 100 µm	*100 - 500 µm*	*500 - 550 µm*
Light intensity (mW/cm²)	20	20	49
Exposure time (s)	4.5	3.5	40
Slice thickness (µm)	0.05	0.05	0.025

Table 4.15 – Optimized printing parameters for MIP dots with Formulation 5

4.1.3.6.3 DPGDA dot with *Formulation 6*

For printed NIP/MIP dots with Formulation 6 (OTC:MAA:DPGDA=1:5:20 and 20 % of salt) the optimized parameters are summarized in Tables 4.16 and 4.17. Moreover, Figures 4.17 and 4.19 show respectively the top view of NIP and MIP dots, obtained through an optical microscope.

NIP

	Burn-in	Range 1	Range 2
	0 - 100 µm	*100 - 500 µm*	*500 - 550 µm*
Light intensity (mW/cm^2)	20	20	49
Exposure time (s)	4.5	3.5	10
Slice thickness (µm)	0.05	0.05	0.025

Table 4.16 – Optimized printing parameters for NIP dots with Formulation 6

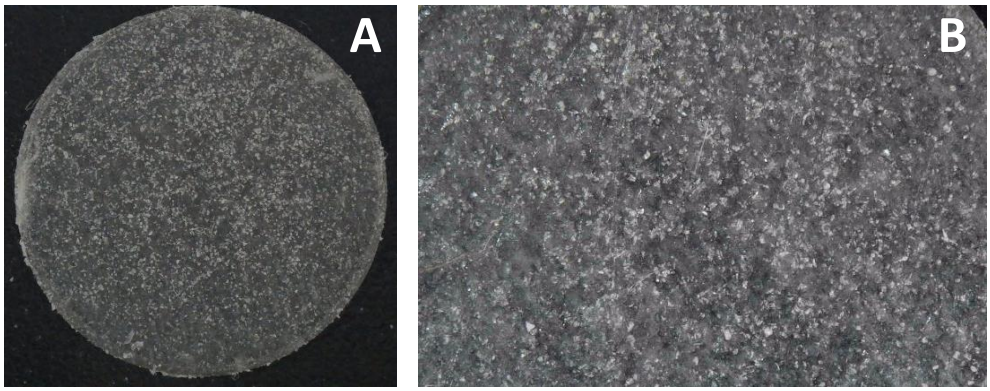

Figures 4.17 – Top view of dot printed with NIP Formulation 6 (A); zoom of the same dot (B)

FESEM microscope was used to analyze the internal structure of these samples too, and to check whether pores were actually created inside the structure. As can be seen in Figure 4.18, some pores have been created, but also in this case they are not interconnected, and their size is not homogeneous.

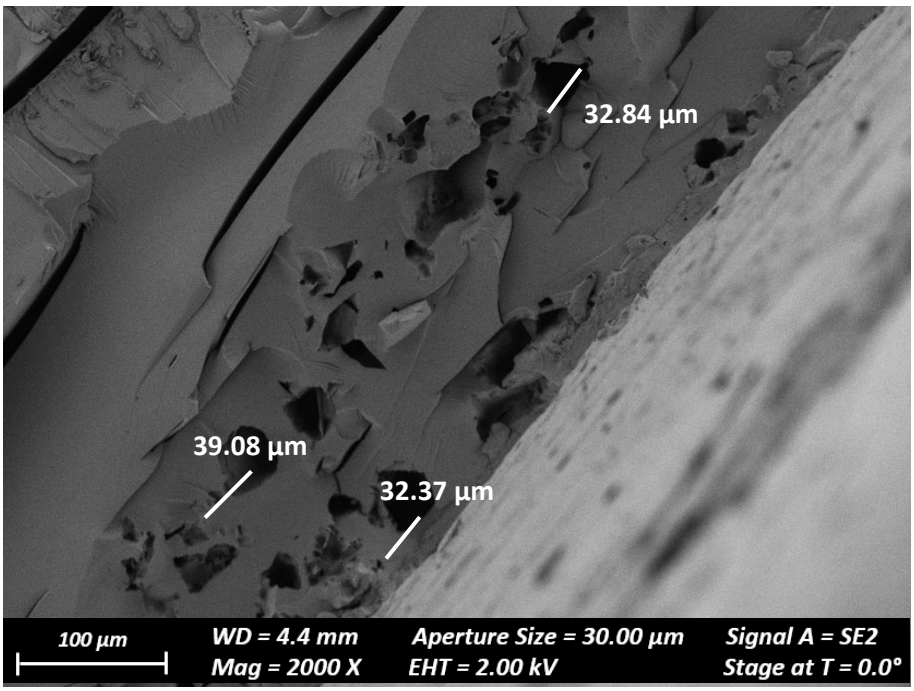

Figure 4.18 – FESEM image of NIP dot, with Formulation 6

MIP

	Burn-in	Range 1	Range 2
	0 - 100 µm	*100 - 500 µm*	*500 - 550 µm*
Light intensity (mW/cm²)	20	20	49
Exposure time (s)	4.5	3.5	40
Slice thickness (µm)	0.05	0.05	0.025

Table 4.17 – Optimized printing parameters for MIP dots with Formulation 6

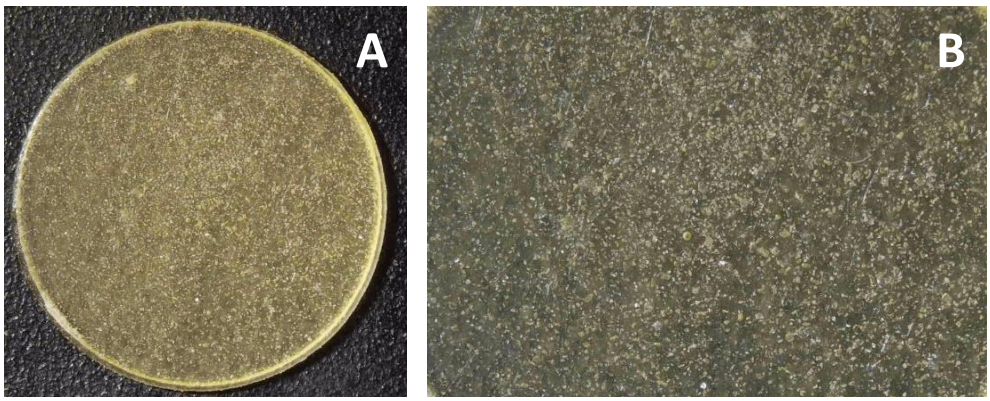

Figures 4.19 – Top view of dot printed with MIP Formulation 6 (A); zoom of the same dot (B)

Figure 4.20, obtained with FESEM, represents the internal structure of MIP dot; in this case, it seems that fewer pores have formed. However, this may

depend on the piece of dot that was used to take the image, considering that porosity is not homogeneous.

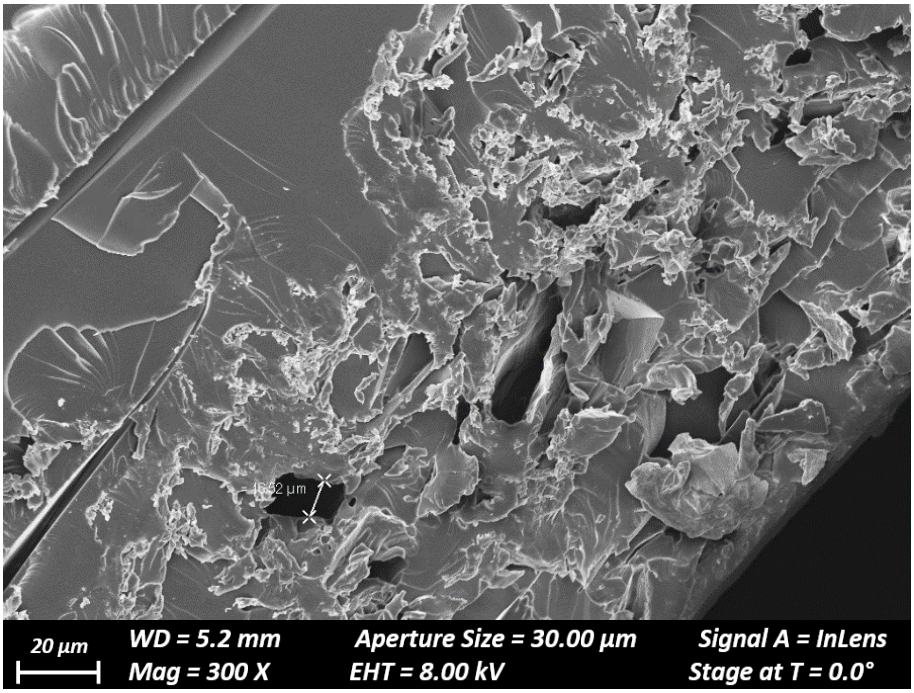

Figure 4.20 – FESEM image of MIP dot, with Formulation 6

4.1.3.7 DPGDA filter with *Formulation 6*

MIP

The starting point was trying to print *Filter 1* geometry, but in all the attempts that were made, only two of the six overall planes were printed (Figure 4.23). The problem that was found was the difficulty of the different levels staying attached to each other, in fact sometimes they remained tied to the building platform. This may be because the surface of the pillars is too small, given the presence of salt particles that make adhesion more difficult. Nevertheless, the resolution on the xy plane is quite satisfactory.

Figure 4.23 – Top view of filter 1 printed with MIP Formulation 6

As a solution to the adhesion problem, *Filter 3* was printed, creating five ranges, including *burn-in*; optimized parameters are summarized in Table 4.18.

	Burn-in	Range 1	Range 2	Range 3	Range 4
	0 - 100 µm	*100 - 300 µm*	*300 - 600 µm*	*600 - 900 µm*	*900 – 1.2 mm*
Light intensity (mW/cm²)	45	45	40	40	40
Exposure time (s)	30	30	25	23	21
Slice thickness (µm)	0.1	0.1	0.1	0.1	0.1

Table 4.18 – Optimized printing parameters for MIP Filter 3 with Formulation 6

From Figures 4.24, it can be noticed the presence of salt particles and overall, the print fidelity is good.

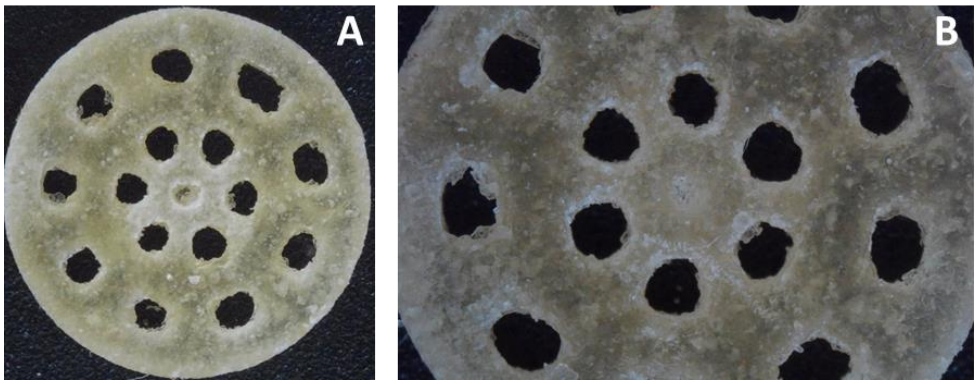

Figures 4.24 – Top view (A) and zoom view (B) of filter 3 printed with MIP Formulation 6

FESEM microscope was used to analyze the internal structure of these samples too and to check whether pores were actually created inside the structure. Indeed, some pores are visible in Figure 4.26, but not as many as expected and there's no interconnection between them.

Another parameter that can be checked is the layer's thickness; theoretically every layer should be 300 µm thick, but as it's shown in Figure 4.25, the thickness ranges from 180 µm to 236 µm.

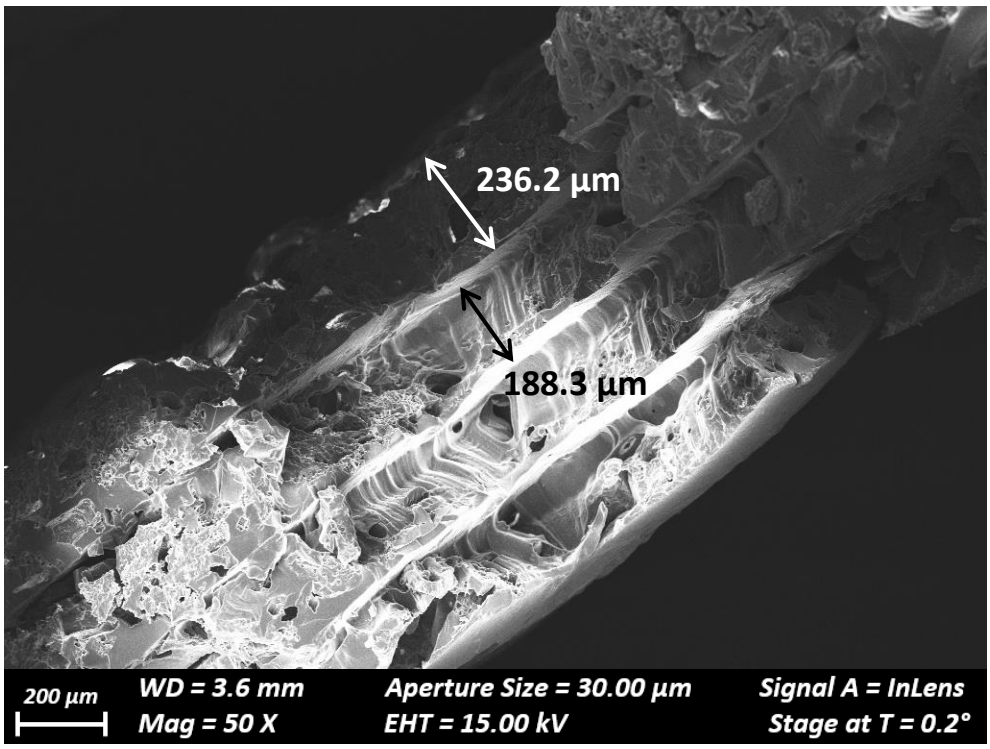

Figure 4.25 – FESEM image of Filter 3, printed with MIP Formulation 6

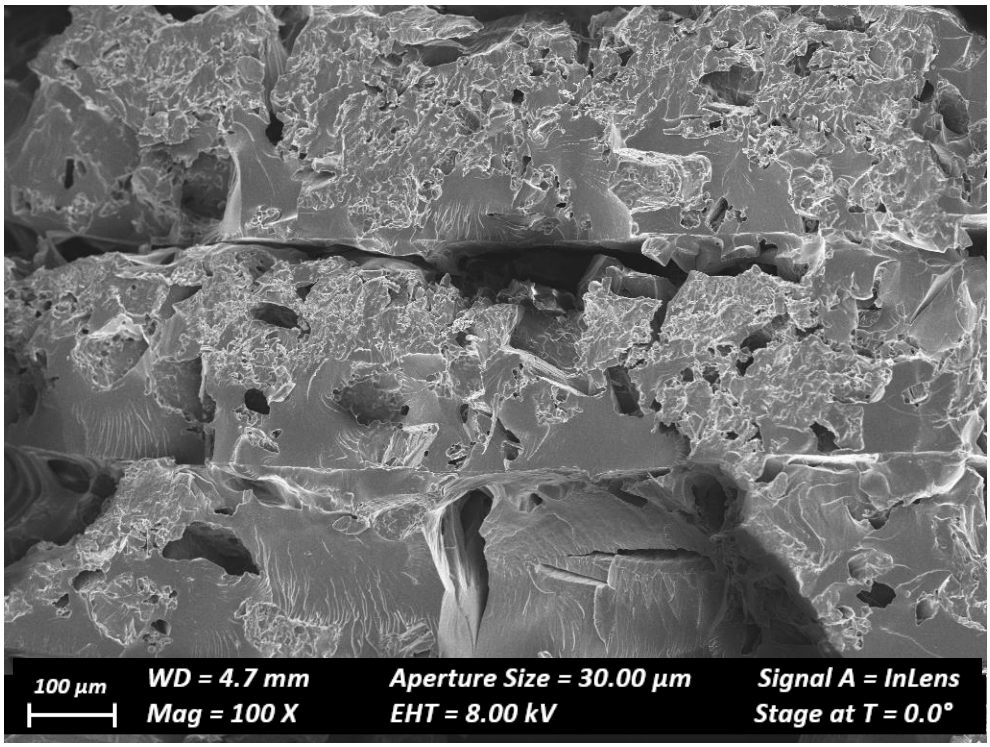

Figure 4.26 – FESEM image of Filter 3, printed with MIP Formulation 6

NIP

To print NIP filters, 0.01 phr of red dye (DR1) was added, to improve resolution (Figure 4.27); Table 4.19 shows the optimized parameters, used to print the filter.

	Burn-in	Range 1	Range 2	Range 3	Range 4
	0 - 100 µm	*100 - 300 µm*	*300 - 600 µm*	*600 - 900 µm*	*900 – 1.2 mm*
Light intensity (mW/cm²)	25	25	25	25	25
Exposure time (s)	5	5	5	5	5
Slice thickness (µm)	0.1	0.1	0.1	0.1	0.1

Table 4.19 – Optimized printing parameters for NIP Filter 3 with Formulation 6

Figure 4.27 – Top view of filter 3 printed with NIP Formulation 6

In this last sample analyzed with FESEM, from Figures 4.28 it can be seen that really few pores have formed.

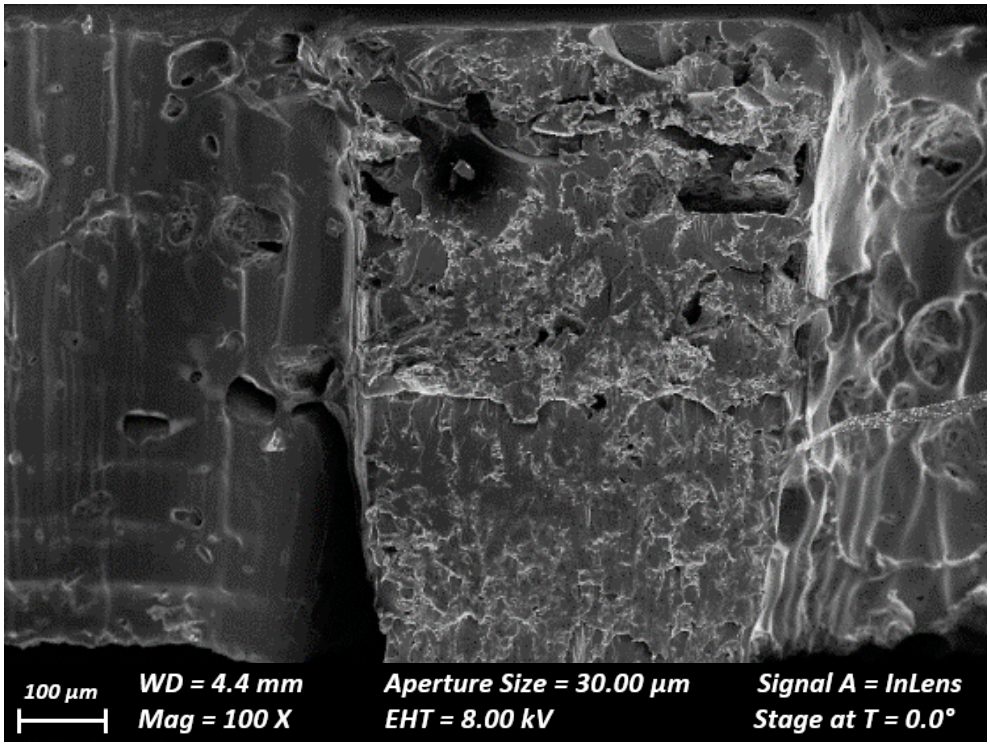

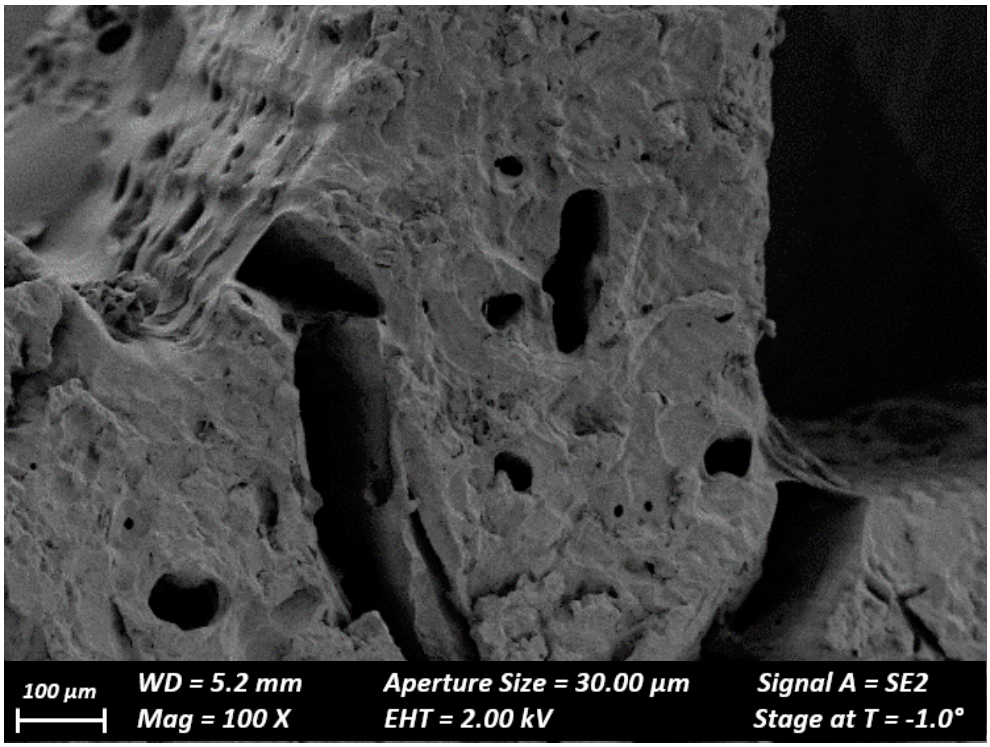

Figures 4.28 – FESEM images of Filter 3, printed with NIP Formulation 6

4.1.4 Post processing of samples

After printing process, every sample described before goes through a post-processing step, that consists of:

- **Removal of the sample** from the building platform: this step was performed using a small blade, with the addition of isopropanol, which should help to remove the object more easily.
- **Cleaning of the sample**: the printed objects were immersed in a vial with ethanol, which was then placed inside the ultrasonic bath; this step was used to remove the unpolymerized resin.
- **Post-curing of the sample**: this step consists of placing the objects into a Robot Factory UV chamber, equipped with a medium-pressure mercury lamp for two minutes; the external UV light increases the final cross-linking density and degree of polymerization, improving the printed samples' long-term structural durability.

At this point, the samples are ready for the next step, template extraction.

4.1.5 Template extraction

First, it's necessary to make a distinction between samples printed without salt and those with; for the latter there is a preliminary step that precedes the removal of the template, i.e., removing the salt particles. Samples were placed

inside a Becher full of demineralized water and left on the magnetic stir all night; to check the effective salt removal, the samples were weighed before and after this washing procedure. Then, the procedure for template removal is the same for samples with and without salt.

The washing solution used to remove OTC from the samples is composed of methanol (MeOH) and acetic acid (AA), with ratio AA:MeOH=1:9; as mentioned in paragraph 3.4.4, the chosen method for the experiments carried out during the thesis is the Ultrasound-Assisted Extraction using an ultrasound bath, along with the use of a rocking platform.

It's important to mention that NIPs were subjected to the washing procedure too, even if they have no template molecule, to be properly compared with MIPs.

The geometry of the sample under consideration has a significant impact on how long it takes to remove the template. This is especially true in this thesis, where NIPs and MIPs have been built using the two distinct geometries described before: dots and filters. It takes roughly 11 hours of ultrasound for filters compared to 6 hours on average for dots. Additionally, the samples were left inside the washing solution on a rocking platform for about 2 nights for the dots and 4 nights for the filters. Moreover, it's important to specify that washing solution needs to be changed when it is saturated with antibiotic (in our case), for two reasons:

- There is the risk that the OTC will be re-captured by the sample rather than be eliminated.
- If the absorption spectrum obtained by the plate reader is saturated, it is not possible to understand whether other OTC was released in subsequent washings.

Additionally, this washing procedure takes a lot of time and, most importantly, an operator's presence to analyze the washing solutions every few hours.

In Figures 4.29, there is an example of *Filter 1* printed with MIP resin, before and after the washing procedure. The evident color shift in the filter indicates that the oxytetracycline, which was the original source of the yellow color, has been eliminated.

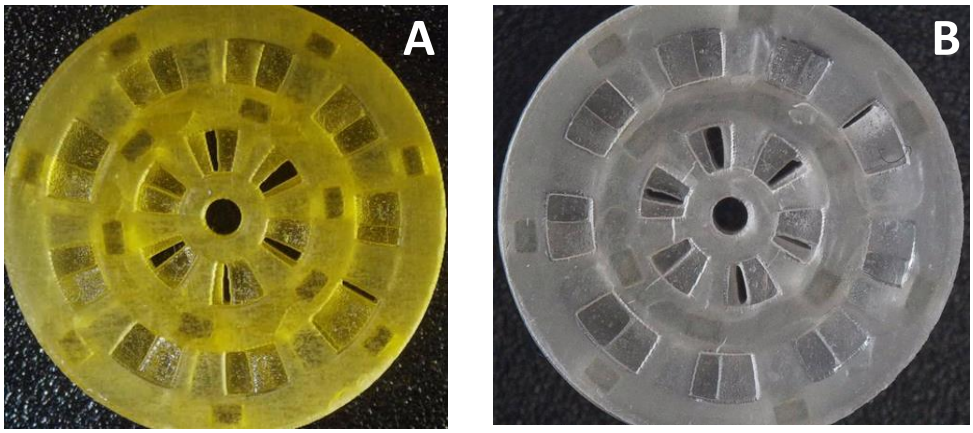

Figure 4.29 – Filter 1 printed with MIP resin, before washing (A) and after washing (B)

To analytically check the removal of the template (OTC), an analysis was carried out using the UV-Visible plate reader described in section 3.6.1. In particular, the absorption spectrum of the washing solutions was obtained after the various cycles in ultrasound and on the platform and the attention was focused on the characteristic peak of the OTC, at 355 nm. The template removal was considered completed when, between one washing and the next, the same absorption spectrum was obtained, because it meant that there was no more OTC to remove.

So, samples are ready for the next step: rebinding procedure.

4.1.6 Rebinding process

As mentioned in the previous chapter, to evaluate the selectivity and the binding ability of MIPs, batch rebinding method has been used. The rebinding solution is composed of OTC dissolved in demineralized water; the samples were placed inside a multiwell plate and then 500 µL of rebinding solution was added; the plate was then placed on the rocking platform for 1-3 nights.

Consequently, 250 µL of the rebinding solution have been collected and placed in another multiwell plate; a preliminary analysis of this solution was carried out using the UV-Visible plate reader, to visually check whether the samples under analysis have captured the template.

The absorption spectrum of the rebinding solution obtained was compared to the spectrum of the “blank” solution, to check if the signal of the rebinding solution is smaller than that of the blank, at 355 nm (characteristic peak of OTC). Then, a more accurate quantitative analysis has been carried out with the use of the calibration curve, that will be described in the next section.

4.1.7 Data analysis

4.1.7.1 OTC calibration curve

To create the calibration curve for OTC, different molarities of the solution have been prepared: 400, 350, 300, 250, 200, 150, 125, 100, 75, 50, 40 and 30 µM. The starting point was the preparation of the stock solution, i.e., 400 µM, starting from dissolving 10 mg of OTC into 50 mL of demineralized water, with the help of the ultrasound bath, according to the following formula:

$g^{OTC} = M*MW*V$, where:

- g^{OTC} is the weight of oxytetracycline in grams.
- M is the molarity of the solution.
- MW is the molecular weight of oxytetracycline.
- V is the volume of the solution in liters.

Then, from the stock solution, all the other solutions were then obtained, by dilution, following the formula below:

$$C_1 \cdot V_1 = C_2 \cdot V_2$$

from which

$$V_2 = \frac{C_1 \cdot V_1}{C_2}$$

where:

- C_1 is the concentration of the starting solution (in this case 400 µM).
- C_2 is the concentration of the desired new solution (in this case 350 µM).
- V_1 is the volume we choose to extract from the solution with concentration C_1 (for example, 10 mL).
- V_2 is the volume of water that is calculated and that must be added to volume V_1 to obtain the desired concentration C_2.

After preparing all the needed solutions, for each of them the absorbance spectrum is obtained, using the plate reader; the blank absorbance spectrum with H2O has also been obtained (Figure 4.30). Then, to display them graphically, the program *OriginPro* has been used:

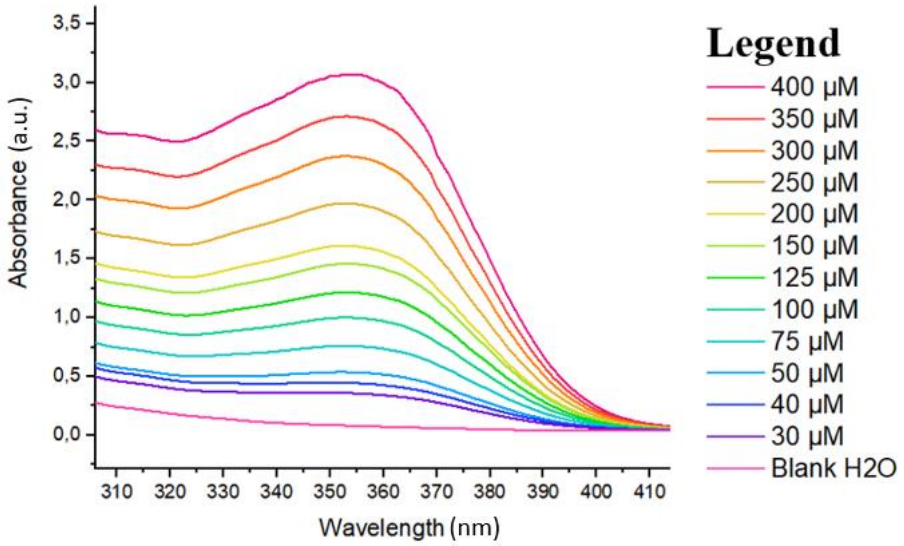

Figure 4.30 – Absorbance spectrum of rebinding solutions with OTC in water

To create the calibration curve, concentration values from 200 µM to 400 µM were excluded because their respective absorption value far exceeds value 1, as explained in section 3.6.1. The remaining concentration values, from 150 µM to 30 µM, have been associated with their respective absorption values at wavelength of 355 nm and Table 4.20 has been created:

Concentration (µM)	150	125	100	75	50	40	30
Absorbance	1.456	1.211	0.999	0.759	0.535	0.445	0.357

Table 4.20 – Table that associates each concentration value with their respective absorption value at 355 nm

From this table is then obtained the calibration curve in Figure 4.31, with the following equation:

$$y = 0.0091x + 0.0794$$

where:

- Y is the absorbance value.
- X is the unknown concentration value.
- 0.0091 is the slope of the calibration curve.
- 0.0794 is the intercept of the calibration curve.

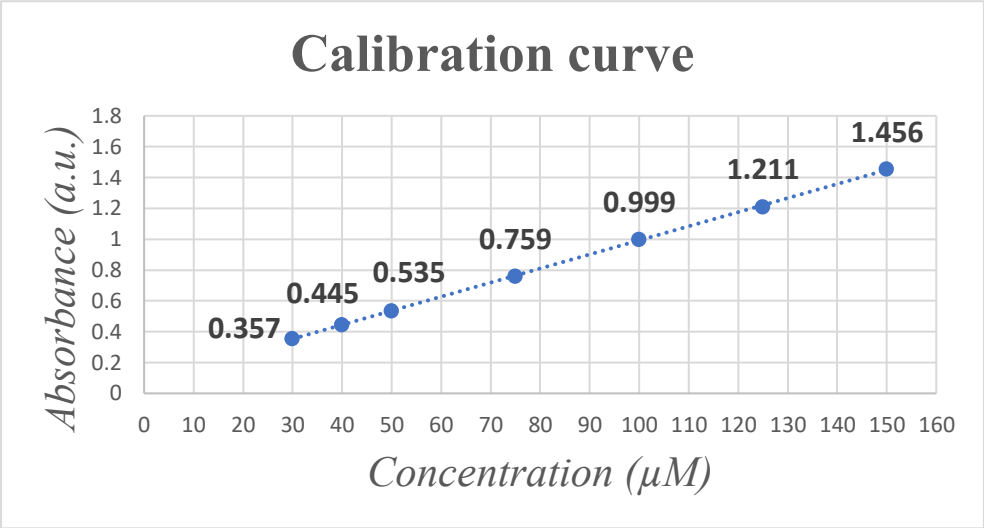

Figure 4.31 – Calibration curve

The data points' dispersion around the fitted regression line is measured using the coefficient of determination, also called *R-squared*. Higher *R-squared* values for the same data set indicate less discrepancy between the fitted values and the observed data. This value is always between 0 and 1 and usually, the larger the R^2, the better the regression model fits the observed data [104]. The calibration curve created has an *R-squared* value of 0.9998, which indicates a good fitting.

At this point, the next step is to obtain the actual concentration values of OTC solutions in water (x), using absorption values from Table 4.20 and the calibration curve:

$$x = \frac{(y - 0.0794)}{0.0091}$$

Specifically:

- $x_{150} = \frac{(1.456-0.0794)}{0.0091} = 151.275\ \mu M$
- $x_{125} = \frac{(1.211-0.0794)}{0.0091} = 124.352\ \mu M$
- $x_{100} = \frac{(0.999-0.0794)}{0.0091} = 101.055\ \mu M$
- $x_{75} = \frac{(0.759-0.0794)}{0.0091} = 74.681\ \mu M$
- $x_{50} = \frac{(0.535-0.0794)}{0.0091} = 50.066\ \mu M$
- $x_{40} = \frac{(0.445-0.0794)}{0.0091} = 40.176\ \mu M$

- $x_{30} = \frac{(0.357-0.0794)}{0.0091} = 30.505\ \mu M$

4.2 Complete experiments

4.2.1 Comparison of different molarities of rebinding solutions

The first experiment was the comparison of three different molarities of the rebinding solution: 150 µM, 100 µM and 50 µM.

The samples printed for each rebinding solution were:

- 3 NIP dots with formulation 1 (OTC:MAA:DPGDA = 1:4:20)
- 3 MIP dots with formulation 1 (OTC:MAA:DPGDA = 1:4:20)

After printing, the samples undergo the post curing and template extraction steps described in the previous sections.

4.2.1.1 Solution 150 µM

After the washing step and once the template was extracted, three NIPs and three MIPs were incubated into blank solutions with molarity 150 µM for one night. Then, 250 µL of rebinding solution were taken from each of the 6 samples and the absorption spectra were obtained using the plate reader, along with the spectrum of the blank solution (Figure 4.32).

Observing the absorption spectra, the signal of the MIPs is lower than the blank signal, and this means that they have captured a certain amount of oxytetracycline.

Instead, since NIPs don't have specific cavities, they shouldn't theoretically be able to catch oxytetracycline. The NIPs signal, however, is lower than the blank signal because there is always some non-specific absorption.

Nevertheless, overall, MIPs caught more OTC than NIPs.

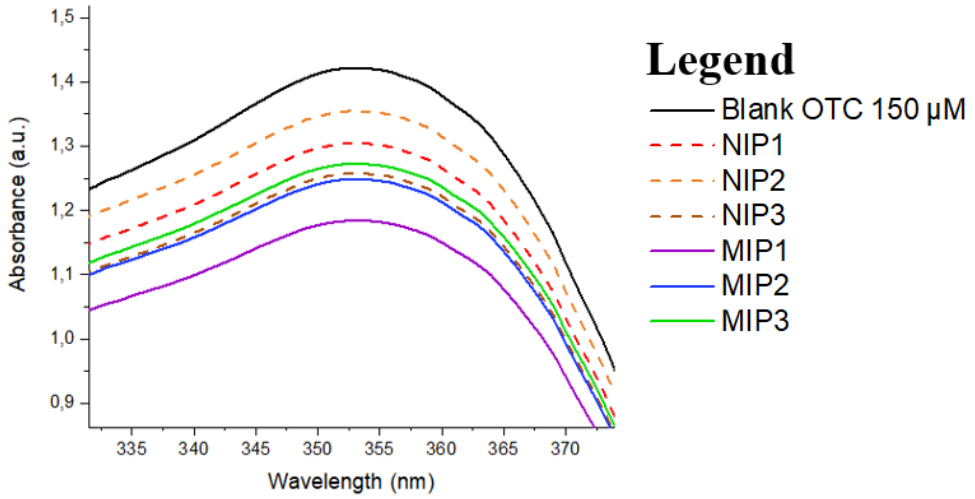

Figure 4.32 – Absorption spectra of three NIPs and MIPs, printed with Formulation 1 and incubated in rebinding solution with molarity 150 µM

At this point, the next step is to obtain the concentration values of OTC rebinding solutions x (column "*Concentration*" of Table 4.21) knowing the absorbance values y (column "*Absorbance*" of Table 4.21) and using the calibration curve:

$$x = \frac{(y - 0.0794)}{0.0091}$$

Then, partition coefficient has been calculated (column "*Partition Coefficient*" of Table 4.21), i.e., the ratio between the substrate bound to the MIP/NIP (Sb) and the substrate still present in solution (Cf):

$$K_p = \frac{S_b}{C_f}$$

Taking as example NIP1, the calculation is the following:

$$K_{pNIP1} = \frac{(147.2088 - 134.3516)}{147.2088} = 0.0873$$

For NIP2, instead:

$$K_{pNIP2} = \frac{(147.2088 - 139.8462)}{147.2088} = 0.0500$$

And so on for all other samples.

Finally, partition coefficients have been graphically represented in Figure 4.33, and the average partition coefficients for NIPs and MIPs have been calculated and represented in Figure 4.34.

	Absorbance	Concentration	Partition coefficient
OTC 150 µM	1.4190	147.2088	
NIP1	1.3020	134.3516	0.0873
NIP2	1.3520	139.8462	0.0500
NIP3	1.2550	129.1868	0.1224
MIP1	1.1820	121.1648	0.1769
MIP2	1.2460	128.1978	0.1291
MIP3	1.2700	130.8352	0.1112

Table 4.21 – Table with absorbance values, concentration values and partition coefficient, for dots printed with Formulation 1 and incubated in rebinding solution 150 µM

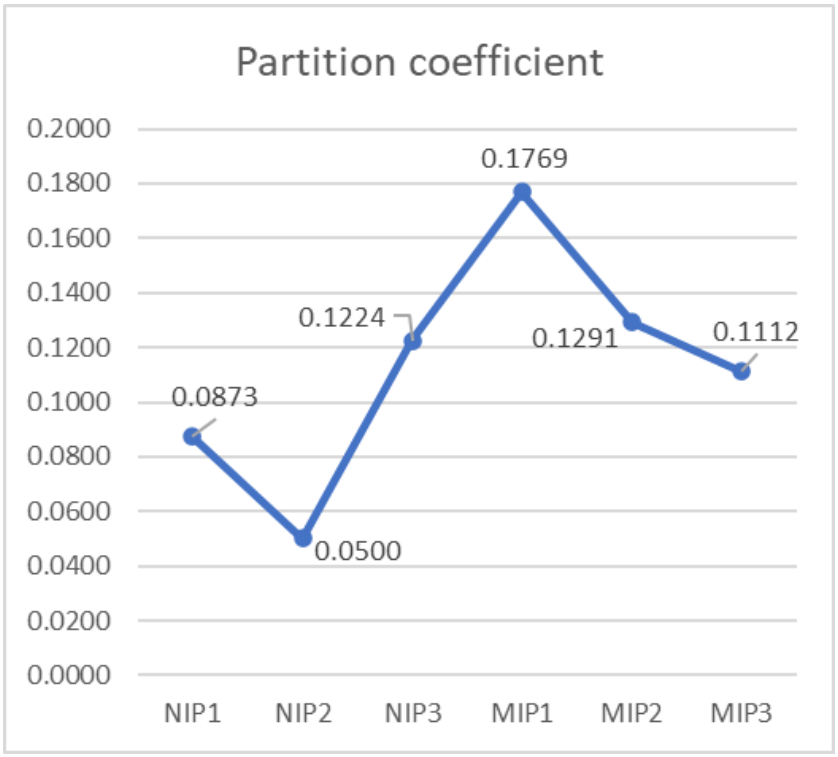

Figure 4.33 – Representation of partition coefficients of NIPs and MIPs printed with Formulation 1 and incubated in rebinding solution 150 µM

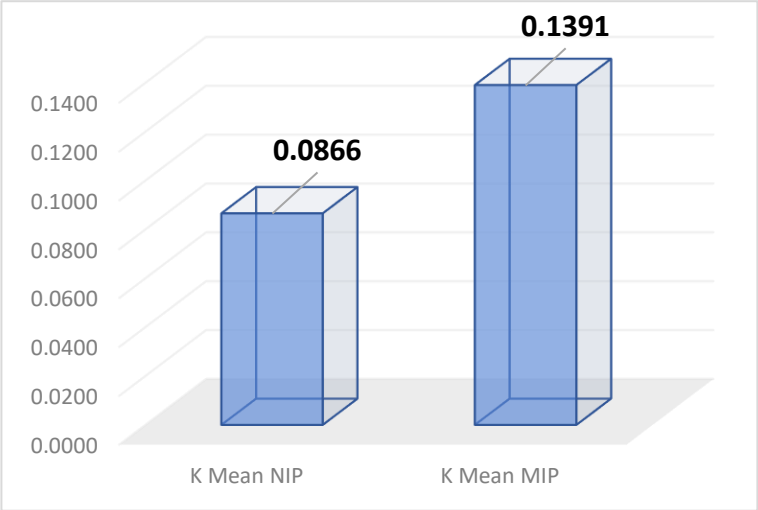

Figure 4.34 – Representation of average partition coefficient for NIPs and MIPs printed with Formulation 1 and incubated in rebinding solution 150 µM

From the comparison between the average partition coefficient of NIPs and MIPs, it can be asserted that MIPs' performance increase of 61.92% compared to NIPs (Figure 4.34).

4.2.1.2 Solution 100 µM

Other six samples, three NIPs and three MIPs, were incubated into blank solutions with molarity 100 µM for one night.

Then, 250 µL of rebinding solution were taken from each of the 6 samples and the absorption spectra were obtained using the plate reader, along with the spectrum of the blank solution (Figure 4.35).

In this case, MIPs performance is not so promising compared to that of NIPs, in fact, as we can see from the picture below, NIP1 is the one that catches the largest amount of OTC than all the other dots.

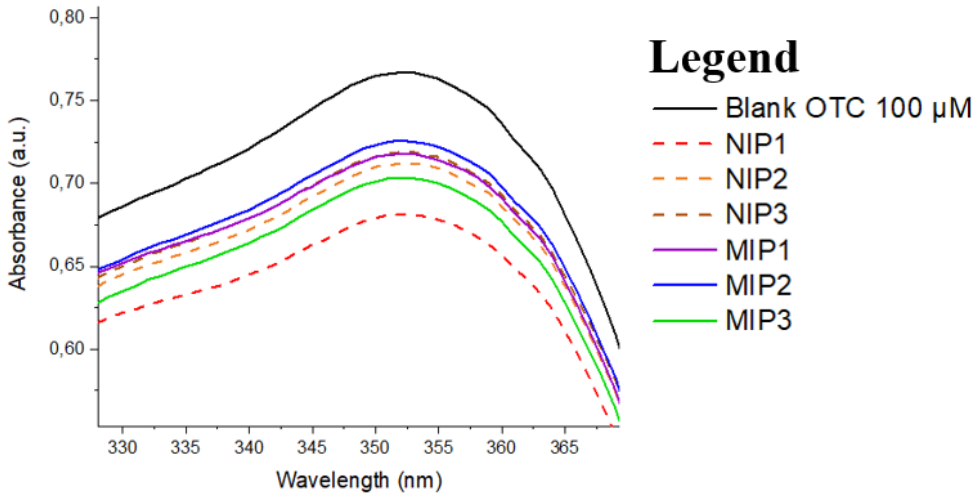

Figure 4.35 – Absorption spectra of three NIPs and MIPs, printed with Formulation 1 and incubated in rebinding solution with molarity 100 µM

In this case, the concentration values of the rebinding solutions, the partition coefficients, and the average partition coefficients for NIPs and for MIPs have also been calculated, proceeding with the same calculations made for the 150 µM solution. All these values are represented in Table 4.22, Figures 4.36 and 4.37.

	Absorbance	Concentration	Partition coefficient
OTC 100 µM	0.7630	75.1209	
NIP1	0.6780	65.7802	0.1243
NIP2	0.7090	69.1868	0.0790
NIP3	0.7160	69.9560	0.0688
MIP1	0.7140	69.7363	0.0717
MIP2	0.7220	70.6154	0.0600
MIP3	0.7000	68.1978	0.0922

Table 4.22 – Table with absorbance values, concentration values and partition coefficient, for dots printed with Formulation 1 and incubated in rebinding solution 100 µM

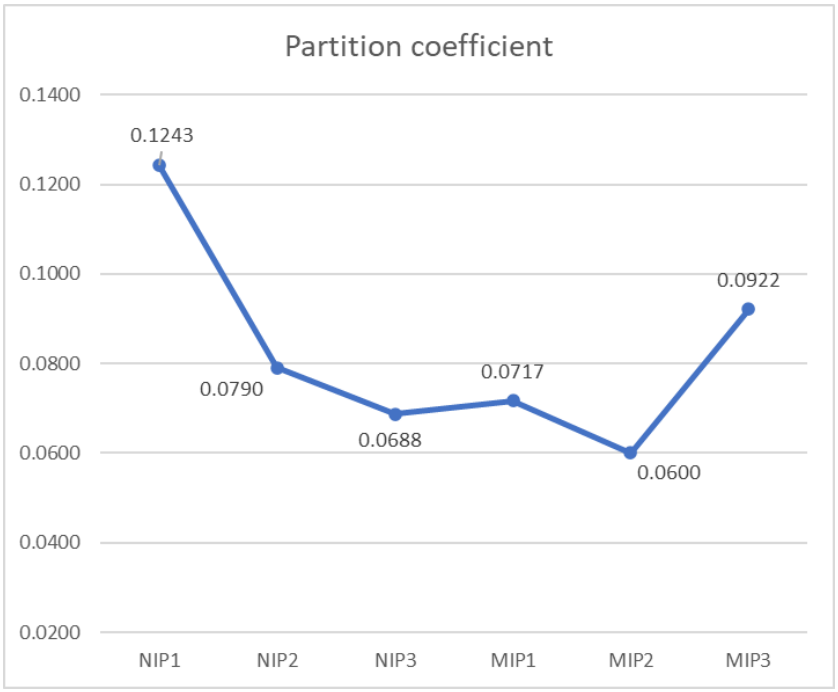

Figure 4.36 – Representation of partition coefficients of NIPs and MIPs printed with Formulation 1 and incubated in rebinding solution 100 µM

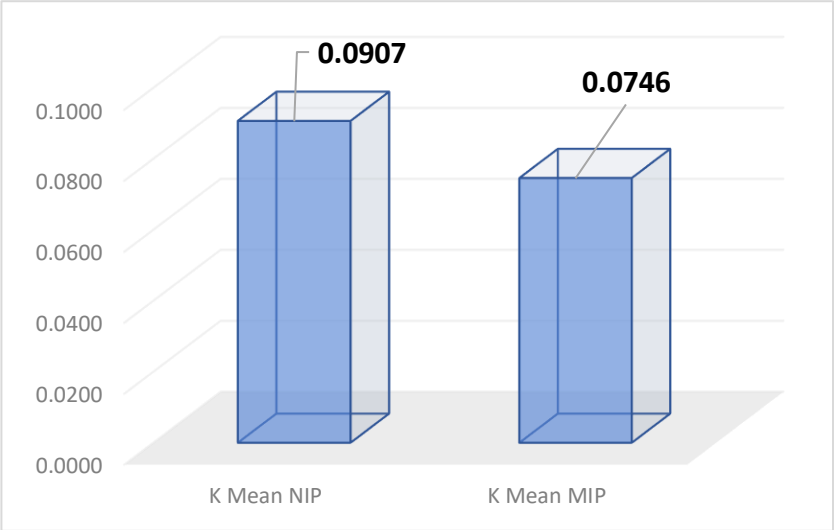

Figure 4.37 – Representation of average partition coefficient for NIPs and MIPs printed with Formulation 1 and incubated in rebinding solution 100 µuM

From the comparison between the average partition coefficient of NIPs and MIPs (Figure 4.37), it can be noted that there is a decrease of 17.58% in the performance of MIPs compared to that of NIPs.

4.2.1.3 Solution 50 µM

Finally, the last six NIPs and MIPs were incubated into blank solutions with molarity 50 µM for one night. The absorption spectra were obtained using the plate reader, taking 250 µL of rebinding solutions and the blank solution (Figure 4.38).

In this case, the overall performance of MIPs is slightly better than that of NIPs.

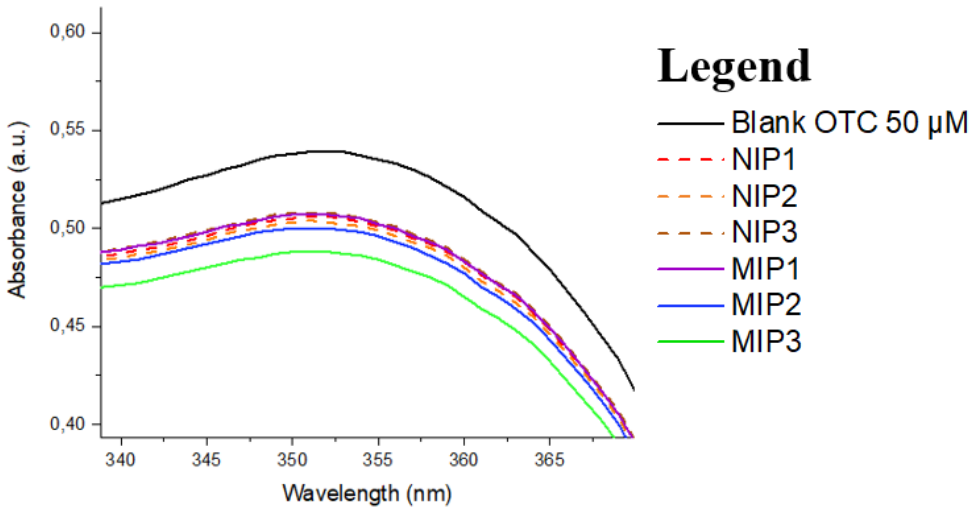

Figure 4.38 – Absorption spectra of three NIPs and MIPs, printed with Formulation 1 and incubated in rebinding solution with molarity 50 µM

The same calculations of the previous cases have been used to obtain absorbance values, concentration values, partition coefficients and average partition coefficients for NIPs and MIPs, as can be seen in Table 4.23, in Figures 4.39 and 4.40.

	Absorbance	Concentration	Partition coefficient
OTC 50 µM	0.5350	50.0659	
NIP1	0.5010	46.3297	0.0746
NIP2	0.4990	46.1099	0.0790
NIP3	0.5030	46.5495	0.0702
MIP1	0.5020	46.4396	0.0724
MIP2	0.4960	45.7802	0.0856
MIP3	0.4840	44.4615	0.1119

Table 4.23 – Table with absorbance values, concentration values and partition coefficient, for dots printed with Formulation 1 and incubated in rebinding solution 50 µM

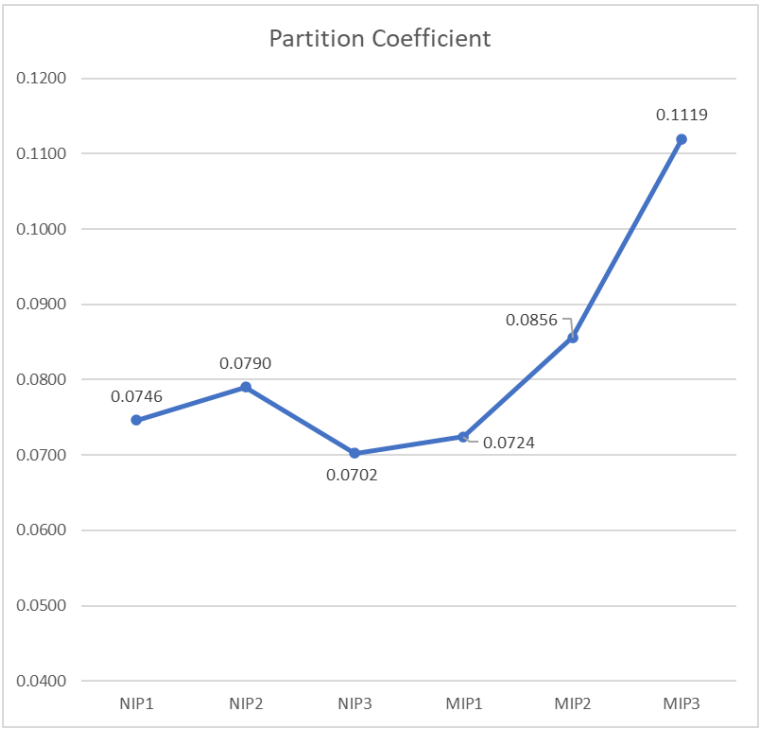

Figure 4.39 – Representation of partition coefficients of NIPs and MIPs printed with Formulation 1 and incubated in rebinding solution 50 µM

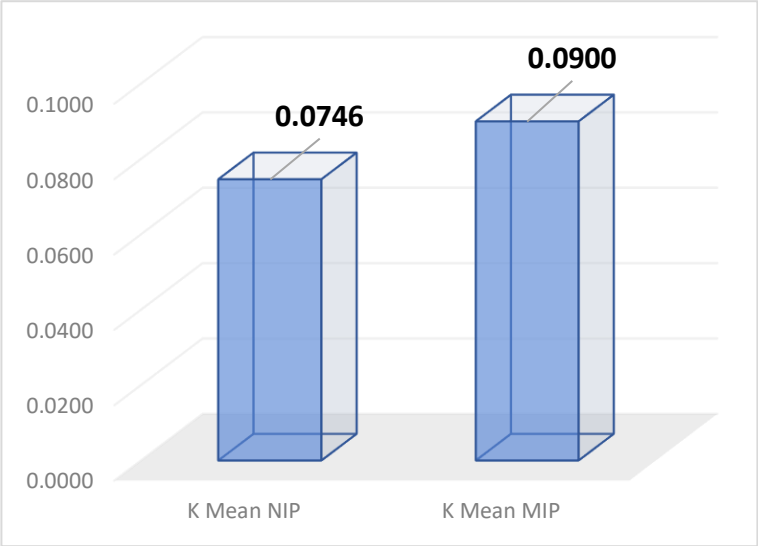

Figure 4.40 – Representation of average partition coefficient for NIPs and MIPs printed with Formulation 1 and incubated in rebinding solution 50 μM

Observing the average partition coefficient of NIPs and MIPs (Figure 4.40), there is a 20% increase of MIPs' performance compared to NIPs.

4.2.2 Comparison of different OTC/MAA ratios

In this section the experiments were conducted using:

- Formulation 2 (OTC:MAA:DPGDA=1:5:20)
- Formulation 3 (OTC:MAA:DPGDA=1:6:20)

For each of the two formulations, 3 repetitions were made, printing for each of them 3 NIPs and 3 MIPs, with the printing parameters described in sections 4.1.3.2 and 4.1.33.

After printing, the samples were subjected to the post curing and template extraction steps described in sections 4.1.4 and 4.1.5. Finally, all samples were incubated inside the 48-multiwell in rebinding solution with molarity 100 μM for three nights.

Subsequently, 250 μL of rebinding solution were taken from each sample and the absorption spectra were obtained using the plate reader, for each of the repetitions performed.

The same parameters as previous experiments have been calculated:

- Concentration values of rebinding solutions using the absorption values at 355 nm and the calibration curve.
- Partition coefficients using the procedure described in section 4.2.1.1.
- Average partition coefficient of NIPs and MIPs.

Then, for each of the two formulations used (2 and 3), an average of the partition coefficients of the NIPs and MIPs of the three repetitions performed was made and the results are reported below.

4.2.2.1 Ratio OTC:MAA:DPGDA=1:5:20

The average partition coefficient of NIPs and MIPs of the three repetitions is represented in Figure 4.41, that shows an increase in performance of MIPs of 28.38% compared to that of NIPs.

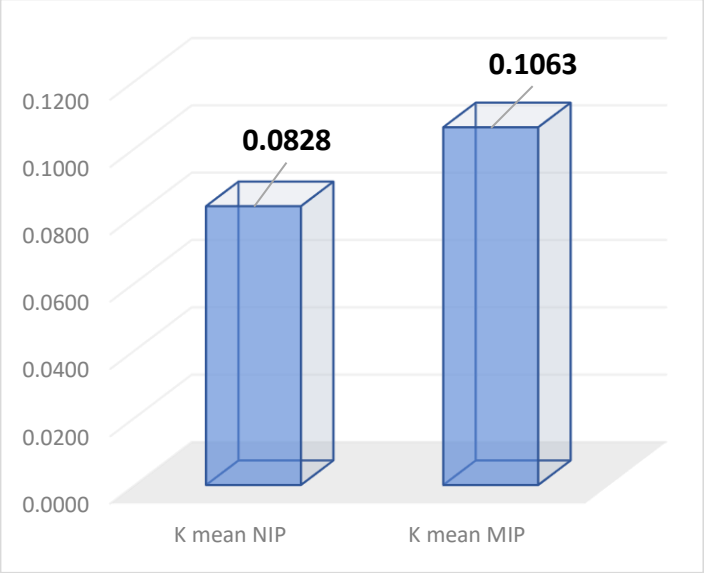

Figure 4.41 – Representation of average partition coefficient for NIPs and MIPs of three repetitions, printed with Formulation 3 and incubated in rebinding solution 100 µM

4.2.2.2 Ratio OTC:MAA:DPGDA=1:6:20

The average partition coefficient of NIPs and MIPs of the three repetitions is represented in Figure 4.42, that shows an increase in performance of MIPs of 29.98% compared to that of NIPs.

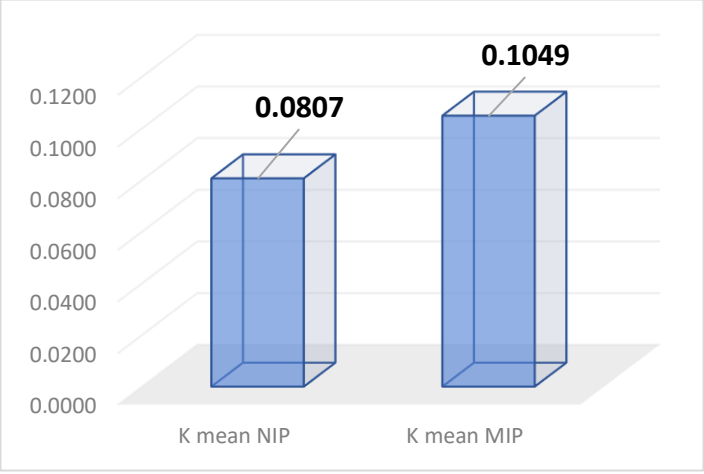

Figure 4.42 – Representation of average partition coefficient for NIPs and MIPs of three repetitions, printed with Formulation 3 and incubated in rebinding solution 100 µM

4.2.3 *Filter 1* with *Formulation 1*

The third macro experiment conducted was the analysis of *Filter 1* selectivity. Two filters were printed with MIP resin with ratio OTC:MAA=1:4, using the parameters described in section 4.1.3.4.

After printing, template was extracted, as showed in Figure 4.29 in section 4.1.5; then, the samples were incubated into blank solution of OTC with molarity 150 µM for three nights.

Finally, 250 µL of rebinding solution were taken from each sample and the absorption spectra were obtained using the plate reader, along with the spectrum of the blank solution (Figure 4.43). Even in this case, the signals of both MIPs post rebinding is lower than that of the solution pre rebinding, meaning that the filters have capture a certain amount of OTC.

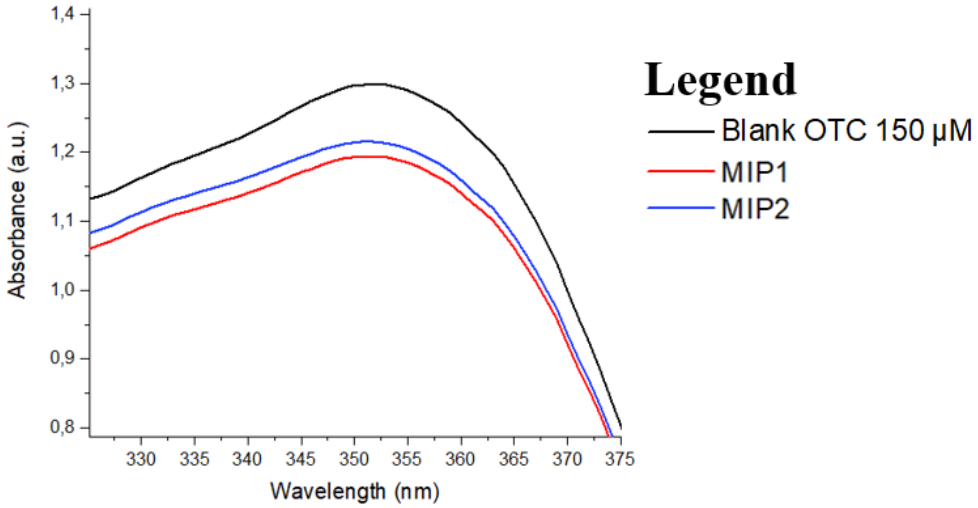

Figure 4.43 – Absorption spectra of two Filter 1, printed with Formulation 1 and incubated in rebinding solution with molarity 150 µM

Then, concentration values have been calculated with the help of the calibration curve and reported in Table 4.24.

	Absorbance	Concentration
OTC 150 µM	1.2900	133.0329
MIP1	1.1950	122.5934
MIP2	1.1850	121.4945
Average of MIP1 and MIP2		122.0439

Table 4.24 – Table with absorbance values and concentration values Filter 1 printed with Formulation 1 and incubated in rebinding solution 150 µM

Finally, an average of the concentration values of MIP1 and MIP2 has been calculated and represented in red in Table 4.24. In Figure 4.44 the concentration of the blank solution 150 µM and the average concentration calculated before are represented. It can be noticed that the filters capture an average of 10 µM of OTC.

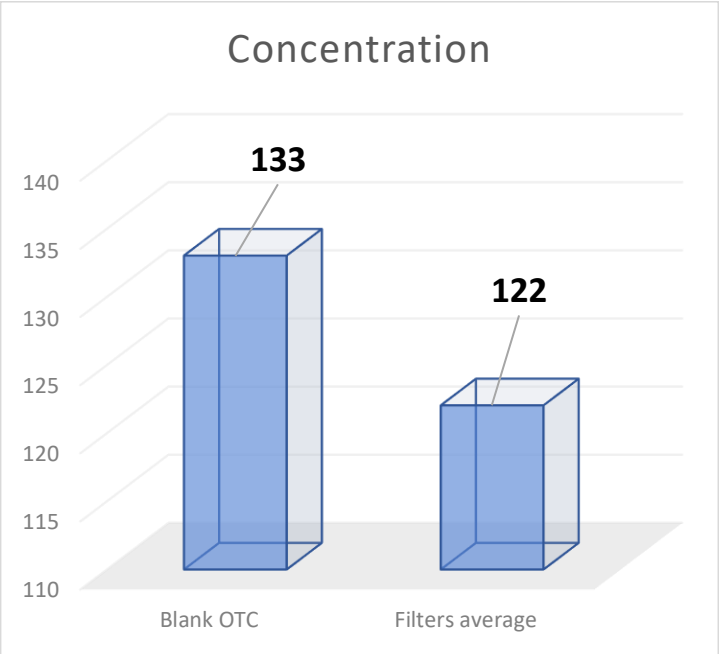

Figure 4.44 – Representation of concentrations of OTC blank solution 150 µM and average concentration of MIP1 and MIP2.

4.2.4 *Filter 3* with *Formulation 6*

The experiment with use of salt was conducted using Formulation 6 (OTC:MAA:DPGDA=1:5:20 with 20% salt); three *Filter 3* with NIP resin and three *Filter 3* with MIP resin were printed, using the parameters described in section 4.1.3.7.

After printing, salt and template were extracted, following the procedures described in the previous sections. Then, the 6 samples were incubated into blank solutions with molarity 100 µM for three nights.

After that, 250 µL of rebinding solution were taken from each of the 6 samples and the absorption spectra were obtained using the plate reader, along with the spectrum of the blank solution (Figure 4.45).

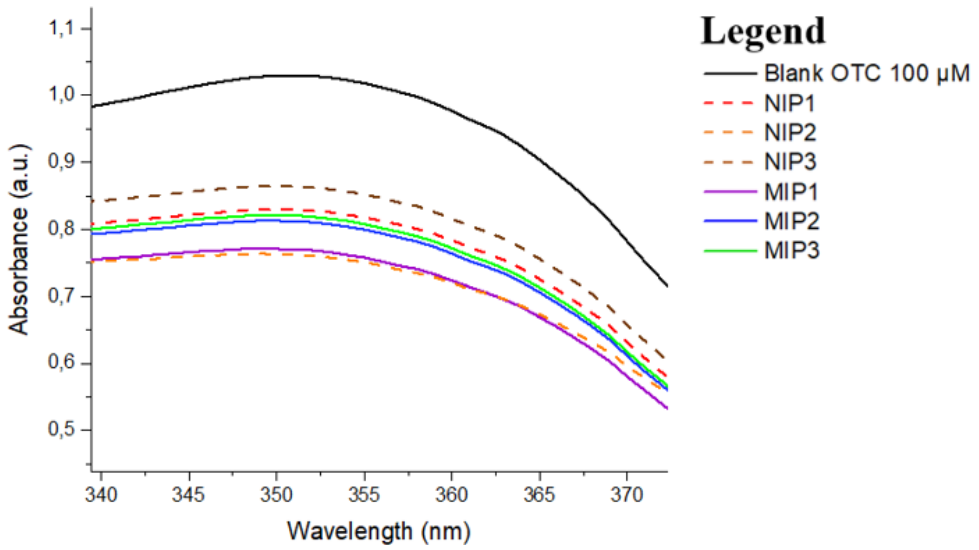

Figure 4.45 – Absorption spectra of three NIPs and MIPs, printed with Formulation 6 and incubated in rebinding solution with molarity 100 µM

The same parameters as previous experiments have been calculated and represented too (Table 4.25 and Figure 4.46):

- Concentration values of rebinding solutions using the absorption values at 355 nm and the calibration line.
- Partition coefficients using the procedure described in section 4.2.1.1.
- Average partition coefficient of NIPs and MIPs.

	Absorbance	Concentration	Partition coefficient
OTC 100 µM	1.0180	103.1429	
NIP1	0.8180	81.1648	0.2131
NIP2	0.7510	73.8022	0.2845
NIP3	0.8520	84.9011	0.1769
MIP1	0.7580	74.5714	0.2770
MIP2	0.8000	79.1868	0.2323
MIP3	0.8080	80.0659	0.2237

Table 4.25 – Table with absorbance values, concentration values and partition coefficient, for dots printed with Formulation 6 and incubated in rebinding solution 100 µM

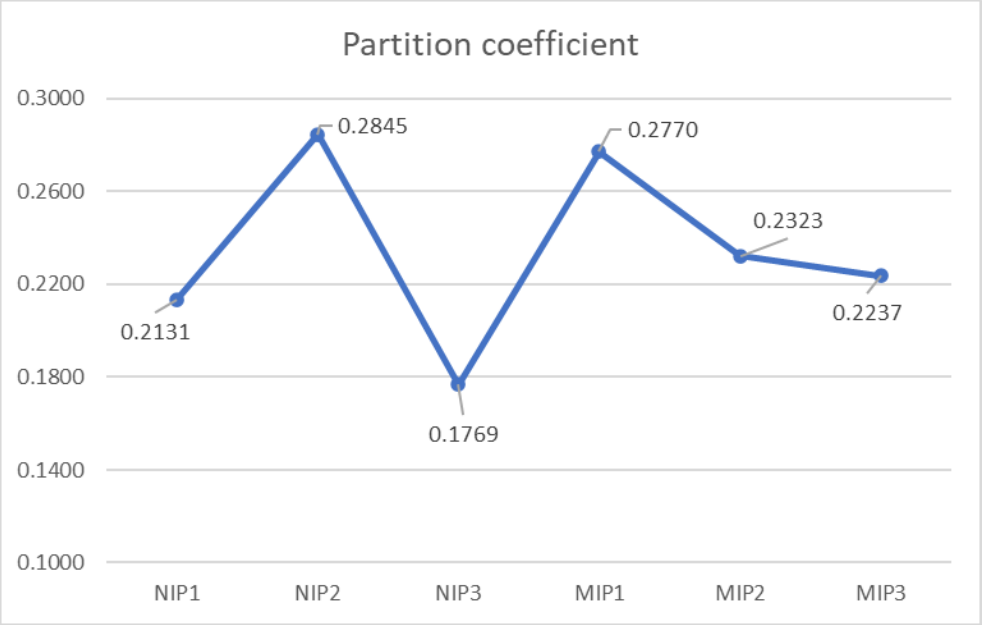

Figure 4.46 – Representation of partition coefficients of NIPs and MIPs printed with Formulation 6 and incubated in rebinding solution 100 µM

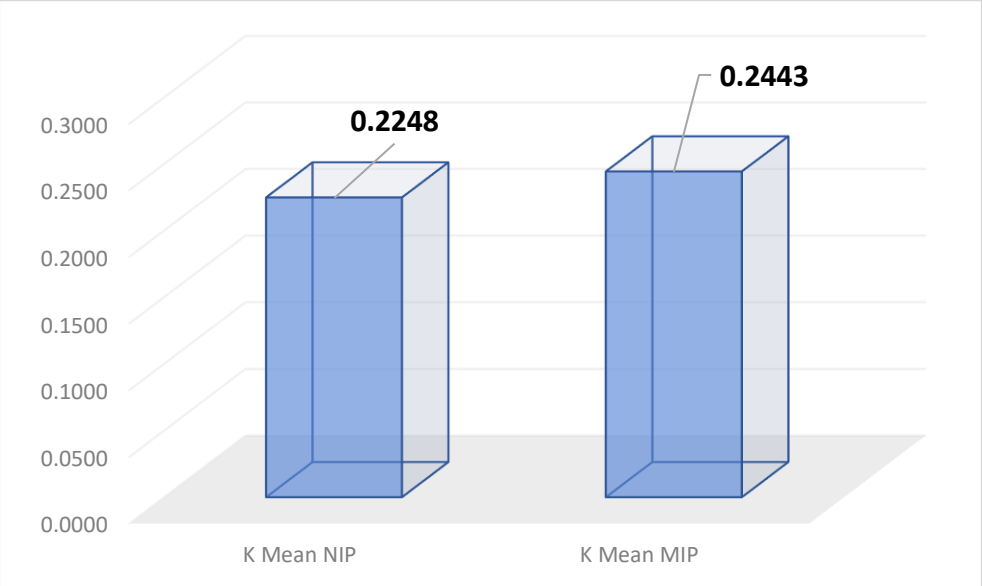

Figure 4.47 – Representation of average partition coefficient for NIPs and MIPs printed with Formulation 6 and incubated in rebinding solution 100 µM

Observing the average partition coefficient of NIPs and MIPs (Figure 4.47), there is an 8,56 % increase of MIPs' performance compared to NIPs.

4.2.5 Experiments' results

The first experiment using rebinding solutions with different molarities provided the following results:

- 150 µM – MIPs' performance increase of 61.92% compared to NIPs.
- 100 µM – MIPs' performance decrease of 17.58% compared to NIPs.
- 50 µM – MIPs' performance increase of 20% compared to NIPs.

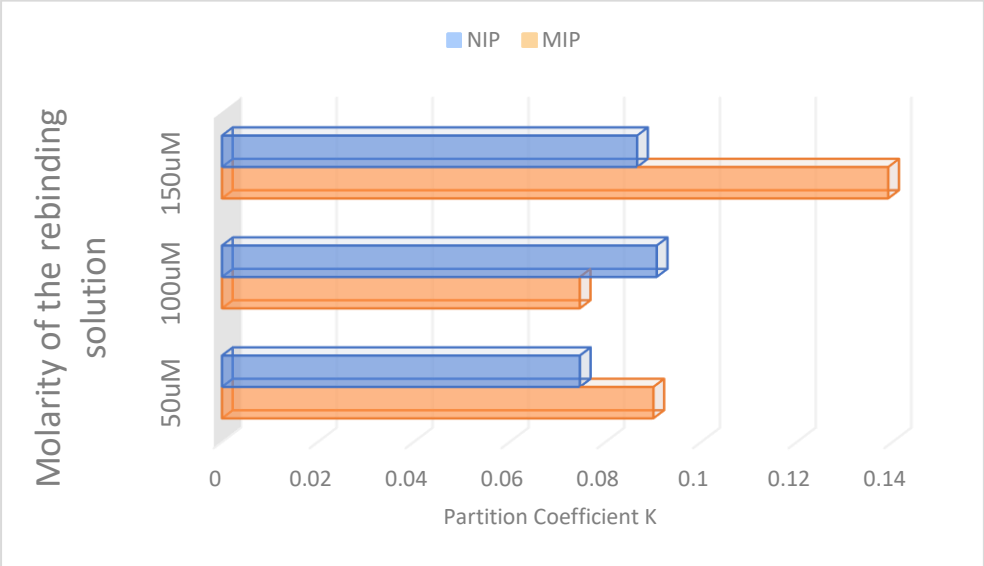

Figure 4.48 – Comparison of partition coefficients for NIPs and MIPs printed with Formulation 1 and incubated in rebinding solutions with different molarities

So, as it can be noticed in Figure 4.48, the best result is obtained with the rebinding solution with molarity of 150 µM. Nevertheless, more repetitions under the same conditions are required to obtain results that are significantly more reliable.

In second experiment, the increase in MIPs' performance compared to that of NIPs is about 30% for both formulations, but the one with OTC:MAA=1:6 seems to work slightly better than that with OTC:MAA=1:5 (Figure 4.49).

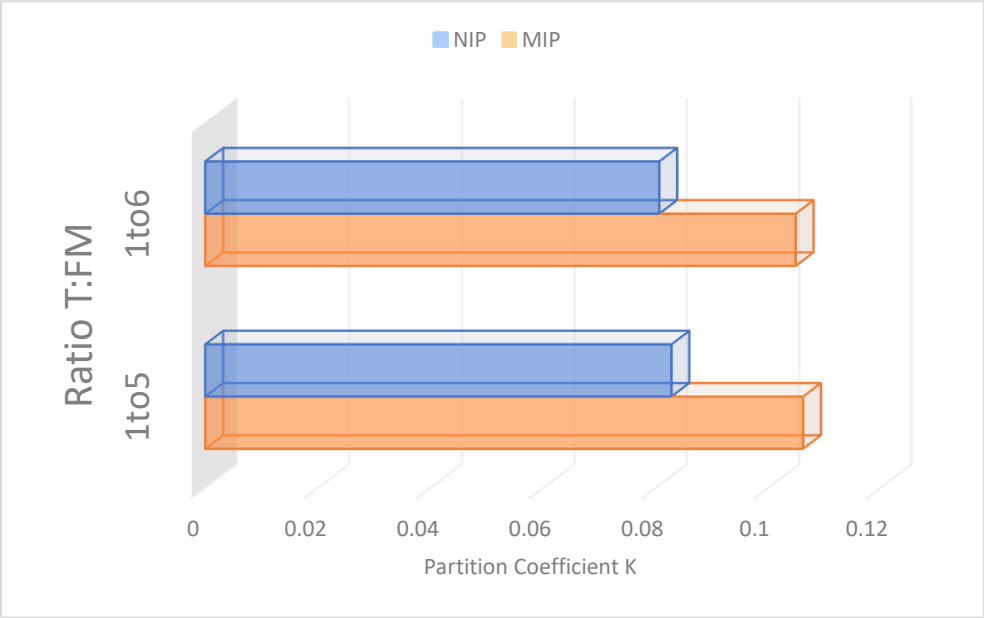

Figure 4.49 – Comparison of partition coefficients for NIPs and MIPs printed with Formulation 2 and , incubated in rebinding solution 100 µM

The results of the third experiment show that the filters made with MIP resin captured an average of 10 µM of OTC; however, it is not possible to compare them with NIPs because, as explained in section 4.1.3.4, it was difficult to print the geometry Filter 1 with NIP resin.

Finally, the fourth experiment conducted with formulation 6 (OTC:MAA=1:5 and 20% of salt) provided an 8.56 % increase of MIPs' performance compared to NIPs. It is not a very encouraging result, because the percentage of increase is really low. However, even in this case it is necessary to perform a greater number of repetitions of the same experiment to have more reliable results.

To sum up, although the results obtained from all the experiments carried out are discreetly good and promising, there is still work to be done to improve the imprinting and therefore the ability of MIPs compared to NIPs to capture the target molecule. Furthermore, it is also necessary to carry out further experiments with the salt-containing formulation, to create interconnected porosities that were not obtained in the samples printed during this thesis.

Chapter 5: Conclusions and future works

The aim of my thesis was to fabricate Molecularly Imprinted Polymers (MIPs), which are synthetic receptors that imitate the natural molecular recognition mechanism of biological receptors, and they are capable of detecting targets in a non-invasive manner.

MIPs could be fabricated using a lot of different techniques, already extensively studied in literature, but in this thesis work Additive Manufacturing, and in particular Digital Light Processing (DLP) has been used. This is a type of VAT printing technique that uses UV light to photopolymerize liquid resin. DLP has been chosen because it is a promising method for creating complex 3D structures, which are precisely defined, self-standing and with high resolution.

First, different geometries have been realized using a CAD software, i.e., a simple dot and three types of filters, constituted by the alternation of planes and pillars; then, different formulations have been prepared, with different ratios within the ingredients (template, functional monomer and crosslinker). Finally, to improve the surface area and to create porosities within the matrix, formulations with different percentages of salt were prepared too.

The most important passage was to optimize the printing parameters (light intensity, time of exposure and slice thickness) for each geometry and formulation. Once the samples were printed, the ability of the investigated materials to operate as MIPs was assessed, i.e., the capacity to capture the target molecule used during the imprinting procedure. To do so, the batch rebinding method was used, comparing rebinding solutions with different molarities, by means of UV-Vis spectroscopy.

Samples printing was successful and high resolution was achieved for:

- Dots with all the formulations, with and without salt, both NIPs and MIPs.
- Filter 1, printed with MIP Formulation 1 (OTC:MAA:DPGDA=1:4:20).
- Filter 3 with Formulation 6 (OTC:MAA:DPGDA=1:4:20 and 20% of salt), both NIPs and MIPs.

From the analysis of the results obtained using different formulations, those that have provided the best results are the one with ratio OTC:MAA=1:5 and OTC:MAA=1:6; in fact, the performance of the MIPs was approximately 30% higher than that of the NIPs for both formulations.

Considering the different rebinding solutions used, the one that has provided the best results is that with molarity of 150 μM.

Finally, concerning the formulation with 20% salt, samples with matrix that presents discrete porosity were obtained and a performance of MIPs about 8% higher than that of NIPs was obtained too. However, this percentage of increase is really low and so it's necessary to perform a greater number of repetitions of the same experiment to have more reliable results and to obtain interconnected porosities, that should improve the ability of MIPs to capture the target molecule.

So, to continue this thesis project and to obtain better results, future works could include:

- Further repetition of the same experiments carried out during this thesis to improve the reliability of the obtained results.
- Print filters with different formulations than the one used (for example, formulations with OTC:MAA=1:5 and OTC:MAA=1:6).
- Test other ingredients to prepare the formulations, for example using a different functional monomer or crosslinker.
- Test MIPs' specificity by performing the batch rebinding in solutions that contain different target molecules than the one used during the imprinting procedure.
- Improve the creation of interconnected porosities with controlled size within the samples' matrix, for example grinding salt particles and then sieving them.
- Develop a technique to automate the washing procedure, so that there is no need for the constant presence of the operator.
- Discover more about aspects like long-term toxicity, biodegradability, biocompatibility and distributions in fluids to enable the use of MIPs in vivo applications.

In conclusion, Molecularly Imprinted Polymers are an extremely valuable resource in many different fields of science, and they have a wide range of potential applications. For example, chromatographic separation, environment/food purification, recognition elements for sensors and biosensors, catalysis, targeted drug delivery. So, it is worthwhile to keep researching about them, and to optimize their fabrication through 3D printing.

References

[1] Murray A, Örmeci B. Application of molecularly imprinted and non-imprinted polymers for removal of emerging contaminants in water and wastewater treatment: a review. *Environmental Science and Pollution Research*. 2012;19(9):3820-3830. doi:10.1007/s11356-012-1119-2

[2] Wang GN, Yang K, Liu HZ, Feng MX, Wang JP. Molecularly imprinted polymer-based solid phase extraction combined high performance liquid chromatography for determination of fluoroquinolones in milk. *Analytical Methods*. 2016;8(27):5511-5518. doi:10.1039/c6ay00810k

[3] BelBruno JJ. Molecularly imprinted polymers. *Chemical Reviews*. 2018;119(1):94-119. doi:10.1021/acs.chemrev.8b00171

[4] Lichtenthaler FW. 100 Years"Schlüssel-Schloss-Prinzip": What Made Emil Fischer Use this Analogy? *Angewandte Chemie*. 1995;33(2324):2364-2374. doi:10.1002/anie.199423641

[5] Vasapollo G, Del Sole R, Mergola L, et al. Molecularly Imprinted Polymers: present and Future Prospective. *International Journal of Molecular Sciences*. 2011;12(9):5908-5945. doi:10.3390/ijms12095908

[6] Supraja. Mechanism of enzyme action (Activation Energy and Lock and Key hypothesis diagram). *Biology Brain*. Published online May 12, 2022. https://www.biologybrain.com/mechanism-of-enzyme-action/

[7] Sajini T, Mathew B. A brief overview of molecularly imprinted polymers: Highlighting computational design, nano and photo-responsive imprinting. *Talanta Open*. 2021;4:100072. doi:10.1016/j.talo.2021.100072

[8] Frost J. How To Interpret R-squared in Regression Analysis. *Statistics by Jim*. Published online July 7, 2023. https://statisticsbyjim.com/regression/interpret-r-squared-regression/

[9] Hu Y, Pan J, Zhang K, Lian H, Li G. Novel applications of molecularly-imprinted polymers in sample preparation. *Trends in Analytical Chemistry*. 2013;43:37-52. doi:10.1016/j.trac.2012.08.014

[10] Akgönüllü S, Kılıç S, Esen C, Denizli A. Molecularly imprinted Polymer-Based sensors for protein detection. *Polymers*. 2023;15(3):629. doi:10.3390/polym15030629

[11] Wulff G, Vesper W, Grobe-Einsler R, Sarhan A. Enzyme-analogue built polymers, 4†. On the synthesis of polymers containing chiral cavities and their use for the resolution of racemates. *Die Makromolekulare Chemie*. 1977;178(10):2799-2816. doi:10.1002/macp.1977.021781004

[12] Wulff G, Vietmeier J. Enzyme-analogue built polymers, 26†. Enantioselective synthesis of amino acids using polymers possessing chiral cavities obtained by an imprinting procedure with template molecules. *Die Makromolekulare Chemie*. 1989;190(7):1727-1735. doi:10.1002/macp.1989.021900724

[13] Wulff G, Best W, Akelah A. Enzyme-analogue built polymers, 17 Investigations on the racemic resolution of amino acids. *Reactive Polymers, Ion Exchangers, Sorbents*. 1984;2(3):167-174. doi:10.1016/0167-6989(84)90132-6

[14] Sallacan N, Zayats M, Bourenko T, Kharitonov AAB, Willner I. Imprinting of Nucleotide and Monosaccharide Recognition Sites in Acrylamidephenylboronic Acid−Acrylamide Copolymer Membranes Associated with Electronic Transducers. *Analytical Chemistry*. 2002;74(3):702-712. doi:10.1021/ac0109873

[15] Wulff G, Schauhoff S. Enzyme-analog-built polymers. 27. Racemic resolution of free sugars with macroporous polymers prepared by molecular imprinting. Selectivity dependence on the arrangement of functional groups versus spatial requirements. *Journal of Organic Chemistry*. 1991;56(1):395-400. doi:10.1021/jo00001a071

[16] Shea KJ, Dougherty TK. Molecular recognition on synthetic amorphous surfaces. The influence of functional group positioning on the effectiveness of molecular recognition. *Journal of the American Chemical Society*. 1986;108(5):1091-1093. doi:10.1021/ja00265a046

[17] Shea KJ, Sasaki DY. An analysis of small-molecule binding to functionalized synthetic polymers by 13C CP/MAS NMR and FT-IR spectroscopy. *Journal of the American Chemical Society*. 1991;113(11):4109-4120. doi:10.1021/ja00011a009

[18] Wulff G, Wolf G. Zur Chemie von Haftgruppen, VI. Über die Eignung verschiedener Aldehyde und Ketone als Haftgruppen für Monoalkohole. *Chemische Berichte*. 1986;119(6):1876-1889. doi:10.1002/cber.19861190610

[19] Wulff G. Enzyme-like catalysis by molecularly imprinted polymers. *Chemical Reviews*. 2001;102(1):1-28. doi:10.1021/cr980039a

[20] Haupt K, Linares A, Bompart M, Bui BTS. Molecularly Imprinted Polymers. In: *Topics in Current Chemistry*. Springer Science+Business Media; 2011:1-28. doi:10.1007/128_2011_307

[21] Arshady R, Mosbach K. Synthesis of substrate-selective polymers by host-guest polymerization. *Macromol Chem Phys*. 1981;182(2):687-692. doi:10.1002/macp.1981.021820240

[22] Shah N. A brief overview of molecularly imprinted polymers: from basics to applications. *ResearchGate*. Published online January 1, 2012. https://www.researchgate.net/publication/281069506_A_Brief_Overview_of_Molecularly_Imprinted_Polymers_From_Basics_to_Applications

[23] Umpleby RJ, Baxter SD, Chen Y, Shah RN, Shimizu KD. Characterization of Molecularly Imprinted Polymers with the Langmuir−Freundlich Isotherm. *Analytical Chemistry*. 2001;73(19):4584-4591. doi:10.1021/ac0105686

[24] Whitcombe MJ, Rodriguez M, Villar P, Vulfson EN. A New Method for the Introduction of Recognition Site Functionality into Polymers Prepared by Molecular Imprinting: Synthesis and Characterization of Polymeric Receptors for Cholesterol. *Journal of the American Chemical Society*. 1995;117(27):7105-7111. doi:10.1021/ja00132a010

[25] Chen L, Xu S, Li J. Recent advances in molecular imprinting technology: current status, challenges and highlighted applications. *Chemical Society Reviews*. 2011;40(5):2922. doi:10.1039/c0cs00084a

[26] Sellergren B. *Molecularly Imprinted Polymers - Man-Made Mimics of Antibodies and Their Applications in Analytical Chemistry*.; 2001. doi:10.1016/s0167-9244(01)x8001-3

[27] Ellwanger A, Berggren C, Bayoudh S, et al. Evaluation of methods aimed at complete removal of template from molecularly imprinted polymers. *Analyst*. 2001;126(6):784-792. doi:10.1039/b009693h

[28] Chen L, Xu S, Li J. Recent advances in molecular imprinting technology: current status, challenges and highlighted applications. *Chemical Society Reviews*. 2011;40(5):2922. doi:10.1039/c0cs00084a

[29] El-Schich Z, Zhang Y, Feith M, et al. Molecularly imprinted polymers in biological applications. *BioTechniques*. 2020;69(6):406-419. doi:10.2144/btn-2020-0091

[30] Salas A, Zanatta M, Sans V, Roppolo I. Chemistry in light-induced 3D printing. *ChemTexts*. 2023;9(1). doi:10.1007/s40828-022-00176-z

[31] Spivak DA. Optimization, evaluation, and characterization of molecularly imprinted polymers. *Advanced Drug Delivery Reviews*. 2005;57(12):1779-1794. doi:10.1016/j.addr.2005.07.012

[32] Sellergren B, Shea KJ. Influence of polymer morphology on the ability of imprinted network polymers to resolve enantiomers. *Journal of Chromatography A*. 1993;635(1):31-49. doi:10.1016/0021-9673(93)83112-6

[33] Andersson LI. Application of Molecular Imprinting to the Development of Aqueous Buffer and Organic Solvent Based Radioligand Binding Assays for (*S*)-Propranolol. *Analytical Chemistry*. 1996;68(1):111-117. doi:10.1021/ac950668

[34] Bengtsson H, Roos U, Andersson LI. Molecular imprint based radioassay for direct determination of S-Propranolol in human plasma. *Analytical Communications*. 1997;34(9):233-235. doi:10.1039/a703977h

[35] Hu Y, Liu R, Zhang Y, Li G. Improvement of extraction capability of magnetic molecularly imprinted polymer beads in aqueous media via dual-phase solvent system. *Talanta*. 2009;79(3):576-582. doi:10.1016/j.talanta.2009.04.029

[36] Yan H, Row KH, Yang G. Water-compatible molecularly imprinted polymers for selective extraction of ciprofloxacin from human urine. *Talanta*. Published online November 9, 2007. doi:10.1016/j.talanta.2007.11.002

[37] Benito-Peña E, Martins SAM, Orellana G, Moreno-Bondi MC. Water-compatible molecularly imprinted polymer for the selective recognition of fluoroquinolone antibiotics in biological samples. *Analytical and Bioanalytical Chemistry*. 2008;393(1):235-245. doi:10.1007/s00216-008-2405-1

[38] Yang Y, Long Y, Cao Q, Li K, Liu F. Molecularly imprinted polymer using β-cyclodextrin as functional monomer for the efficient recognition of bilirubin. *Analytica Chimica Acta*. 2008;606(1):92-97. doi:10.1016/j.aca.2007.10.044

[39] Kyzas GZ, Bikiaris DN, Lazaridis NK. Selective separation of basic and reactive dyes by molecularly imprinted polymers (MIPs). *Chemical Engineering Journal*. 2009;149(1-3):263-272. doi:10.1016/j.cej.2008.11.002

[40] Yang K, Berg MM, Zhao C, Ye L. One-Pot synthesis of hydrophilic molecularly imprinted nanoparticles. *Macromolecules*. 2009;42(22):8739-8746. doi:10.1021/ma901761z

[41] Spivak DA, Gilmore M, Shea KJ. Evaluation of binding and origins of specificity of 9-Ethyladenine imprinted polymers. *Journal of the American Chemical Society*. 1997;119(19):4388-4393. doi:10.1021/ja963510v

[42] Kempe M, Mosbach K. Binding studies on substrate- and Enantio-Selective molecularly imprinted polymers. *Analytical Letters*. Published online July 1, 1991. doi:10.1080/00032719108052959

[43] Wulff G, Kemmerer R, Vietmeier J, Hg P. CHIRALITY OF VINYL POLYMERS. THE PREPARATION OF CHIRAL CAVITIES IN SYNTHETIC POLYMERS. *NOUVEAU JOURNAL DE CHIMIE*. Published online January 1, 1982. http://pascal-francis.inist.fr/vibad/index.php?action=getRecordDetail&idt=PASCAL83X0498348

[44] Sellergren B. Molecular imprinting by noncovalent interactions. Enantioselectivity and binding capacity of polymers prepared under conditions favoring the formation of template complexes. *Die Makromolekulare Chemie*. 1989;190(11):2703-2711. doi:10.1002/macp.1989.021901104

[45] Kim HJ, Spivak DA. New Insight into Modeling Non-Covalently Imprinted Polymers. *Journal of the American Chemical Society*. 2003;125(37):11269-11275. doi:10.1021/ja0361502

[46] Kim HJ, Spivak DA. New Insight into Modeling Non-Covalently Imprinted Polymers. *Journal of the American Chemical Society*. 2003;125(37):11269-11275. doi:10.1021/ja0361502

[47] Chianella I, Lotierzo M, Piletsky SA, et al. Rational design of a polymer specific for Microcystin-LR using a computational approach. *Analytical Chemistry*. 2002;74(6):1288-1293. doi:10.1021/ac010840b

[48] Wu L, Li Y. Study on the recognition of templates and their analogues on molecularly imprinted polymer using computational and conformational analysis approaches. *Journal of Molecular Recognition*. 2004;17(6):567-574. doi:10.1002/jmr.688

[49] Yañez F, Chianella I, Piletsky SA, Concheiro A. Computational modeling and molecular imprinting for the development of acrylic polymers with high affinity for bile salts. *Analytica Chimica Acta*. 2010;659(1-2):178-185. doi:10.1016/j.aca.2009.11.054

[50] Andersson HS, Karlsson JG, Piletsky SA, Koch-Schmidt AC, Mosbach K, Nicholls IA. Study of the nature of recognition in molecularly imprinted polymers, II. *Journal of Chromatography A*. 1999;848(1-2):39-49. doi:10.1016/s0021-9673(99)00483-5

[51] Ramstroem O, Andersson LI, Mosbach K. Recognition sites incorporating both pyridinyl and carboxy functionalities prepared by molecular imprinting. *Journal of Organic Chemistry*. 1993;58(26):7562-7564. doi:10.1021/jo00078a041

[52] Lübke C, Lübke M, Whitcombe MJ, Vulfson EN. Imprinted Polymers Prepared with Stoichiometric Template−Monomer Complexes: Efficient Binding of Ampicillin from Aqueous Solutions. *Macromolecules*. 2000;33(14):5098-5105. doi:10.1021/ma000467u

[53] Piletsky SA, Andersson HS, Nicholls IA. Combined hydrophobic and electrostatic Interaction-Based recognition in molecularly imprinted polymers. *Macromolecules*. 1999;32(3):633-636. doi:10.1021/ma9812736

[54] Ramström O, Ansell RJ. Molecular imprinting technology: challenges and prospects for the future. *Chirality*. 1998;10(3):195-209. doi:10.1002/(sici)1520-636x(1998)10:3

[55] Yin J, Yang G, Chen Y. Rapid and efficient chiral separation of nateglinide and its l-enantiomer on monolithic molecularly imprinted polymers. *Journal of Chromatography A*. 2005;1090(1-2):68-75. doi:10.1016/j.chroma.2005.06.078

[56] Simon R, Houck S, Spivak DA. Comparison of particle size and flow rate optimization for chromatography using one-monomer molecularly imprinted polymers versus traditional non-covalent molecularly imprinted polymers. *Analytica Chimica Acta*. 2005;542(1):104-110. doi:10.1016/j.aca.2005.03.048

[57] Gao D, Zhang Z, Wu M, Xie C, Guan G, Wang D. A surface functional Monomer-Directing strategy for highly dense imprinting of TNT at surface of silica nanoparticles. *Journal of the American Chemical Society*. 2007;129(25):7859-7866. doi:10.1021/ja070975k

[58] Rezanavaz R, Petcu M, Guen MJL, Dubois A. Three-Dimensional Printing of Molecularly Imprinted Polymers by Digital Light Processing for Copper Ion Sequestration. *ResearchGate*. Published online September 27, 2022. doi:10.1089/3dp.2022.0107

[59] Lorenzo RA, Carro AM, Alvarez-Lorenzo C, Concheiro A. To remove or not to remove? The challenge of extracting the template to make the cavities available in molecularly imprinted polymers (MIPs). *International Journal of Molecular Sciences*. 2011;12(7):4327-4347. doi:10.3390/ijms12074327

[60] Martin P, Jones GR, Stringer F, Wilson ID. Comparison of normal and reversed-phase solid phase extraction methods for extraction of β-blockers from plasma using molecularly imprinted polymers. *Analyst*. 2003;128(4):345-350. doi:10.1039/b211787h

[61] Fu G, Yu H, Zhu J. Imprinting effect of protein-imprinted polymers composed of chitosan and polyacrylamide: A re-examination. *Biomaterials*. 2008;29(13):2138-2142. doi:10.1016/j.biomaterials.2008.01.019

[62] De Castro MDL, Priego-Capote F. Soxhlet extraction: Past and present panacea. *Journal of Chromatography A*. 2010;1217(16):2383-2389. doi:10.1016/j.chroma.2009.11.027

[63] Eskilsson CS, Björklund E. Analytical-scale microwave-assisted extraction. *Journal of Chromatography A*. 2000;902(1):227-250. doi:10.1016/s0021-9673(00)00921-3

[64] Forchheimer D, Luo G, Montelius L, Ye L. Molecularly imprinted nanostructures by nanoimprint lithography. *Analyst*. 2010;135(6):1219. doi:10.1039/c0an00132e

[65] Salmean C, Dimartino S. 3D-Printed Stationary Phases with Ordered Morphology: State of the Art and Future Development in Liquid Chromatography. *Chromatographia*. 2018;82(1):443-463. doi:10.1007/s10337-018-3671-5

[66] Reddy R. ADDITIVE MANUFACTURING TECHNOLOGIES. *BEST: International Journal of Management, Information Technology and Engineering*. 2016;4(7). https://www.researchgate.net/profile/Solomon-Tolcha-2/publication/334545466_ADDITIVE_MANUFACTURING_TECHNOLOGIES/links/5d30943a92851cf4408fb599/ADDITIVE-MANUFACTURING-TECHNOLOGIES.pdf

[67] North E. 3D printing vs CNC Machining – Key differences. *AdvancedAdditiveManufacuring Ltd - 3DPrintUK*. Published online October 3, 2019. https://www.advancedadditivemanufacturing.co.uk/blog/3d-printing-vs-cnc-machining-key-differences/

[68] Siddique THM, Sami I, Nisar MZ, Naeem M, Karim A, Usman M. Low Cost 3D Printing for Rapid Prototyping and its Application. *Conference: 2019 Second International Conference on Latest Trends in Electrical Engineering and Computing Technologies*. Published online November 1, 2019. doi:10.1109/intellect47034.2019.8954983

[69] Gokhare VG, Raut DN, Shinde D. A Review paper on 3D-Printing Aspects and Various Processes Used in the 3D-Printing. *International Journal of Engineering Research and Technology*. 2017;6(6). https://www.ijert.org/research/a-review-paper-on-3d-printing-aspects-and-various-processes-used-in-the-3d-printing-IJERTV6IS060409.pdf

[70] Huang SH, Liu P, Mokasdar A, Hou L. Additive manufacturing and its societal impact: a literature review. *The International Journal of Advanced Manufacturing Technology*. 2012;67(5-8):1191-1203. doi:10.1007/s00170-012-4558-5

[71] Layani M, Wang X, Magdassi S. Novel materials for 3D printing by photopolymerization. *Advanced Materials*. 2018;30(41):1706344. doi:10.1002/adma.201706344

[72] Palmara G, Frascella F, Roppolo I, Chiappone A, Chiadò A. Functional 3D printing: Approaches and bioapplications. *Biosensors and Bioelectronics*. 2021;175:112849. doi:10.1016/j.bios.2020.112849

[73] Sun HB, Kawata S. Two-Photon photopolymerization and 3D lithographic microfabrication. In: *Advances in Polymer Science*. ; 2006:169-273. doi:10.1007/b94405

[74] Kaur M, Srivastava AK. PHOTOPOLYMERIZATION: a REVIEW. *Journal of Macromolecular Science, Part A*. 2002;42(4):481-512. doi:10.1081/mc-120015988

[75] Schmidleithner C. *Stereolithography*.; 2018.

[76] Bagheri A, Jin J. Photopolymerization in 3D printing. *ACS Applied Polymer Materials*. 2019;1(4):593-611. doi:10.1021/acsapm.8b00165

[77] Piedra-Cascón W, Krishnamurthy VR, Att W, Revilla-León M. 3D printing parameters, supporting structures, slicing, and post-processing procedures of vat-polymerization additive manufacturing technologies: A narrative review. *Journal of Dentistry*. 2021;109:103630. doi:10.1016/j.jdent.2021.103630

[78] Alsoussi A. Learn en. *Printie 3D*. Published online April 26, 2020. https://www.printie3d.com/learn-more-about-3d-printing/

[79] Kadry H, Wadnap S, Xu C, Ahsan F. Digital light processing (DLP) 3D-printing technology and photoreactive polymers in fabrication of modified-release tablets. *European Journal of Pharmaceutical Sciences*. 2019;135:60-67. doi:10.1016/j.ejps.2019.05.008

[80] Zhao Z, Xia T, Song X. Engineering materials with light: recent progress in digital light processing based 3D printing. *Journal of Materials Chemistry C*. 2020;8(40):13896-13917. doi:10.1039/d0tc03548c

[81] Bae SU, Kim BJ. Effects of cellulose nanocrystal and inorganic nanofillers on the morphological and mechanical properties of digital light processing (DLP) 3D-Printed photopolymer composites. *Applied Sciences*. 2021;11(15):6835. doi:10.3390/app11156835

[82] Denk W, Strickler JH, Webb WW. Two-Photon laser scanning fluorescence microscopy. *Science*. 1990;248(4951):73-76. doi:10.1126/science.2321027

[83] Yan H, Row KH. Characteristic and synthetic approach of molecularly imprinted polymer. *International Journal of Molecular Sciences*. 2006;7(5):155-178. doi:10.3390/i7050155

[84] Guidechem chemical B2B network provides information on china and global chemical market quotation and relative chemical Information.Guidechem Chemical Network providing the most complete information of the chemical industry. GuideChem. https://www.guidechem.com/

[85] Kaale E, Chambuso M, Kitwala J. Analysis of residual oxytetracycline in fresh milk using polymer reversed-phase column. *Food Chemistry*. 2008;107(3):1289-1293. doi:10.1016/j.foodchem.2007.08.075

[86] KuKanich B, Gehring R, Webb AI, Craigmill AL, Riviere JE. Effect of formulation and route of administration on tissue residues and withdrawal times. *Javma-journal of the American Veterinary Medical Association*. 2005;227(10):1574-1577. doi:10.2460/javma.2005.227.1574

[87] Lv YK, Li-Min W, Yang L, Zhao C, Sun H. Synthesis and application of molecularly imprinted poly(methacrylic acid)–silica hybrid composite material for selective solid-phase extraction and high-performance liquid chromatography determination of oxytetracycline residues in milk. *Journal of Chromatography A*. 2012;1227:48-53. doi:10.1016/j.chroma.2011.12.108

[88] DPGDA - allnex. Allnex. https://allnex.com/en/product/82a3a083-2bdd-46a5-abcc-11eb48f59dfd/dpgda

[89] Max – Asiga. https://www.asiga.com/max/

[90] Kleger N, Cihova M, Masania K, Studart AR, Löffler JF. 3D Printing of Salt as a Template for Magnesium with Structured Porosity. *Advanced Materials*. 2019;31(37):1903783. doi:10.1002/adma.201903783

[91] Conde Y, Despois J, Goodall R, et al. Replication processing of highly porous materials. *Advanced Engineering Materials*. 2006;8(9):795-803. doi:10.1002/adem.200600077

[92] Penner MH. Basic principles of spectroscopy. In: *Food Science Text Series*. ; 2017:79-88. doi:10.1007/978-3-319-45776-5_6

[93] Gitika. Beer Lambert Law Equation Derivation, Formula, Examples. *Adda247*. Published online September 5, 2023. https://www.adda247.com/school/beer-lambert-law/

[94] Perkampus H h. *UV-VIS Spectroscopy and Its Applications*.; 1992. doi:10.1007/978-3-642-77477-5

[95] Mäntele W, Deniz E. UV–VIS absorption spectroscopy: Lambert-Beer reloaded. *Spectrochimica Acta Part A: Molecular and Biomolecular Spectroscopy*. 2017;173:965-968. doi:10.1016/j.saa.2016.09.037

[96] TuttoChimica.it - Spettrofotometro. http://www.tuttochimica.it/chimica_analitica_spettrofotometro.asp

[97] Chiappone A, Pedico A, Porcu S, Pirri CF, Lamberti A, Roppolo I. Photocurable 3D-Printable Systems with Controlled Porosity towards CO2 Air Filtering Applications. *Polymers*. 2022;14(23):5265. doi:10.3390/polym14235265

[98] Scanner da laboratorio 3Shape – Serie E. 3Shape. https://www.3shape.com/it/scanners/e-series

[99] Zhou W, Apkarian RP, Wang ZL, Joy DC. Fundamentals of Scanning Electron Microscopy (SEM). In: *Springer EBooks*. ; 2006:1-40. doi:10.1007/978-0-387-39620-0_1

[100] Scanning Electron Microscopy (SEM). Techniques. https://serc.carleton.edu/research_education/geochemsheets/techniques/SEM.html

[101] Field Emission Scanning Electron Microscopy (FESEM) – PhotoMetrics. https://photometrics.net/field-emission-scanning-electron-microscopy-fesem/

[102] https://support.asiga.com/approach-failed-max/#:~:text=1